Development of Novel Models to Study Ovarian Cancer Stem Cells

by

Daniela Vanesa Burgos Ojeda

A dissertation submitted in partial fulfillment
of the requirements for the degree of
Doctor of Philosophy
(Cellular and Molecular Biology)
in the University of Michigan
2014

Doctoral Committee:

Associate Professor Ronald J. Buckanovich, Chair
Professor Kathleen R. Cho
Professor Andrzej A. Dlugosz
Assistant Professor Marina Pasca di Magliano
Professor Max S. Wicha

DEDICATION

This dissertation is dedicated to my family and my loved country Venezuela. Specially to my loving parents, Luis Alberto Burgos Briceno and Dalia Ojeda, whose support and words of encouragement kept me continuing this journey. My siblings, Luis Alejandro Burgos Ojeda and Dalia Esther Burgos Ojeda whose were always there for me to listen and supported me throughout the process. My best friend and husband, Peter Andres Sabatini Muniz, for all your support and love throughout the entire doctorate program. To our precious daughter Isabella Alejandra Sabatini Burgos thank you for supporting me, even though you are so young I know you understand and helped mommy throughout this experience. And finally to our little one who is coming to our lives, who accompanied me and supported me during the dissertation writing.

Finally to my loving Venezuela, no matter all your problems, I will always love you and be proud of coming from you. I will always keep you in my heart and put your name high.

Orgullosa de ser Venezolana, tu hija, tu hermana, tu esposa y tu mama,

Daniela Burgos Ojeda de Sabatini

ACKNOWLEDGEMENTS

I wish to thank my committee members who were more than generous with their expertise and precious time. A special thanks to Dr. Ronald Buckanovich, my committee chairman and mentor, for his countless hours of teaching, encouraging, proof-reading and most of all patience throughout the entire process. Thank you for always being there for me, all your advice and teaching. I have learned so much from you and I will always admire you as a scientist and as a person. Thank you Dr. Kathleen Cho, Dr. Andrzej Dlugosz, Dr. Marina Pasca di Magliano and Dr. Max S. Wicha for agreeing to serve on my committee. Specially, Dr. Kathleen Cho for providing us all the mice needed.

I would like to acknowledge all the Buckanovich Laboratory members, especially Dr. Karen McLean who trained me, taught me, proof-read all my writing and was always there for me even during her busiest time. Ines Silva, for all your teaching about organization and planning skills to be able to manage my time during my doctoral degree. Yunjung Choi and Shoumei Bai, for all the teaching, listening, patience and help with my experiments. Kun Yang, for always being supportive and willing to help.

Finally I would like to acknowledge and thank the program in Cellular and Molecular Biology from allowing me to conduct my research and providing any assistance requested.

Thank you all for making this an enjoyable experience.

TABLE OF CONTENTS

LIST OF TABLES

TABLE

LIST OF FIGURES

FIGURE

GENERAL ABSTRACT

Cancer stem cells (CSC) are rare cells within a tumor reported to be resistant to standard chemotherapy, which can serve to populate the bulk of a tumor with more differentiated daughter cells and potentially contribute to recurrent disease and metastasis. A better understanding of ovarian CSC could lead to novel therapeutic approaches to specifically target CSC. We developed two in vivo models for the study of ovarian CSC. We first generated a human embryonic stem cell derived teratoma (hESCT) tumor model, creating a human tumor microenvironment for CSC growth. We demonstrate that unlike other tumor models, this model has human tumor vessels, a critical part of the CSC niche. These vessels express tumor vascular specific markers (TVMs). We showed the ability of the hESCT model, with human tumor vascular niche, to enhance the engraftment rate of primary human ovarian cancer stem-like cells. Furthermore, this model can be used to test anti-human specific TVM immunotherapeutics.

Unfortunately, the study of human CSC can be hampered by heterogeneity of primary tumor samples, long requirements for tumor growth in vivo, and the need for tumor growth in immune-deficient mice. We therefore evaluated CSC in a transgenic murine model of ovarian cancer. Using flow cytometry to characterize a cell line derived from this tumor model we identified that $CD24^+$ cells have a enhanced ability to form tumor spheres, to passage, and to initiate tumors in vivo; hallmarks of CSC. $CD24^+$ cells preferentially express stem cell markers Nanog and c-myc and demonstrate preferential phosphorylation of STAT3. Suggesting an important role for STAT3 in $CD24^+$ CSC, $CD24^+$ cells were preferentially sensitive to inhibition

of STAT3 phosphorylation with the JAK2 inhibitor TG101209. Finally, in vivo therapy with TG101209 appeared to decrease tumor metastasis and combined with chemotherapy, prolonged overall survival. Furthermore, preliminary data suggests a role of $CD24^{+}$ cells in tumor migration. Combined we have characterized two distinct models for the characterization of ovarian CSC targeted therapeutics.

GENERAL INTRODUCTION

Ovarian Cancer

Epithelial ovarian cancer (EOC) is the most lethal gynecologic cancer in the western world, accounting for more deaths than endometrial and cervical cancer combined (1), and is the fifth leading cause of cancer-related death among women. Most patients with ovarian cancer present with advanced stage disease (stage III or stage IV). These patients are treated with surgical removal of disease plus chemotherapy, which results in a median progression-free survival of 16-22 months and a 5-year survival rate of 27% although better results are now being reported with improvements in therapy (2, 3).

There are four major histologic types of epithelial ovarian cancer, serous, endometrioid, clear cell and mucinous (4, 5). The different subtypes are characterized by distinct genetic alterations (6). 85% of mucinous ovarian cancers have *KRAS* gene mutations while *KRAS* mutations are less common in clear cell, endometrioid and high grade serous carcinomas (7). Mutations of the *CTNNB1* gene encoding *ß-catenin* are observed in 16-38% of ovarian endometrioid adenocarcinomas (OEAs) (8). With the exception of *TP53*, mutated in more than 95% of serous ovarian cancers, there is no predominant mutation in serous ovarian cancers (9, 10) (See Table 2). Recently an alternative classification of ovarian cancer has been proposed where it is divided into two types (11, 12). Type I EOC includes endometrioid, clear cell,

mucinous and low-grade carcinomas, which usually originate from precursor lesions like endometriosis or borderline tumors (11, 13). In contrast, type II EOC includes high-grade serous carcinomas that are biologically aggressive tumors with a tendency for metastasis (11, 13). Type I and type II ovarian cancers can have overlapping features, suggesting that a subset of EOC may undergo type I to type II progression along with the acquisition of somatic *TP53* mutations (12, 13).

Origin of Ovarian Cancer

It is currently debated whether the origin of ovarian cancer is in the ovarian surface epithelium (OSE) of mesothelial origin (14) or the fallopian tube (15). It has been proposed that ovarian tumorigenesis is associated with ovulation wound repair and/or inflammation, possibly leading to abnormal stem cell expansion in the OSE (16). The dilemma of the theory of ovarian cancer arising from the OSE is that there are different types of ovarian cancers based on histology, which are not necessarily derived from the mesothelium (17). These subtypes have diverse histological origins and different clinical and pathological behaviors. Therefore, it is unlikely that all these tumors originate from the same cell or the same lesion (18). Recently it has been proposed that migratory cancer cells may come from the fallopian tube or from other sites from the female reproductive tract and travel through the fallopian tubes and arrive to the OSE (12, 18, 19).

In addition to the exact tissue of origin regarding cancer, further controversy exists regarding specific cell type which leads to tumor initiation. It has been proposed that specifically normal stem cells which incur genetic and epigenetic changes can become cancer stem cells

(CSC) to initiate tumors. Alternatively, it is possible that non-stemlike cells can gain stem cell like functions via genetic changes.

Ovarian Cancer Stem Cells

The majority of ovarian cancer patients achieve complete clinical remission following initial treatment. Unfortunately, most will relapse and succumb to their disease. This is consistent with the cancer stem cell hypothesis, which theorizes that within a heterogeneous population of cancer cells, rare chemotherapy-resistant cells with stem cell like qualities can serve to populate the bulk of a tumor with more differentiated daughter cells and potentially contribute to recurrent disease (20, 21). In the past five years a significant amount of work has been done to identify ovarian cancer cells with characteristics of stem cells (22-31).

Within an ovarian cancer, all tumor cells are not equal; tumor cells display a great deal of heterogeneity. More specifically, within a given tumor (or even tumor cell line), there are abundant distinct tumor cell populations expressing different markers. These unique cell populations have differential capacities for growth, survival, metastasis and resistance to chemotherapy and radiation therapy. Cancer stem cells make up a small proportion of malignant cells within a tumor, typically 0.01-1%. Cancer stem cells have the capacity to undergo either symmetric or asymmetric divisions to recreate a tumor with the complete original complex pool of tumor cells in immune-suppressed mice (32, 33). Moreover, these highly specialized cell populations reportedly have unlimited division potential and therefore are capable of serial passages in vitro and in vivo. These cells have been termed cancer stem cells (CSC), tumor

initiating cells (TICs), cancer initiating stem cells (CIC) and tumor propagating cells (TPC). For the purpose of this thesis dissertation we will refer to these cells as CSC.

Ovarian CSC are, for the most part, shown to be resistant to chemotherapy and radiation therapy (22, 27, 29, 34). Based on their resistance to traditional cancer therapies and presumed ability to recapitulate the original tumor, CSC are believed to be the source of recurrent ovarian cancer. Consequently, there is a strong interest to identify, functionally characterize the pathobiology of, and eventually target ovarian CSC. To date, the study of CSC in ovarian cancer has been extremely challenging for several reasons, patient-to-patient heterogeneity, long requirements to grow and the use of immunosuppressed mice. It has been postulated that CSC may arise from genetic changes in normal stem cells (28, 35). Thus, one way to identify CSC is to characterize cells within a tumor that express known stem cell markers for the tissue of origin. There are several ovarian CSC markers that have been previously reported in the last five years.

CD24

CD24 is a P-selectin ligand for human tumor tissue, also known as a heat-stable antigen. It is a glycoprotein that is expressed in neutrophils, B cells, immature thymocytes, and red blood cells (36). CD24 was initially detected in hematologic cancers such as leukemia and lymphoma, and later found to be overexpressed in solid tumors such as small cell lung carcinoma and ovarian cancer (37-39). CD24 is expressed on the cancer cell surface, and is a cell adhesion molecule that binds to P-selectin on platelets or vascular endothelial cells to promote cancer metastasis (40), suggesting CD24 may play a role in tumor progression. CD24 has been identified as a CSC marker in pancreatic (41) and liver cancers (42). Interestingly, in breast

cancer, CSC are reported to be $CD24^-$ or $CD24^{dim}$. The differences in CD24 expression in different CSC may relate to the different tissues of origin.

Ovarian cancer patients whose tumors have a high level of CD24 expression have high grade tumors with poorer prognosis and shorter survival times (36). Gao et al. recently reported CD24 as a putative CSC marker in ovarian cancer. They established primary ovarian cancer cell lines from serous and mucinous cystadenocarcinomas and found that cells with the CSC characteristics of quiescence, chemoresistance, and tumor initiation capacity were enriched for CD24 expression (26). $CD24^+$ cells expressed stemness related genes such as Nestin, ß-catenin, Bmi-1, Oct4, Oct3/4, Notch1, and Notch4 when compared to $CD24^-$ cells. Interestingly, they found expression of both CD133 and CD117 in the majority of $CD24^+$ cell clones generated. Approximately 1% of $CD24^+$ cells co-expressed CD133 and approximately 1% of $CD24^+$ cells co-expressed CD117. More recently, this same group analyzed cell clones generated from cells located in the center of a tumor and cells at the tumor periphery (43). They hypothesized that cells at the tumor's leading edge would be enriched for CSC. They found that cells from the leading edge had a higher proportion of side population cells (43). Side population (SP) cells are defined by Hoechst dye exclusion in flow cytometry, are enriched by stem cell markers and are believed to be chemo-resistant (44). Within the SP cells they found enriched expression of CD24 and CD117. Once again approximately 1% of cells co-expressed CD24 and CD117. Unfortunately, the tumorigenicity of these cells was not assessed.

CD24 expression in combination with CD44 and the epithelial cell adhesion molecule (EpCam) was also assessed in conjunction with SP cells (45). In established cell lines OVCAR-3, SKOV-3 and IGROV-1 treated with chemotherapy, the percentage of cells expressing all three cell surface markers was found to increase. In addition, when compared to $CD24^-$, $CD44^-$,

EpCam$^-$ cells, these 'triple positive' cells demonstrated greater invasion into matrigel and more rapid tumor growth in vivo. This triplet of markers was not functionally assessed in human tumors.

Interestingly, CD24 has been reported to promote self-renewal through STAT3 and Nanog signaling in liver cancer (42). In ovarian cancer, CD24 and Nanog have been shown to co-localize in the ovarian surface epithelium and premalignant cysts (46). Schreiber et al. showed that higher the malignancy of ovarian cancer higher the percentage of co-localization of Nanog and CD24 in premalignant cysts, which have been proposed as one of the sites that may cause ovarian cancer. Briefly they mentioned that in benign ovarian tumors 37% of specimens were positive to CD24 and Nanog labeling with 26% of CD24$^+$ cells localized in cyst walls. In contrast, 79% of serous borderline tumors were positive for CD24 and 42% were localized in cysts walls. 32% of CD24$^+$ cells showed co-localization Nanog. In serous ovarian carcinomas 81% of specimens were labeled with CD24 antibodies and 45% of CD24$^+$ cells co-localized with Nanog (46). These findings may be relevant to ovarian cancer since it can be utilized for its early detection and may indicate a relationship to the source of this disease.

CD133 and Aldehyde Dehydrogenase

One of the most widely described ovarian CSC markers is CD133. CD133 or Prominin is a membrane glycoprotein encoded by the *CD133/Prom-1* gene. It was first detected as a marker of hematopoietic stem cells and since then has been demonstrated to be a marker of numerous normal and cancer stem cell populations (47-53). In one of the first indications that CD133 may be a marker of ovarian CSC, Ferrandina et al. analyzed expression of CD133 in 41 ovarian

tumors, 8 normal ovaries, and 5 benign ovarian tumors (54). They found that primary ovarian cancer $CD133^{+}CK7^{+}$ cells had greater colony forming potential and had a higher proliferative potential than $CD133^{-}CK7^{+}$ cells (55). Interestingly, they also found that normal ovaries and benign tumors had significantly lower expression of CD133 than ovarian carcinomas (55). In one of the first functional characterizations of CD133 as an ovarian CSC marker, Baba and colleagues demonstrated that $CD133^{+}$ cells from established cell lines had greater tumor initiating capacity than $CD133^{-}$ cells (22). Similarly, consistent with a CSC phenotype, $CD133^{+}$ cells demonstrated greater resistance to chemotherapy. They also reported that CD133 expression in tumor cells was regulated at the level of promoter methylation, suggesting that epigenetic events could be responsible for the induction of tumor 'stemness'.

The study by Baba and colleagues relied primarily on established cell lines. Curley et al. used an alternate approach to study CSC in primary human tumor samples (25). They established 11 primary xenografts from freshly isolated human ovarian carcinomas and then characterized the ability of different cell populations derived from the primary xenografts to initiate new tumors and their ability to continue to undergo serial passages in immunocompromised mice. For both serous and clear cell ovarian cancers, the $CD133^{+}$ high expressing cell fraction demonstrated greater tumor initiating capacity than $CD133^{-}$ cells. In addition $CD133^{+}$ cells gave rise to $CD133^{-}$ cells and a tumor with histologic characteristics of the primary tumor. In one instance a 99% pure $CD133^{-}$ fraction gave rise to a tumor, albeit with a much longer latency period. However an interesting point was the resulting tumor had just over 10% CD133 positive cells suggesting that either $CD133^{-}$ cells can become $CD133^{+}$ cells or the < 1% $CD133^{+}$ fraction was sufficiently amplified to become 10% of the resulting tumor.

Finally, our group and one other group recently analyzed the combined expression of CD133 and the stem cell marker aldehyde dehydrogenase (ALDH) as ovarian CSC markers (29, 56). We found that in cell lines and primary human ovarian tumors in which tumor cells lacked CD133 expression, FACS isolated $ALDH^+$ activity cancer cells were capable of initiating tumors in mice whereas limiting dilutions of $ALDH^-$ activity cells were not. This is in accordance with the work of Landen and colleagues demonstrating specifically $ALDH1A1^+$ cells are ~50 fold more tumorigenic than $ALDH1A1^-$ cells (27). In established cell lines and primary human tumors in which tumor cells expressed CD133, $CD133^+ALDH^+$ (or $CD133^+$ cells with ALDH activity) cells had far greater tumor initiating capacity and shorter tumor latencies than $CD133^-$ $ALDH^-$ cells. Interestingly, while $CD133^+ALDH^-$ cells isolated from cell lines were highly tumorigenic, $CD133^+ALDH^-$ cells isolated from primary tumors were unable to initiate tumors in immunocompromised mice. Whether these cells truly have restricted tumor initiating capacity, or are more sensitive to isolation procedures remains to be determined. Both $ALDH^+$ activity CSC and $CD133^+ALDH^+$ human ovarian CSC were highly angiogenic. This is consistent with studies suggesting ovarian CSC from tumor metastases are capable of attracting endothelial progenitors to promote angiogenesis (57).

CD44 and CD117

CD44 is the receptor of hyaluronate and has been identified as a marker of CSC in breast (58), prostate (50), colorectal (59), pancreatic (41), and head and neck squamous cell carcinomas (60). CD117, also known as c-kit, is another well-characterized stem cell marker, which has been implicated as a CSC marker in several solid tumors. In the first study to consider ovarian CSC,

Szotek and colleagues use hoechst dye exclusion to identify side-population (SP) cells with CSC characteristics within a murine ovarian cancer cell line. These SP cells were enriched for CD117 expression. However, they found human ovarian cancer ascites SP cells lacked CD117 expression. In contrast, Bapat et al. isolated tumor cells from the ascites of a patient diagnosed with serous ovarian cancer and established 19 spontaneously immortalized clones (23). Molecular characterization of these clones identified the expression of CD44, CD117, and scatter factor - the ligand for CD117. Interestingly, only one of these clones demonstrated tumorigenicity in vivo, suggesting the presence of cells with different tumor initiating capacity within the ovarian tumor associated ascites. Alternatively, one could speculate this clone had acquired additional genetic changes due to in vitro culture. Consistent with this, a second clone underwent spontaneous transformation during culture.

Similarly, Zhang et al. analyzed tumor spheroids generated from the ascites of 5 patients with serous ovarian cancer (31). After approximately ten serial passages in a stem cell based media (lacking serum and addition of growth factors such as FGF, EGF and other factors such as insulin, hydrocortisone and ß-mercaptoethanol) they observed that the remaining spheroid cells were highly enriched for CD44 and CD117 expression. Like the studies above for CD133 (22, 29), $CD44^{+}CD117^{+}$ spheroid cells were resistant to chemotherapy, and were able to initiate and serially propagate tumors in mice. Finally, using primary tumor xenografts similar to the CD133 study above (25), Luo et al. reported that tumorigenic $CD117^{+}$ lineage cells were isolated from 3 of 14 tumor xenografts. These cells were capable of serial transplantation and asymmetric division, and the presence of these cells was correlated with chemoresistance (61).

Subsequently, Alvero et al. analyzed epithelial ovarian tumors from 147 patients prior to chemotherapy and found that all had a subset of CD44 positive cells, and the expression of CD44

was higher in metastatic tumors and tumor ascites (24). They then generated primary cell lines from human tumors or ascites and then injected $CD44^+$ cells from the lines into immunocompromised mice. They found that $CD44^+$ cells recapitulated the original tumor and were able to undergo multiple passages in vivo (24). Complicating the interpretation of this study, they injected a large number of cells ($1x10^6$) and they did not test the tumorigenicity of $CD44^-$ cells. Expression analysis of $CD44^+$ and $CD44^-$ cells revealed that Myeloid Differentiation Factor 88 (MyD88), an activator of the NFkB signaling pathway, was upregulated by 10 fold in $CD44^+$ cells, potentially linking CD44 expressing cells and chronic inflammatory responses of cancer (24). In a follow-up study, the same group showed that xenograft tumors derived from $CD44^+$ cells gave rise to human CD34 expressing blood vessels, suggesting that these tumor cells have the potential to differentiate into vessels or direct other cells for the formation of vessels (62). Finally, a study performed using vital dyes to identify 'label retaining cells' i.e. quiescent CSC, demonstrated that nearly 100% of the label retaining cells were $CD44^+CD117^+$ (63). However, this study was performed with a murine tumor cell line so the applicability to human cancer remains uncertain.

Using Novel Models to Study Ovarian Cancer Stem Cells

The study of human ovarian cancer stem cells has been hampered by low engraftment rates and long requirements for tumor growth in mice. During the past five years only three groups could grow primary ovarian cancer stem cells in a xenograft (25, 29, 64). Other groups used primary tumor spheres, metastatic tissue and cell lines due to the difficulty of primary tumor cells to engraft in the mouse (see Table 1). Therefore new models are necessary for the

study of human ovarian cancer stem cells. We propose to study ovarian cancer stem cells in two new models.

Cancer Stem Cells and the Tumor Microenvironment

Within the adult organism, stem cells reside in defined anatomical microenvironments called niches. These architecturally diverse microenvironments serve to balance stem cell self-renewal and differentiation (65). The same concept can be applied to the tumor microenvironment, which is a complex network of different cell types, soluble factors, signaling molecules and extracellular matrix components, which orchestrate the fate of tumor progression (66). In the tumor microenvironment, CSC receive growth factor and cytokine cues from tumor cells, stroma and vasculature to self-renew, differentiate, induce epithelial-mesenchymal transition (EMT) or simply remain quiescent. Unfortunately, the study of CSC has been hampered by the difficulty of these cells to engraft in mouse xenografts. Engraftment rates of primary cells are ~40%. These low engraftment rates might be due to the difference of species and the lack of survival cues coming from the human microenvironment. In addition primary CSC xenografts can take up to 9 months to grow (29), which is both impractical for most studies and can be complicated by spontaneous tumors, which can develop in immunosuppressed mice.

Studying Human Ovarian Cancer Stem Cells in a Human Microenvironment

Several models have been developed to study cancer cell characteristics such as proliferation, migration, invasion, neoangiogenesis and metastasis. These include in vitro model systems to grow cell lines and primary cells in tissue culture plates, anchorage-independent systems, transwell culture systems, and 3D culture systems. The majority of in vivo model

systems involve the injection of tumor cells at various sites into immunocompromised mice. However these models all lack a human microenvironment. One of the factors within the microenvironment that these models lack is human tumor endothelial cells, a critical component of the CSC niche.

Human brain CSC have been shown to grow near the tumor vasculature (67) where human endothelial cells provide secreted factors that maintain these cells in a self-renewing and undifferentiated state. Other studies have shown that when human brain CSC are xenotransplanted orthotopically, they grow near the murine vasculature (68). In order to understand the interaction of CSC with the tumor microenvironment, it is necessary to study human CSC in a human tumor microenvironment in the mouse. Several techniques have been proposed with the goal of recreating a human microenvironment in the mouse with human vessels. One approach is the use of primary xenografts that contain tumor cells. For example, human renal cell and prostate carcinoma primary xenografts established from biopsy have previously been shown to contain human vessels even one month after implantation (69). However, studies with colorectal cancer biopsy xenografts have shown a rapidly replacement of human vessels with their murine counterparts by nearly 50% by day 10 after implantation (70).

Stable and functional human blood vessels can be engineered in immunodeficient mice after co-implantation of primary human endothelial cells and human mesenchymal stem cells (71-73) or spheroid-based endothelial cell transplantation (74). The human vasculature constructed under these conditions was found to be similar to normal vessels at both the molecular and cellular levels. However, these tumors still lack total recapitulation of the tumor microenvironment. Co-injection of human endothelial cells with tumor cells has been studied by us (unpublished data) and others (75) and still is not an accurate substitute of the tumor

microenvironment. Interestingly, Alonso-Camino et al. showed that when tumor cells were co-injected with human endothelial cells and mesenchymal stem cells in mice that underwent sublethal whole-body exposure to radiation, human vessels were maintained within the tumor for 30 days before the murine vasculature reconstitutes the tumor vasculature (76). Additionally, the same group showed that the former mentioned organoids with human blood vessels formed by co-injection of human endothelial cells plus mesenchymal stem cells are appealing to human breast cancer circulating cells (77).

The human vasculatures engineered in the previous models are similar to normal vasculature. However, several studies have shown that tumor vasculature is different from normal vasculature in colon (78), breast (79, 80), brain (81), and ovarian (82, 83) cancers. Furthermore, these studies have shown that there are tumor specific differences among tumor endothelial markers. Tumor growth depends on the tumor vasculature (84, 85). Tumor vasculature is derived from the formation of new vessels (angiogenesis), modification of existing vessels or recruitment and differentiation of endothelial precursors from bone marrow (vasculogenesis), all of which contribute to vascular heterogeneity in and among tumors (86).

Another widely used technique to create a human microenvironment in the mouse is the use of human mammary fat pads to grow human breast CSC (87). Kupperwasser et al. first developed this technique for xenotransplantation of normal mammary epithelial cells. This consists of clearing fat pads of pre-pubescent mice and then replacing them by injecting a mixture of irradiated and non-irradiated immortalized human fibroblasts (88). The irradiated fibroblasts support the growth of normal and cancer epithelial cells by secreting a number of growth factors, collagen and possibly directly interacting with the epithelial cells (87, 89). The

use of human mammary fat pads in the mouse partially recapitulates a human microenvironment orthotopically and allows the engraftment of breast CSC.

Another technique to create a human microenvironment in the mouse is the use of human embryonic stem cells (hESC), as these cells have been shown to form a teratoma if injected in immunosuppressed mice (90). Human embryonic stem cell derived teratoma (hESCT) is a benign tumor containing the three germ layers including human vessels. It has been previously shown hESCT can support the growth of human tumor cells (91, 92) and interestingly tumor cells are found near hESCT-derived vessels (93). The same group also demonstrated that hESCT supported the growth of primary ovarian cancer ascites (94). Primary tumor cells injected subcutaneously took 45-65 days to form a tumor, whereas primary tumor cells took 21-24 days to grow within the teratoma. Furthermore, tumors growing within hESCT showed more obvious differentiated glandular structures similar to the original cancer histology as compared with standard xenograft tumors (94). The investigators were able to identify the growth of primary ovarian cancer clear cell carcinoma stem cells intra-hESCT using the CSC markers CD44 and ALDH (95). These studies suggest a human microenvironment in the mouse will better support CSC growth.

Mouse Model to Study Ovarian Cancer Stem Cells

Given current deficits in the study of human CSC; poor engraftment rates, slow tumor growth, significant interpatient heterogeneity, and the need to grow cells in an immune-suppressed background, murine models offer an appealing alternative approach to study CSC.

However, before these models can be used to study CSC, CSC need to be defined in these models.

Investigators have attempted to create mouse models of human ovarian cancer by introducing the common genetic alterations of this disease into mice. The generation of genetically engineered mouse models of ovarian cancer in which the fallopian tube or the OSE is specifically targeted has been hampered by the lack of defined transcriptional promoters active specifically in these cell types (96). Specifically, promoters used to express genes in OSE are also active in other tissues of Mullerian origin (fallopian tube, uterus, cervix and ovarian granulosa cells) (96). Cre-Lox system has been used to induce targeted deletion of tumor suppressor genes and to activate oncogenes. The Cre-Lox system consist of a single enzyme, Cre recombinase that recombines a pair of short target sequences called the Lox sequences. Placing Lox sequences appropriately allows genes to be activated, repressed, or exchanged for other genes. For example, the Mullerian inhibiting substance II receptor (MISRII) promoter drives transgene expression in the OSE and ovarian granulosa cells, but is also expressed in the mesenchyme of the oviduct (96). One mouse model utilized the MISRII promoter to drive expression of the SV40 large T antigen (SV40-Tag), which is a viral oncogene that binds to and inactivates TP53 and retinoblastoma (Rb), both of which are altered in ovarian cancer (96-98). However, only 50% of the mice in this model system developed large undifferentiated ovarian adenocarcinomas and took 90-100 days for tumors to form (97).

Adenoviral vectors that express Cre recombinase can be used to selectively express or delete genes in the ovary, by injecting the vector into the ovarian bursa. This theoretically results in the Cre-expressing adenovirus only reaching oviductal, ovarian surface epithelial and bursa

cells. However, in practice they sometimes leak out through the injection site and reach uterine tissue.

The BRCA1 and 2 genes are either mutated or silenced by methylation in approximately 20% of all high-grade ovarian cancers and approximately 95% harbor TP53 mutations (10). Loss of BRCA1 in combination with *TP53* (BRCA1$^{LoxP/LoxP}$ TP53$^{LoxP/LoxP}$) mice developed leiomosarcoma but not serous ovarian cancer (99). Mice with MISRII-Cre; Pten$^{fl/fl}$; Dicer$^{fl/fl}$ developed tumors resembling high-grade serous ovarian cancer in the mesenchyme of the oviduct that metastasized to the peritoneum and formed ascites (100). However the tumors did not have mutations in BRCA and TP53, which are features of high grade serous ovarian cancer.

Wu et al. developed a mouse model that resembles human endometrioid adenocarcinoma with conditional inactivation of the APC and PTEN tumor suppressor genes (101). This mouse model belongs to the type I ovarian cancer tumor classification (for reference to type I and type II ovarian cancers see page 2 on the ovarian cancer section of this dissertation document). Recently, Wu et al. developed a new mouse model of ovarian cancer with conditional inactivation of the APC and PTEN tumor suppressors with the addition of TP53 deletion, resulting in a more aggressive phenotype, shortened survival and more widespread metastasis (like type II ovarian cancers) (13). This new model is more applicable to the majority of ovarian cancer patients, which have a type II ovarian cancer disease than their previous mouse model with only APC and PTEN somatic mutations, which resembles human endometrioid adenocarcinoma (more like type I ovarian cancers) (101). In this newest mouse model of ovarian cancer, tumors develop following injection of adenovirus cre recombinase (AdCre) into the ovarian bursa of Apc$^{flox/flox}$; Pten$^{flox/flox}$; TP53 $^{flox/flox}$ mice at 8-10 weeks of age (13). These mice developed metastases in locations similar to those seen in patients with stage IV ovarian cancer,

and show similar morphology, biological behavior and gene expression patterns to their human counterpart (13). 76% of mice develop ascites. This mouse model is an excellent tool to study ovarian cancer since tumors formed as early as 6 weeks following AdCre injection. Importantly, these mice are immunocompetent. Therefore we can analyze the possible effects of the tumor microenvironment on therapeutic response.

Ovarian Surface Epithelium Stem Cells

The origin of CSCs is not known. Potentially CSC could originate from normal stem cells that acquired mutation over time. Surprisingly few studies have been performed characterizing normal epithelial ovarian stem cells. The first attempt to identify a stem cell population in murine OSE was reported by Szotek et al. Using BrdU and histone2B-GFP transgenic mice they identified a population of label retaining cells in the OSE which was quiescent and enriched in the Hoechst stain 'side population' (102). More recently, a population of murine OSE cells in the hilum between the ovary and oviduct were found to be responsible for repopulation of the OSE (103). These cells were were found to be relatively quiescent, and expressed the stem cell markers ALDH, CD133 and LGR5 (103). Importantly, when TP53 and Rb1 mutations were introduced into these cells, two relevant mutations in human ovarian cancer, these cells had increased tumor initiation capacity. These studies suggest that there may be a murine OSE stem cells that when mutated act as CSC. However, more detailed studies remain to be carried out to test this hypothesis.

Ovarian cancer stem cell studies have been hampered by patient heterogeneity, low engraftment in mice, long requirements for tumor growth and the use of immunosuppressed mice. We developed two distinct murine tumor models to study ovarian cancer stem cells. One model expands the human ESCT model to generate confirmed human tumor vessels recreating the human tumor microenvironment for human primary ovarian cancer stem cells to engraft. Another model, which we know its genetics deficits, therefore making it homogeneous, provides rapid tumor growth and importantly offers an immunocompetent microenvironment. With both of these models we can test immunotherapeutics targeting ovarian cancer stem cells.

Table 1. Previously published ovarian cancer stem cell markers

Marker	Source of ovarian CSC injected in xenografts
CD44	Primary cancer cell lines and spheres (24)
CD117 and CD44	Primary spheres (31)
CD133	Cell line (22), **Primary tumor cells** (25)
ALDH	Cell line (104), Omental metastasis bulk tissue (27)
ALDH and CD133	**Primary tumor cells** (29) (64)
CD24	Primary patient clones passaged (cell line) (26)
Sox2	Cell line (105)
ALDH and Side population	Cell line (106)

Table 2. Prevalence of histologic types of epithelial ovarian cancer and their associated molecular genetic changes (adapted from Kurman et. al)(12).

Ovarian Cancer Type	Histology	Frequent mutations
II	High grade serous	*TP53* Chromosomal instability Inactivation of *BRCA1/2*
I	Mucinous	*KRAS*
	Clear Cell	*ARIDIA* *PIK3CA* *ZNF217* *PPP2RIA*
	Low-grade serous	*KRAS* *BRAF* *ERBB2* *PIK3CA*
	Endometrioid	*ARIDIA* *CTNNB1* *PTEN* *PIK3CA* *PP2RIA*

REFERENCES

1. Ozols RF, Bookman MA, Connolly DC, Daly MB, Godwin AK, Schilder RJ, et al. Focus on epithelial ovarian cancer. Cancer Cell. 2004;5:19-24.
2. Institute NC. SEER Statistics Review, 1975-2005.
3. Kipps E, Tan DS, Kaye SB. Meeting the challenge of ascites in ovarian cancer: new avenues for therapy and research. Nat Rev Cancer. 2013;13:273-82.
4. Guppy AE, Nathan PD, Rustin GJ. Epithelial ovarian cancer: a review of current management. Clin Oncol (R Coll Radiol). 2005;17:399-411.
5. Farley J, Ozbun LL, Birrer MJ. Genomic analysis of epithelial ovarian cancer. Cell Res. 2008;18:538-48.
6. Bell DA. Origins and molecular pathology of ovarian cancer. Mod Pathol. 2005;18 Suppl 2:S19-32.
7. Enomoto T, Weghorst CM, Inoue M, Tanizawa O, Rice JM. K-ras activation occurs frequently in mucinous adenocarcinomas and rarely in other common epithelial tumors of the human ovary. Am J Pathol. 1991;139:777-85.
8. Wu R, Zhai Y, Fearon ER, Cho KR. Diverse mechanisms of beta-catenin deregulation in ovarian endometrioid adenocarcinomas. Cancer Res. 2001;61:8247-55.
9. Ahmed AA, Etemadmoghadam D, Temple J, Lynch AG, Riad M, Sharma R, et al. Driver mutations in TP53 are ubiquitous in high grade serous carcinoma of the ovary. J Pathol. 2010;221:49-56.
10. Integrated genomic analyses of ovarian carcinoma. Nature. 2011;474:609-15.
11. Kurman RJ, Shih Ie M. Pathogenesis of ovarian cancer: lessons from morphology and molecular biology and their clinical implications. Int J Gynecol Pathol. 2008;27:151-60.
12. Kurman RJ, Shih Ie M. Molecular pathogenesis and extraovarian origin of epithelial ovarian cancer--shifting the paradigm. Hum Pathol. 2011;42:918-31.
13. Wu R, Baker SJ, Hu TC, Norman KM, Fearon ER, Cho KR. Type I to type II ovarian carcinoma progression: mutant Trp53 or Pik3ca confers a more aggressive tumor phenotype in a mouse model of ovarian cancer. Am J Pathol. 2013;182:1391-9.
14. Auersperg N. Ovarian surface epithelium as a source of ovarian cancers: Unwarranted speculation or evidence-based hypothesis? Gynecol Oncol. 2013.
15. Karst AM, Levanon K, Drapkin R. Modeling high-grade serous ovarian carcinogenesis from the fallopian tube. Proc Natl Acad Sci U S A. 2011;108:7547-52.
16. Ness RB, Cottreau C. Possible role of ovarian epithelial inflammation in ovarian cancer. J Natl Cancer Inst. 1999;91:1459-67.
17. Lee KR, Young RH. The distinction between primary and metastatic mucinous carcinomas of the ovary: gross and histologic findings in 50 cases. Am J Surg Pathol. 2003;27:281-92.
18. Mor G, Alvero A. The duplicitous origin of ovarian cancer. Rambam Maimonides Med J. 2013;4:e0006.

19. Piek JM, van Diest PJ, Zweemer RP, Jansen JW, Poort-Keesom RJ, Menko FH, et al. Dysplastic changes in prophylactically removed Fallopian tubes of women predisposed to developing ovarian cancer. J Pathol. 2001;195:451-6.
20. Steg AD, Bevis KS, Katre AA, Ziebarth A, Alvarez RD, Zhang K, et al. Stem cell pathways contribute to clinical chemoresistance in ovarian cancer. Clinical Cancer Research.
21. Latifi A, Abubaker K, Castrechini N, Ward AC, Liongue C, Dobill F, et al. Cisplatin treatment of primary and metastatic epithelial ovarian carcinomas generates residual cells with mesenchymal stem cell-like profile. J Cell Biochem. 2011;112:2850-64.
22. Baba T, Convery PA, Matsumura N, Whitaker RS, Kondoh E, Perry T, et al. Epigenetic regulation of CD133 and tumorigenicity of CD133+ ovarian cancer cells. Oncogene. 2009;28:209-18.
23. Bapat SA, Mali AM, Koppikar CB, Kurrey NK. Stem and progenitor-like cells contribute to the aggressive behavior of human epithelial ovarian cancer. Cancer Res. 2005;65:3025-9.
24. Alvero AB, Chen R, Fu HH, Montagna M, Schwartz PE, Rutherford T, et al. Molecular phenotyping of human ovarian cancer stem cells unravels the mechanisms for repair and chemoresistance. Cell Cycle. 2009;8:158-66.
25. Curley MD, Therrien VA, Cummings CL, Sergent PA, Koulouris CR, Friel AM, et al. CD133 expression defines a tumor initiating cell population in primary human ovarian cancer. Stem Cells. 2009;27:2875-83.
26. Gao MQ, Choi YP, Kang S, Youn JH, Cho NH. CD24+ cells from hierarchically organized ovarian cancer are enriched in cancer stem cells. Oncogene. 2010;29:2672-80.
27. Landen CN, Jr., Goodman B, Katre AA, Steg AD, Nick AM, Stone RL, et al. Targeting aldehyde dehydrogenase cancer stem cells in ovarian cancer. Mol Cancer Ther. 2010;9:3186-99.
28. Murphy SK. Targeting ovarian cancer-initiating cells. Anticancer Agents Med Chem. 2010;10:157-63.
29. Silva IA, Bai S, McLean K, Yang K, Griffith K, Thomas D, et al. Aldehyde dehydrogenase in combination with CD133 defines angiogenic ovarian cancer stem cells that portend poor patient survival. Cancer Res. 2011;71:3991-4001.
30. Steffensen KD, Alvero AB, Yang Y, Waldstrom M, Hui P, Holmberg JC, et al. Prevalence of epithelial ovarian cancer stem cells correlates with recurrence in early-stage ovarian cancer. J Oncol. 2011;2011:620523.
31. Zhang S, Balch C, Chan MW, Lai HC, Matei D, Schilder JM, et al. Identification and characterization of ovarian cancer-initiating cells from primary human tumors. Cancer Res. 2008;68:4311-20.
32. Medema JP, Vermeulen L. Microenvironmental regulation of stem cells in intestinal homeostasis and cancer. Nature. 2011;474:318-26. 33. Vermeulen L, Sprick MR, Kemper K, Stassi G, Medema JP. Cancer stem cells--old concepts, new insights. Cell Death Differ. 2008;15:947-58.
34. Kurrey NK, Jalgaonkar SP, Joglekar AV, Ghanate AD, Chaskar PD, Doiphode RY, et al. Snail and slug mediate radioresistance and chemoresistance by antagonizing p53-mediated apoptosis and acquiring a stem-like phenotype in ovarian cancer cells. Stem Cells. 2009;27:2059-68.

35. Naora H. Developmental patterning in the wrong context: the paradox of epithelial ovarian cancers. Cell Cycle. 2005;4:1033-5.
36. Zhu J, Zhang G, Lu H. CD24, COX-2, and p53 in epithelial ovarian cancer and its clinical significance. Front Biosci (Elite Ed). 2012;4:2745-51.
37. Senner V, Sturm A, Baur I, Schrell UH, Distel L, Paulus W. CD24 promotes invasion of glioma cells in vivo. J Neuropathol Exp Neurol. 1999;58:795-802.
38. Jackson D, Waibel R, Weber E, Bell J, Stahel RA. CD24, a signal-transducing molecule expressed on human B cells, is a major surface antigen on small cell lung carcinomas. Cancer Res. 1992;52:5264-70.
39. Kristiansen G, Denkert C, Schluns K, Dahl E, Pilarsky C, Hauptmann S. CD24 is expressed in ovarian cancer and is a new independent prognostic marker of patient survival. Am J Pathol. 2002;161:1215-21.
40. Aigner S, Sthoeger ZM, Fogel M, Weber E, Zarn J, Ruppert M, et al. CD24, a mucin-type glycoprotein, is a ligand for P-selectin on human tumor cells. Blood. 1997;89:3385-95.
41. Li C, Heidt DG, Dalerba P, Burant CF, Zhang L, Adsay V, et al. Identification of pancreatic cancer stem cells. Cancer Res. 2007;67:1030-7.
42. Lee TK, Castilho A, Cheung VC, Tang KH, Ma S, Ng IO. CD24(+) liver tumor-initiating cells drive self-renewal and tumor initiation through STAT3-mediated NANOG regulation. Cell Stem Cell. 2011;9:50-63.
43. Choi YP, Shim HS, Gao M-Q, Kang S, Cho NH. Molecular portraits of intratumoral heterogeneity in human ovarian cancer. Cancer Letters.307:62-71.
44. Szotek PP, Pieretti-Vanmarcke R, Masiakos PT, Dinulescu DM, Connolly D, Foster R, et al. Ovarian cancer side population defines cells with stem cell-like characteristics and Mullerian Inhibiting Substance responsiveness. Proc Natl Acad Sci U S A. 2006;103:11154-9.
45. Wei X, Dombkowski D, Meirelles K, Pieretti-Vanmarcke R, Szotek PP, Chang HL, et al. Mullerian inhibiting substance preferentially inhibits stem/progenitors in human ovarian cancer cell lines compared with chemotherapeutics. Proc Natl Acad Sci U S A. 2010;107:18874-9.
46. Schreiber L, Raanan C, Amsterdam A. CD24 and Nanog identify stem cells signature of ovarian epithelium and cysts that may develop to ovarian cancer. Acta Histochem. 2013.
47. Yin AH, Miraglia S, Zanjani ED, Almeida-Porada G, Ogawa M, Leary AG, et al. AC133, a novel marker for human hematopoietic stem and progenitor cells. Blood. 1997;90:5002-12.
48. Hristov M, Erl W, Weber PC. Endothelial progenitor cells: isolation and characterization. Trends Cardiovasc Med. 2003;13:201-6.
49. Singh SK, Clarke ID, Hide T, Dirks PB. Cancer stem cells in nervous system tumors. Oncogene. 2004;23:7267-73.
50. Collins AT, Berry PA, Hyde C, Stower MJ, Maitland NJ. Prospective identification of tumorigenic prostate cancer stem cells. Cancer Res. 2005;65:10946-51.
51. Hess DA, Wirthlin L, Craft TP, Herrbrich PE, Hohm SA, Lahey R, et al. Selection based on CD133 and high aldehyde dehydrogenase activity isolates long-term reconstituting human hematopoietic stem cells. Blood. 2006;107:2162-9.
52. Gentry T, Deibert E, Foster SJ, Haley R, Kurtzberg J, Balber AE. Isolation of early hematopoietic cells, including megakaryocyte progenitors, in the ALDH-bright cell population of cryopreserved, banked UC blood. Cytotherapy. 2007;9:569-76.

53. O'Brien CA, Pollett A, Gallinger S, Dick JE. A human colon cancer cell capable of initiating tumour growth in immunodeficient mice. Nature. 2007;445:106-10.
54. Ferrandina G, Martinelli E, Petrillo M, Prisco MG, Zannoni G, Sioletic S, et al. CD133 antigen expression in ovarian cancer. BMC Cancer. 2009;9:221.
55. Ferrandina G, Bonanno G, Pierelli L, Perillo A, Procoli A, Mariotti A, et al. Expression of CD133-1 and CD133-2 in ovarian cancer. International Journal of Gynecological Cancer. 2008;18:506-14.
56. Kryczek I, Liu S, Roh M, Vatan L, Szeliga W, Wei S, et al. Expression of aldehyde dehydrogenase and CD133 defines ovarian cancer stem cells. Int J Cancer. 2011.
57. Kusumbe AP, Mali AM, Bapat SA. CD133-expressing stem cells associated with ovarian metastases establish an endothelial hierarchy and contribute to tumor vasculature. Stem Cells. 2009;27:498-508.
58. Al-Hajj M, Wicha MS, Benito-Hernandez A, Morrison SJ, Clarke MF. Prospective identification of tumorigenic breast cancer cells. Proc Natl Acad Sci U S A. 2003;100:3983-8.
59. Dalerba P, Dylla SJ, Park IK, Liu R, Wang X, Cho RW, et al. Phenotypic characterization of human colorectal cancer stem cells. Proc Natl Acad Sci U S A. 2007;104:10158-63.
60. Prince ME, Sivanandan R, Kaczorowski A, Wolf GT, Kaplan MJ, Dalerba P, et al. Identification of a subpopulation of cells with cancer stem cell properties in head and neck squamous cell carcinoma. Proc Natl Acad Sci U S A. 2007;104:973-8.
61. Luo L, Zeng J, Liang B, Zhao Z, Sun L, Cao D, et al. Ovarian cancer cells with the CD117 phenotype are highly tumorigenic and are related to chemotherapy outcome. Exp Mol Pathol. 2011;91:596-602.
62. Alvero AB, Fu HH, Holmberg J, Visintin I, Mor L, Marquina CC, et al. Stem-like ovarian cancer cells can serve as tumor vascular progenitors. Stem Cells. 2009;27:2405-13.
63. Kusumbe AP, Bapat SA. Cancer stem cells and aneuploid populations within developing tumors are the major determinants of tumor dormancy. Cancer Research. 2009;69:9245-53.
64. Kryczek I, Liu S, Roh M, Vatan L, Szeliga W, Wei S, et al. Expression of aldehyde dehydrogenase and CD133 defines ovarian cancer stem cells. Int J Cancer. 2012;130:29-39.
65. Brafman DA. Constructing stem cell microenvironments using bioengineering approaches. Physiol Genomics. 2013.
66. Catalano V, Turdo A, Di Franco S, Dieli F, Todaro M, Stassi G. Tumor and its microenvironment: A synergistic interplay. Semin Cancer Biol. 2013.
67. Calabrese C, Poppleton H, Kocak M, Hogg TL, Fuller C, Hamner B, et al. A perivascular niche for brain tumor stem cells. Cancer Cell. 2007;11:69-82.
68. Lathia JD, Gallagher J, Myers JT, Li M, Vasanji A, McLendon RE, et al. Direct in vivo evidence for tumor propagation by glioblastoma cancer stem cells. PLoS One. 2011;6:e24807.
69. Gray DR, Huss WJ, Yau JM, Durham LE, Werdin ES, Funkhouser WK, Jr., et al. Short-term human prostate primary xenografts: an in vivo model of human prostate cancer vasculature and angiogenesis. Cancer Res. 2004;64:1712-21.
70. Sanz L, Cuesta AM, Salas C, Corbacho C, Bellas C, Alvarez-Vallina L. Differential transplantability of human endothelial cells in colorectal cancer and renal cell carcinoma primary xenografts. Lab Invest. 2009;89:91-7.

71. Nor JE, Peters MC, Christensen JB, Sutorik MM, Linn S, Khan MK, et al. Engineering and characterization of functional human microvessels in immunodeficient mice. Lab Invest. 2001;81:453-63.
72. Koike N, Fukumura D, Gralla O, Au P, Schechner JS, Jain RK. Tissue engineering: creation of long-lasting blood vessels. Nature. 2004;428:138-9.
73. Sanz L, Santos-Valle P, Alonso-Camino V, Salas C, Serrano A, Vicario JL, et al. Long-term in vivo imaging of human angiogenesis: critical role of bone marrow-derived mesenchymal stem cells for the generation of durable blood vessels. Microvasc Res. 2008;75:308-14.
74. Alajati A, Laib AM, Weber H, Boos AM, Bartol A, Ikenberg K, et al. Spheroid-based engineering of a human vasculature in mice. Nat Methods. 2008;5:439-45.
75. Kumar P, Ning Y, Polverini PJ. Endothelial cells expressing Bcl-2 promotes tumor metastasis by enhancing tumor angiogenesis, blood vessel leakiness and tumor invasion. Lab Invest. 2008;88:740-9.
76. Alonso-Camino V, Santos-Valle P, Ispizua MC, Sanz L, Alvarez-Vallina L. Engineered human tumor xenografts with functional human vascular networks. Microvasc Res. 2011;81:18-25.
77. Fernandez-Perianez R, Molina-Privado I, Rojo F, Guijarro-Munoz I, Alonso-Camino V, Zazo S, et al. Basement membrane-rich organoids with functional human blood vessels are permissive niches for human breast cancer metastasis. PLoS One. 2013;8:e72957.
78. St Croix B, Rago C, Velculescu V, Traverso G, Romans KE, Montgomery E, et al. Genes expressed in human tumor endothelium. Science. 2000;289:1197-202.
79. Parker BS, Argani P, Cook BP, Liangfeng H, Chartrand SD, Zhang M, et al. Alterations in vascular gene expression in invasive breast carcinoma. Cancer Res. 2004;64:7857-66.
80. Bhati R, Patterson C, Livasy CA, Fan C, Ketelsen D, Hu Z, et al. Molecular characterization of human breast tumor vascular cells. Am J Pathol. 2008;172:1381-90.
81. Madden SL, Cook BP, Nacht M, Weber WD, Callahan MR, Jiang Y, et al. Vascular gene expression in nonneoplastic and malignant brain. Am J Pathol. 2004;165:601-8.
82. Buckanovich RJ, Sasaroli D, O'Brien-Jenkins A, Botbyl J, Hammond R, Katsaros D, et al. Tumor vascular proteins as biomarkers in ovarian cancer. J Clin Oncol. 2007;25:852-61.
83. Lu C, Bonome T, Li Y, Kamat AA, Han LY, Schmandt R, et al. Gene alterations identified by expression profiling in tumor-associated endothelial cells from invasive ovarian carcinoma. Cancer Res. 2007;67:1757-68.
84. Kerbel R, Folkman J. Clinical translation of angiogenesis inhibitors. Nat Rev Cancer. 2002;2:727-39.
85. Ferrara N, Kerbel RS. Angiogenesis as a therapeutic target. Nature. 2005;438:967-74.
86. Junttila MR, de Sauvage FJ. Influence of tumour micro-environment heterogeneity on therapeutic response. Nature. 2013;501:346-54.
87. Ginestier C, Hur MH, Charafe-Jauffret E, Monville F, Dutcher J, Brown M, et al. ALDH1 is a marker of normal and malignant human mammary stem cells and a predictor of poor clinical outcome. Cell Stem Cell. 2007;1:555-67.
88. Kuperwasser C, Chavarria T, Wu M, Magrane G, Gray JW, Carey L, et al. Reconstruction of functionally normal and malignant human breast tissues in mice. Proc Natl Acad Sci U S A. 2004;101:4966-71.

89. Orimo A, Gupta PB, Sgroi DC, Arenzana-Seisdedos F, Delaunay T, Naeem R, et al. Stromal fibroblasts present in invasive human breast carcinomas promote tumor growth and angiogenesis through elevated SDF-1/CXCL12 secretion. Cell. 2005;121:335-48.
90. Thomson JA, Itskovitz-Eldor J, Shapiro SS, Waknitz MA, Swiergiel JJ, Marshall VS, et al. Embryonic stem cell lines derived from human blastocysts. Science. 1998;282:1145-7.
91. Tzukerman M, Skorecki K. A novel experimental platform for investigating tumorigenesis and anti-cancer therapy in a human microenvironment derived from embryonic stem cells. Discov Med. 2003;3:51-4.
92. Tzukerman M, Rosenberg T, Ravel Y, Reiter I, Coleman R, Skorecki K. An experimental platform for studying growth and invasiveness of tumor cells within teratomas derived from human embryonic stem cells. Proc Natl Acad Sci U S A. 2003;100:13507-12.
93. Tzukerman M, Rosenberg T, Reiter I, Ben-Eliezer S, Denkberg G, Coleman R, et al. The influence of a human embryonic stem cell-derived microenvironment on targeting of human solid tumor xenografts. Cancer Res. 2006;66:3792-801.
94. Katz E, Skorecki K, Tzukerman M. Niche-dependent tumorigenic capacity of malignant ovarian ascites-derived cancer cell subpopulations. Clin Cancer Res. 2009;15:70-80.
95. Abelson S, Shamai Y, Berger L, Shouval R, Skorecki K, Tzukerman M. Intratumoral heterogeneity in the self-renewal and tumorigenic differentiation of ovarian cancer. Stem Cells. 2012;30:415-24.
96. Lengyel E, Burdette JE, Kenny HA, Matei D, Pilrose J, Haluska P, et al. Epithelial ovarian cancer experimental models. Oncogene. 2013.
97. Connolly DC, Bao R, Nikitin AY, Stephens KC, Poole TW, Hua X, et al. Female mice chimeric for expression of the simian virus 40 TAg under control of the MISIIR promoter develop epithelial ovarian cancer. Cancer Res. 2003;63:1389-97.
98. Flesken-Nikitin A, Choi KC, Eng JP, Shmidt EN, Nikitin AY. Induction of carcinogenesis by concurrent inactivation of p53 and Rb1 in the mouse ovarian surface epithelium. Cancer Res. 2003;63:3459-63.
99. Quinn BA, Brake T, Hua X, Baxter-Jones K, Litwin S, Ellenson LH, et al. Induction of ovarian leiomyosarcomas in mice by conditional inactivation of Brca1 and p53. PLoS One. 2009;4:e8404.
100. Kim J, Coffey DM, Creighton CJ, Yu Z, Hawkins SM, Matzuk MM. High-grade serous ovarian cancer arises from fallopian tube in a mouse model. Proc Natl Acad Sci U S A. 2012;109:3921-6.
101. Wu R, Hendrix-Lucas N, Kuick R, Zhai Y, Schwartz DR, Akyol A, et al. Mouse model of human ovarian endometrioid adenocarcinoma based on somatic defects in the Wnt/beta-catenin and PI3K/Pten signaling pathways. Cancer Cell. 2007;11:321-33.
102. Szotek PP, Chang HL, Brennand K, Fujino A, Pieretti-Vanmarcke R, Lo Celso C, et al. Normal ovarian surface epithelial label-retaining cells exhibit stem/progenitor cell characteristics. Proc Natl Acad Sci U S A. 2008;105:12469-73.
103. Flesken-Nikitin A, Hwang CI, Cheng CY, Michurina TV, Enikolopov G, Nikitin AY. Ovarian surface epithelium at the junction area contains a cancer-prone stem cell niche. Nature. 2013;495:241-5.
104. Kuroda T, Hirohashi Y, Torigoe T, Yasuda K, Takahashi A, Asanuma H, et al. ALDH1-high ovarian cancer stem-like cells can be isolated from serous and clear cell

adenocarcinoma cells, and ALDH1 high expression is associated with poor prognosis. PLoS One. 2013;8:e65158.
105. Bareiss PM, Paczulla A, Wang H, Schairer R, Wiehr S, Kohlhofer U, et al. SOX2 Expression Associates with Stem Cell State in Human Ovarian Carcinoma. Cancer Res. 2013;73:5544-55.
106. Yasuda K, Torigoe T, Morita R, Kuroda T, Takahashi A, Matsuzaki J, et al. Ovarian cancer stem cells are enriched in side population and aldehyde dehydrogenase bright overlapping population. PLoS One. 2013;8:e68187.
107. Burgos-Ojeda D, McLean K, Bai S, Pulaski H, Gong Y, Silva I, et al. A novel model for evaluating therapies targeting human tumor vasculature and human cancer stem-like cells. Cancer Res. 2013;73:3555-65.

CHAPTER I

A novel model for evaluating therapies targeting human tumor vasculature and human cancer stem-like cells

Daniela Burgos-Ojeda[1], Karen McLean[2], Shoumei Bai[1], Heather Pulaski[2], Yusong Gong[3], Ines Silva[3], Karl Skorecki[4], Maty Tzukerman[4], and Ronald .J. Buckanovich[1,2,3]

[1]Cell and Molecular Biology Program,
[2]Department of Obstetrics and Gynecology, Division of Gynecologic Oncology,
[3]Department of Internal Medicine, Division Hematology-Oncology,
University of Michigan, Ann Arbor, MI.

[4]Rambam Medical Center and Sohnis-Forman Stem Cell Center at the Technion-Israel Institute of Technology, Haifa Israel

ABSTRACT

Human tumor vessels express tumor vascular markers (TVMs), proteins that are not expressed in normal blood vessels. Antibodies targeting TVMs could act as potent therapeutics. Unfortunately, preclinical in vivo studies testing anti-human TVM therapies have been difficult to perform due to a lack of in vivo models with confirmed expression of human TVMs. We therefore evaluated TVM expression in a human embryonic stem cell derived teratoma (hESCT) tumor model previously shown to have human vessels. We now report that, in the presence of tumor cells, hESCT tumor vessels express human TVMs. The addition of mouse embryonic fibroblasts and human tumor endothelial cells significantly increases the number of human tumor vessels. TVM induction is mostly tumor type specific with ovarian cancer cells inducing primarily ovarian TVMs while breast cancer cells induce breast cancer specific TVMs. We demonstrate the utility of this model to test an anti-human specific TVM immunotherapeutics;

anti-human Thy-1 TVM immunotherapy results in central tumor necrosis and a three-fold reduction in human tumor vascular density. Finally, we tested the ability of the hESCT model, with human tumor vascular niche, to enhance the engraftment rate of primary human ovarian cancer stem-like cells (CSC). $ALDH^+$ CSC from patients (n=6) engrafted in hESCT within 4-12 weeks whereas none engrafted in the flank. ALDH- ovarian cancer cells showed no engraftment in the hESCT or flank (n=3). Thus this model represents a useful tool to test anti-human TVM therapy and evaluate in vivo human CSC tumor biology.

INTRODUCTION

The tumor vasculature expresses numerous genes not expressed in normal vasculature (78, 107-110). This is in part due to the increased expression of genes associated with physiologic angiogenesis, as many tumor vascular antigens are also upregulated in angiogenic tissues (78, 111, 112). However, if the angiogenic signature is the primary difference between tumor vasculature and normal vasculature, one might anticipate a significant overlap between vascular profiles of different tumor types. Indeed this is not the case; the vascular expression profile of different tumor types appears to be distinct (81, 83, 108, 110, 112, 113). This is consistent with murine studies suggesting physiologic and pathologic angiogenesis have distinct gene signatures (111), and indicates that the influence of the cancer cell on the tumor microenvironment may play a role in the induction of tumor specific vascular proteins.

Tumor vascular markers (TVMs), antigens specifically expressed in tumor vessels and not expressed in normal vessels, represent a potentially important therapeutic target. In particular, those with extracellular exposure are ideal targets for immunotherapeutics (107, 113-115). As therapeutic targets, TVMs would be accessible to drug, and the restricted nature of TVM expression should limit therapy-associated side effects on normal tissues. Proof-of-principle studies in rodents demonstrated the potency of tumor vascular targeted therapy. Immunotherapeutics targeting a tumor vascular specific splice variant of fibronectin demonstrated profound restriction of tumor growth (116). More recently, antibodies targeting the

anthrax receptor (Tem8) have been shown to specifically inhibit pathologic angiogenesis, and restrict tumor growth (117, 118). Phase I clinical trials using an immunotherapeutic targeting the TVM FOLH1 suggest anti-tumor vascular immunotherapeutics are safe and potentially efficacious (119).

Broader development of anti-TVM therapies has been hindered by the absence of an experimental system with confirmed human TVM expression with which to test potential therapies. Most mouse tumor models generate murine vessels and therefore cannot be used to test antibodies specific to human antigens. While models of human tumor vasculature have been proposed, these models have been difficult to reproduce, have limited long term viability, and/or do not have confirmed expression of TVMs (70, 120, 121).

Beyond their role in providing nutrients to the tumor, tumor vascular cells are also a critical host component of the cancer stem-like cell (CSC) niche. Vascular cells receive angiogenic cues from CSC and in turn provide CSC with critical survival, proliferation, and differentiation signals (67). Thus a model with robust human tumor vasculature could enhance the in vivo study of human CSC, which have been surprisingly difficult to engraft in mice. The difficulty engrafting human CSC in mice could be related to differences in the murine and human microenvironments, including the vasculature.

In the current study we focused on detailed characterization of the vasculature using the previously reported human embryonic stem cell teratoma (hESCT) tumor model previously demonstrated to have human vessels (92, 93). This model has the ease of standard xenograft models, however tumor vessels are derived from the human ESC and are therefore of human origin. It had not been clear if these are ‘normal’ human vessels or true ‘tumor vessels’ that express TVMs. Here, we demonstrate that, when injected with cancer cells, hESCT have vessels

expressing human TVMs. With the addition of mouse embryonic fibroblasts and primary tumor vascular cells, ~80% of the vessels in the tumor are human in origin and persist for up to 12 weeks. Using hESCT ovarian cancer and breast cancer models, we found that several TVMs are induced in a tumor specific fashion. We then used this model to demonstrate the ability to test the therapeutic activity of anti-human tumor vascular specific antibody therapeutics; an anti-THY1 immunotoxin delayed tumor growth and resulted in central tumor necrosis. Finally, we demonstrated that this tumor model, with a human microenvironment, enhances the engraftment and growth of primary ovarian CSC.

MATERIALS AND METHODS

Cell Culture

Use of hESC was approved by the University of Michigan Embryonic Stem Cell Research Oversight Committee. H9 hESC (WiCell Research Institute, Madison, WI) and H7-GFP hESC (a gift from Joseph Wu, Stanford University) were grown as previously described (122). Undifferentiated ESC colonies were initially passaged by manual dissection with final passages performed with enzymatic digestion using TrypLE Select (Invitrogen, Carlsbad, CA). Human ovarian cancer cell line HEY1 and SKOV3 (American Type Culture Collection, Manassas, VA) were grown in RPMI containing 10% FBS. The breast cancer cell line MCF7 (a gift from Dr. Max Wicha, University of Michigan) was grown in MEM containing 10% FBS and 0.01 mg/ml bovine insulin (Invitrogen, Carlsbad, CA). In order to create DsRED expressing cells, both MCF7 and HEY1 cells were transduced with DsRED expressing lentiviral construct (provided by the UMCC Vector core).

In vivo Tumor Models

NOD/SCID mice (Charles River, Wilmington, MA), were housed and maintained in the University of Michigan Unit for Laboratory Animal Medicine. All studies were approved by the University Committee on the Use and Care of Animals. hESCT were generated as previously described (92, 93, 122). Briefly, H9 hESC were cultured on mouse embryonic fibroblasts (MEFs), manually dispersed and passaged. Approximately $5x10^5$ undifferentiated H9 hESC or

H7-GFP ESC were injected subcutaneously into the axilla of NOD/SCID mice (with or without MEFs) with 100 µl of PBS and 200 µl of matrigel (BD Biosciences, San Diego, CA). Once hESCT were palpable, tumor cells in 40 µl of PBS were injected intra-hESCT. $2x10^5$ tumor cells (HEY1-DsREd or MCF7 DsRED) were injected alone or with 5,000 VE-Cadherin$^+$ primary human tumor vascular cells (isolated as previously described) (112). For hESCT injected with primary ovarian CSCs, 700 (n=2), 5000 (n=3), or 10,000 (n=3) primary ALDH$^+$ ovarian cancer cells (from 6 different patients) or 10,000 ALDH$^-$ cells from paired samples were injected (n=3). All tumor were harvested when hESCT-tumor volumes were ~2000 mm^3 (range 4-12 weeks, median 8 weeks). For flank xenografts, $5x10^5$ cells were injected in 100 µl of PBS and 200 µl of matrigel into the axilla of NOD/SCID mice. Tumors were imaged using bio-fluorescence (Xenogen IVIS 2000, Caliper Life Sciences, Hopkinton, MA. Murine tumors were APC/PTEN/p53 mutant mouse ovarian tumors (a gift from Dr. Kathy Cho, University of Michigan) (101, 123).

Isolation of Cancer Stem Cells from Primary Ovarian Cancer Specimens

Informed written consent was obtained from all patients before tissue procurement. All studies were performed with the approval of the Institutional Review Board of the University of Michigan. All tumors were from patients with stage III or IV epithelial ovarian or primary peritoneal cancer. Tumors were mechanically dissected into single-cell suspensions, red cells lysed with ACK buffer, and cell pellets were collected by centrifugation. CSC were then isolated from primary ovarian tumor single cell suspensions using the ALDEFLUOR assay fluorescence activated cell sorting (FACS) as previously described (29). Gating was established using propidium iodide (PI) exclusion for viability. ALDH/DEAB treated cells were used to define

negative gates. FACS was performed using the BD FACSCanto II or FACSAria (Becton Dickinson) under low pressure in the absence of UV light.

Immunofluorescence (IF) and Immunohistochemistry (IHC)

8 μm sections from fresh frozen tumors were fixed in acetone for 10 min and then washed with PBS and blocked for 20 min. Primary antibody was incubated for 2 hr, washed with PBS and incubated with secondary antibody for 1 hr. For IF, slides were washed with PBS and then mounted with Vectashield Mounting Medium for fluorescence with DAPI H-1200 (Vector Laboratories, Burlingame, CA). Antibodies used for IF and IHC are listed in Supplementary Table 1. IHC staining was performed using the Vectastain ABC kit (Vector, Burlingame, CA) per manufacturer's instructions. Select p53 IHC was performed by the Histology/IHC Service at the University of Michigan.

RNA Isolation and RT-PCR

Tumors were sectioned and regions of tumor with human vasculature were confirmed via IHC. Serial sections of were dissolved in Trizol (Invitrogen, Carlsbad, CA) and RNA was extracted (PureLink RNA Mini Kit, Invitrogen, Carlsbad, CA) per manufacturer recommendations. RNA integrity was confirmed on the Agilent 2100 BioAnalyzer. PCR was performed for 40 cycles with primers at 100 nM concentrations (Supplementary Table 2). All transcripts were confirmed using 3% agarose gel electrophoresis.

Quantification of Vessels

Vascular density quantification was performed as previously described (124). Five sections from each of three tumors in each tumor group were evaluated. Total mCD31 and hCD31 stain, as defined by pixel density and hue, was assessed using Olympus Microsuite Biological Suite Software. The area of staining was then compared between mCD31 and hCD31 using a two-sided student t-test. $hCD31^+$ tumor microvascular density following anti-THY1-toxin therapy were similarly assessed. hCD31-PE and Alexa 594 Goat anti-GFP were used to assess human vessels either from tumor endothelial cell origin (PE^+ only) or from hESCT origin (PE^+ and GFP^+). Sections were photographed in toto, and then quantitated using Olympus software as above.

Immunotoxin Development and Delivery

Anti-THY1-saporin immunotoxin was developed as previously described (124). 2 μg of freshly conjugated anti-THY1 antibody and saporin toxin, or an equimolar concentration of strepavidin-saporin, or unlabeled anti-THY1 antibody was incubated with $5x10^4$ mesenchymal stem cells (MSC) in triplicate. After three days of treatment, viability cell was assessed using Trypan Blue. To test the efficacy of anti-TVM therapeutics in vivo hESCT-HEY1 tumors were treated with no treatment (n=3), or 2 mg of rat IgG-saporin (n=3), or anti-THY1-saporin (n=4). Immunotoxin was delivered intravenously every other day for 3 doses. Tumor growth was tracked using biofluorescent imaging with the Xenogen IVIS 200 imaging system and LivingImage software provided by the Center of Molecular Imaging of the University of

Michigan. Mice were monitored the day before and after treatment. This experiment was repeated with rat IgG-saporin controls (n=3) and anti-Thy-1-saporin (n=3).

RESULTS

Vessels in hESCT-Cancer Model Express TVMs in a Cancer Cell Dependent Manner

We generated hESCT-ovarian cancers (HEY1) and hESCT-breast cancers (MCF7) as previously described (122) using DsRED labeled cancer cells. Immunofluorescence demonstrated clear, non-DsRED, human $CD31^+$ vessels consistent with prior reports of human ESC derived vessels (91-93, 125). Human vessels were predominantly found in a peri-tumoral location (Fig I1A), and less frequently within the tumor islets and teratoma tissue. RT-PCR was performed to determine if the ovarian or breast specific TVMs were expressed in (1) HEY1 ovarian cancer cell culture, (2) HEY1 ovarian tumor xenografts, (3) in vivo hESCT, or (4) in vivo hESCT- HEY1 ovarian tumors. In parallel we assessed the expression of ovarian or breast cancer specific TVMs were expressed in (1) MCF7 ovarian cancer cell culture, (2) MCF7 breast cancer xenografts, (3) in vivo hESCT, or (4) in vivo hESCT-MCF7 breast tumors. We evaluated the expression of TVMs that have been reported to be upregulated in numerous tumors, including tumor endothelial marker-7 (TEM7), Integrin ß3, and THY1, as well as for TVMs reported to be ovarian cancer specific including EGFL6, P2Y-like receptor (GPR105), and F2RL1, or breast cancer specific such as FAP, HOXB2, SFRP2, and SLITRTK6. Unfortunately all TVM mRNAs (and every gene we have tested to date) were expressed in both hESCT and the ovarian cancer and breast cancer hESCT-cancer model, thus RT-PCR suggested TVMs were expressed in the hESCT but was otherwise uninformative (Fig I1B).

We next performed immunohistochemistry (IHC) to localize TVM expression within the cell line xenografts, hESCT, hESCT-HEY1 ovarian tumors, and hESCT-MCF7 breast cancers. Within hESCT controls, TVM protein expression could be identified in various developmental tissues, but expression was generally not found in vascular structures (Fig I2). In contrast, the expression of ovarian TVMs could be detected within peri-tumoral vessels within the hESCT-HEY1 ovarian tumors (Fig I2). Some vessels were clearly filled with red blood cells, indicating a connection with the murine vasculature and perfusion (Fig I2 and data not shown). Serial sections stained with anti-hCD31 antibody confirmed these structures as human vessels (Sup. Fig 1). Identical results were obtained in a hESCT-SKOV3 ovarian cancer model (data not shown). Similarly, the breast cancer specific TVMs FAP, SFRP2, SLITRK6, and SMPD3, were all expressed in the hESCT-MCF7 tumors (Fig I2). No vascular expression of any of the TVMs was detected in flank tumor xenografts (Fig I2) or in a murine ovarian tumor model (Supplemental Fig 2), demonstrating the IHC is not detecting murine tumor vessels.

It remained unclear if the distinctions in the tumor vascular expression profile observed for different tumors is related to different methodologies of TVM identification, or a true distinction in the pattern of expression related to the tumor specific microenvironment. We therefore also assessed the vascular expression of 'breast' TVMs in the hESCT-HEY1 ovarian cancer model and the expression of 'ovarian' TVMs within the hESCT-MCF7 breast cancer model. Interestingly vascular expression of the 'ovarian' TVMs F2RL1, GPR105 and EGFL6 was not detected in the hESCT-MCF7 breast cancer model (Fig I2). Similarly the 'breast' TVMs FAP and SFRP2 were not expressed in the vasculature of the hESCT-HEY1 ovarian tumors (Fig I2). Rare vascular expression of the 'breast' TVMs SLITRK6 and SMPD3 was detected in the hESCT-HEY1 ovarian tumor model (Fig I2). These findings suggest that some TVMs are

expressed in a cancer specific manner and therefore likely induced by tumor cells, while others are more promiscuous and may identify angiogenic vessels or vasculogenesis.

Enhancing Human Vascular Density in the hESCT Cancer Model

A primary goal of this study was to determine if this model could be used to test anti-human TVM immunotherapeutics. However, initial studies demonstrated that only a minority of resultant vessels (~15%) were of human origin with the remainder being murine vessels (see below). In order to increase the utility of the model for testing anti-vascular therapeutics, we attempted to increase the percentage of human tumor vessels in the hESCT-cancer model. As fibroblasts in the ovarian tumor microenvironment can significantly promote angiogenesis (31), we co-injected hESC and irradiated mouse embryonic fibroblasts (MEFs) to create a hESCT in which to inject HEY1 ovarian cancer cells. Alternatively hESCT+MEFs we co-injected with HEY1 ovarian cancer cells and 5,000 FACS isolated VE-Cadherin^{+} primary ovarian tumor endothelial cells. Human CD31 IHC demonstrated the greatest number of human vessels in tumors co-injected with MEFs and VE-Cadherin^{+} cells (Fig I3A). Interestingly, while there were regions of the tumor, which had overlapping and interconnected human and murine vessels (Fig I3B), most regions of the tumor were dominated by either human or murine vessels (data not shown). IHC analysis of these vessels confirmed the expression of TVMs (data not shown). Quantification of the vascular density of murine and human vessels using co-IF with human CD31 and murine CD31 revealed that while the hESCT-HEY1 ovarian cancer tumor model alone had ~15% human vessels, the addition of MEFs increased the percentage of human vessels to ~40% (p value of 0.01, Fig I3C). With the addition of VE-Cadherin^{+} tumor endothelial cells nearly 80% of the tumor vessels were human (p value <0.0001, Fig I3C). HEY1 cells co-injected

with 5000 VE-Cadherin^{+} cells in matrigel in the animals flank, demonstrated no human vessels (data not shown) demonstrating the profound human vascularity is unique to the hESCT model. In order to determine if the increase in human vessels in the presence of VE-Cadherin^{+} cells was due to increased angiogenesis from the hESCT cells or proliferation of the VE-Cadherin^{+} cells, we repeated the above experiment using GFP labeled H7 ESC (Fig I3D). Evaluation of tumor vessels demonstrated that 60-80% of the human vessels were GFP$^{(-)}$ and thus derived from the ovarian cancer VE-Cadherin^{+} cells while the remaining 20-40% of human vessels were GFP^{+} and therefore derived from hESCT cells (Fig I3E). These data demonstrate that the addition of human tumor vascular cells to this model leads to a dramatic increase in human tumor vasculature such that the majority of vessels present in the tumor are human in origin.

Testing an Anti-TVM Therapeutic in the hESCT-Ovarian Cancer Model

In order to test the utility of this model for screening anti-human TVM immunotherapeutics, we developed an immunotoxin targeting the human TVM THY1. This antigen was chosen due to the availability of commercial antibodies that can recognize the THY1 antigen in vivo. In order to create the immunotoxin, streptavidin-conjugated saporin toxin was coupled to a biotinylated anti-human THY1 antibody. The cytotoxicity of this immunotoxin was confirmed in vitro against THY1^{+} primary human mesenchymal stem cells (MSC); anti-THY1-immunotoxin resulted in statistically significant MSC death relative to antibody alone or saporin toxin alone controls (Fig I4A). In order to test the efficacy of anti-TVM-immunotoxin in vivo, anti-THY1-saporin (n=7 total in two experiments) immunotoxin or control rat IgG-saporin (n=6 total in two experiments) was delivered intravenously to mice bearing hESCT-HEY1 DsRed tumors. Tumor growth was tracked with biofluorescent imaging. While rat IgG-saporin treated

tumors demonstrated continued growth, THY1-Saporin treated hESCT-HEY1 ovarian tumors demonstrated delayed growth and significant reduction in central tumor viability (the region dependent on human vessels) (Fig I4B-C). Following completion of therapy, growth resumed in peripheral tumor regions that were dependent on murine vessels continued to expand (Fig I4B and data not shown). Control hESCT alone and HEY1-DsRED flank tumors showed no response to either therapy (data not shown).

To further analyze the impact of anti-THY1 therapy on the human vessels, we quantified human tumor microvascular density using anti-hCD31 IHC. There was a three-fold reduction in the number of human vessels in hESCT-HEY1 ovarian tumors treated with anti-THY1 saporin toxin compared with Rat IgG-saporin toxin treated controls (Fig I4D). These results confirm the utility of this model for testing human TVMs specific therapeutics in vivo.

The hESCT Model Promotes the in vivo Growth of Primary Human Cancer Stem Cells

Human ovarian CSC have been particularly challenging to grow in vivo. Engraftment rates of CSC directly isolated from human ovarian tumors are only 20-40% in traditional flank tumor models and 5,000 CSC typically require 6-12 months to create a tumor (29). We hypothesized that the human microenvironment of the hESCT model with a human tumor vascular niche could greatly enhance the growth of ovarian CSC. Using ALDH as an ovarian CSC marker (29), we assessed the efficiency of primary human ovarian CSC engraftment in the hESCT tumor model. We injected FACS isolated $ALDH^+$ primary human ovarian CSC (700-10,000) from 6 ovarian cancer patient samples into either hESCT or subcutaneously. hESCT were allowed to grow until they reached ~2000 mm^3 (4-12 weeks after tumor cell injection). Histochemical analysis of resected hESCT-$ALDH^+$ CSC demonstrated regions consistent with

papillary serous tumor growth (Fig I5A and data not shown). In order to confirm these areas represent ovarian tumor cells, we exploited the recent finding that *TP53* is mutant in >95% of serous ovarian tumors (126). *TP53* IHC clearly identified human *TP53*$^{+}$ serous ovarian tumors in all hESCT injected with ALDH^{+} ovarian cancer cells (Fig I5A and C). Strong *TP53* stain was not identified in hESCT alone or from hESCT injected with ALDH^{+} cells from a benign fibroadenoma (data not shown). ALDH^{+} ovarian cancer cells injected subcutaneously in the flank showed no growth during this time period. Finally we repeated this experiment, directly comparing the growth within hESCT of ALDH^{+} and ALDH^{-} cells within from 3 patients. hESCT injected with ALDH^{+} CSC demonstrated much more rapid growth than hESCT injected with paired ALDH^{-} cells, indicating likely CSC engraftment in hESCT (Fig I5B). Once again, *TP53* IHC of resected hESCT-ALDH^{+} CSC tumors demonstrated stain in regions consistent with papillary serous tumor growth (Fig I5C). No *TP53* stain was noted in any of the hESCT-ALDH^{-} cell tumors, thus the 'tumors' that grow in the ALDH^{-} hESCT represent benign teratoma growth. These data demonstrate that primary ovarian CSC engraft in the human hESCT microenvironment more efficiently than in murine subcutaneous tissue.

DISCUSSION

These data demonstrate that the hESCT-cancer model expresses bona fide *human tumor vessels*. These vessels express not only the expected human vascular markers such as CD31 but also tumor type-specific tumor vascular markers (TVMs) such as EGFL6 and TEM7. A central rationale for the development of such model system is for the testing of novel vascular-targeted therapeutics. A major challenge for developing antibody-based therapies targeting tumor vessels has been the lack of an animal model with a human tumor microenvironment and human vessels; antibodies targeting human antigens cannot be tested in traditional animal tumor models unless the antibodies happen to cross-react between species. The model advanced here addresses this issue and thus allows screening of potential immunotherapeutics targeting human vascular antigens. Similarly, this model can also be used to test the in vivo binding activity of vascular-targeted peptides (122, 127, 128).

The generation of large numbers of human tumor vessels in this model required the addition of VE-Cadherin^{+} human tumor vascular cells. Interestingly, the addition of only 5,000 vascular cells led to nearly 80% human tumor vessels, ~70% of which were not derived from hESC, suggesting that the human VE-Cadherin^{+} cells are proliferating within the hESCT. Importantly, the human vessels in this model persisted throughout the period of tumor growth (4-12 weeks after cancer cell injection).

The need to add freshly isolated human tumor vascular cells could limit the widespread utility of this model. However, a significant number of human vessels (~40%) could still be

generated in the absence of human tumor vascular cells with the addition of irradiated mouse embryonic fibroblasts. It is possible that the addition of other pro-angiogenic cells such mesenchymal stem cells (129) or tumor-associated myeloid cells (130) could further increase the percentage of human vessels. One limitation for therapeutic testing with this model, as with other murine tumor models of human vasculature, is that tumors are still ultimately dependent on the murine vasculature for blood flow. Therefore, even with the complete therapeutic elimination of the human tumor vessels, tumors regions supplied by the murine tumor vasculature will continue to grow.

While we used our model to confirm anti-vascular therapeutics, it can also potentially be used to test vascular imaging agents specifically targeting human vessels. This model allows testing the sensitivity of these compounds to detect tumor vasculature of 'early stage' tumors. We believe that this murine model offers a means to investigate the basic biology of human TVMs in vivo. Specifically, the mechanism of tumor specific TVM induction could be addressed, due to the power to independently modulate the expression patterns of the hESC and the cancer cells themselves. This may be particularly relevant given that we observed differential induction of some tumor-specific TVMs by breast versus ovarian cancer cell lines.

Finally, the above data demonstrate that this model permits direct engraftment of primary human CSC in a manner more efficient than subcutaneous injections. This expands upon and is consistent with previous reports demonstrating improved growth of primary ovarian cell lines within hESCT as compared to tumor flanks (92, 93). Our previous studies using flank models for the engraftment of $ALDH^+$ ovarian CSC demonstrated engraftment rates of ~20%, and tumor growth required 6-12 months (29). Using the hESCT model, we found 100% engraftment from as few as 700 $ALDH^+$ primary human CSC within 4-12 weeks of tumor cell injection within the

hESCT. This model therefore represents a new tool to enhance the efficiency of the study of primary human CSC. This model could potentially be further improved with the addition of cancer associated mesenchymal stem cells (131). These findings emphasize the importance of the interplay between the tumor and the surrounding microenvironment and will allow a dissection of the signals within the tumor microenvironment that support cancer stem cell survival, proliferation, and differentiation.

CONCLUSIONS

We have confirmed the expression of human TVMs in a murine tumor model with robust human tumor vasculature. Importantly many of these TVMs appear to be tumor type specific, indicating a tumor niche dependent induction of these TVMs. This model is a useful tool to study therapeutics targeting human tumor vessels. In addition, this model with its unique human tumor microenvironment allowed 100% engraftment of primary human CSC. The hESCT system will allow deeper probing of the role of the microenvironment dependent induction of TVMs, their role in tumor biology, and interactions in the tumor vascular/cancer stem cell niche.

Acknowledgements: We thank the members of the UMCCC Flow Cytometry and Histology Cores for assistance in the experiments in this manuscript.

Grant Support

This work was initiated with support of the Damon Runyon Cancer Research Foundation and completed with the support of the NIH New Investigator Innovator Directors Award grant #00440377. Breast cancer studies were supported by the University of Michigan Cancer Center Support Grant CA046592. D. Burgos-Ojeda was supported by the NIH Cellular and Molecular Biology Training Grant T32-GM07315. K. Skorecki and M. Tzukerman receive research grant support from the Israel Science Foundation, and the Daniel Soref and Richard Satell Foundations at the American Technion Society.1

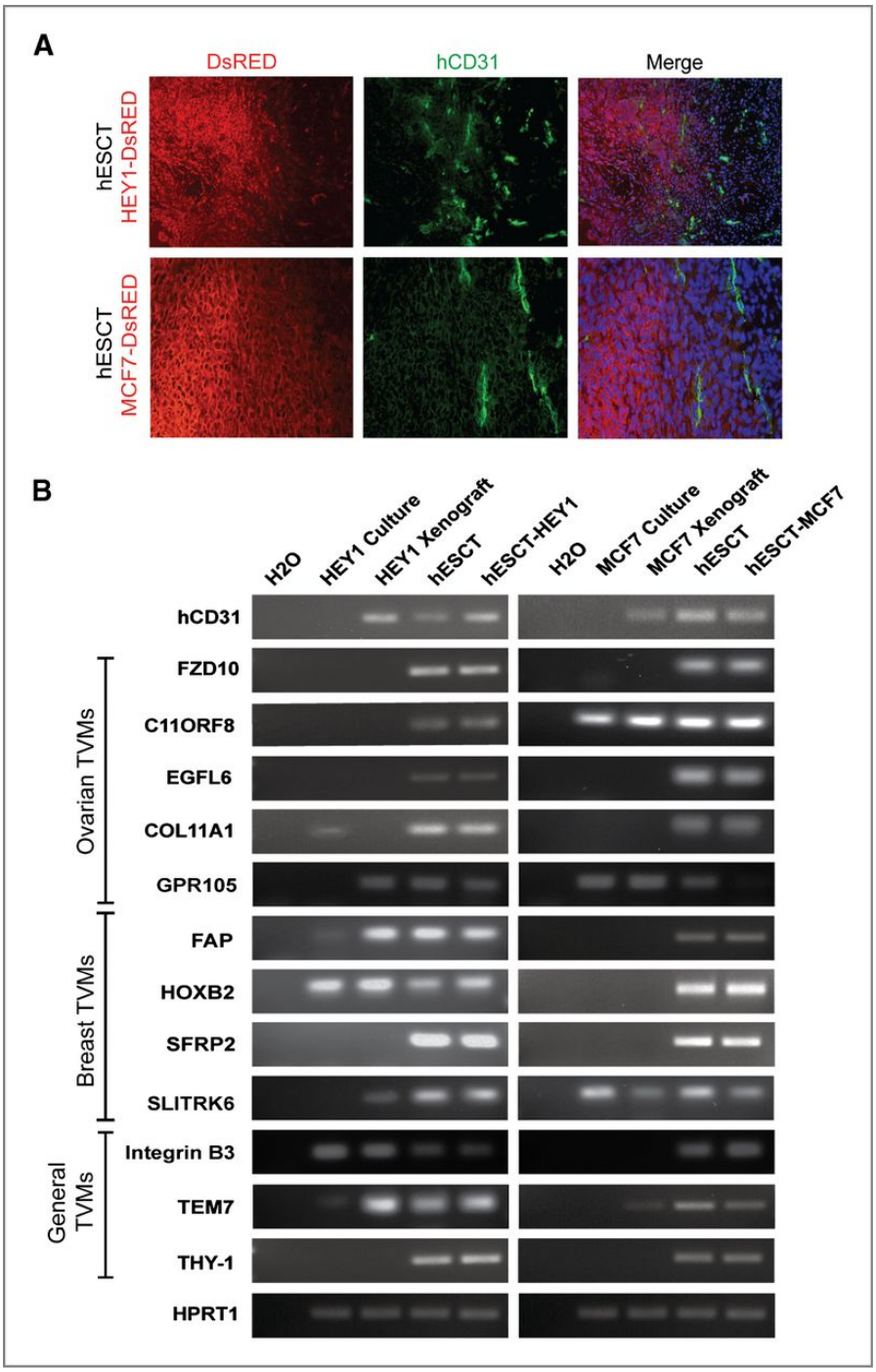

Figure I1. Validation of human vasculature in the hESCT-cancer model. (A) Co-IF demonstrating the presence of hCD31^{+} (green) vascular structures in a peritumoral location with DsRed cancer cells. **(B)** RT-PCR of TVMs expression in the indicated cancer cell line cultures, tumor cell line xenografts, hESCT, and hESCT-cancer models.

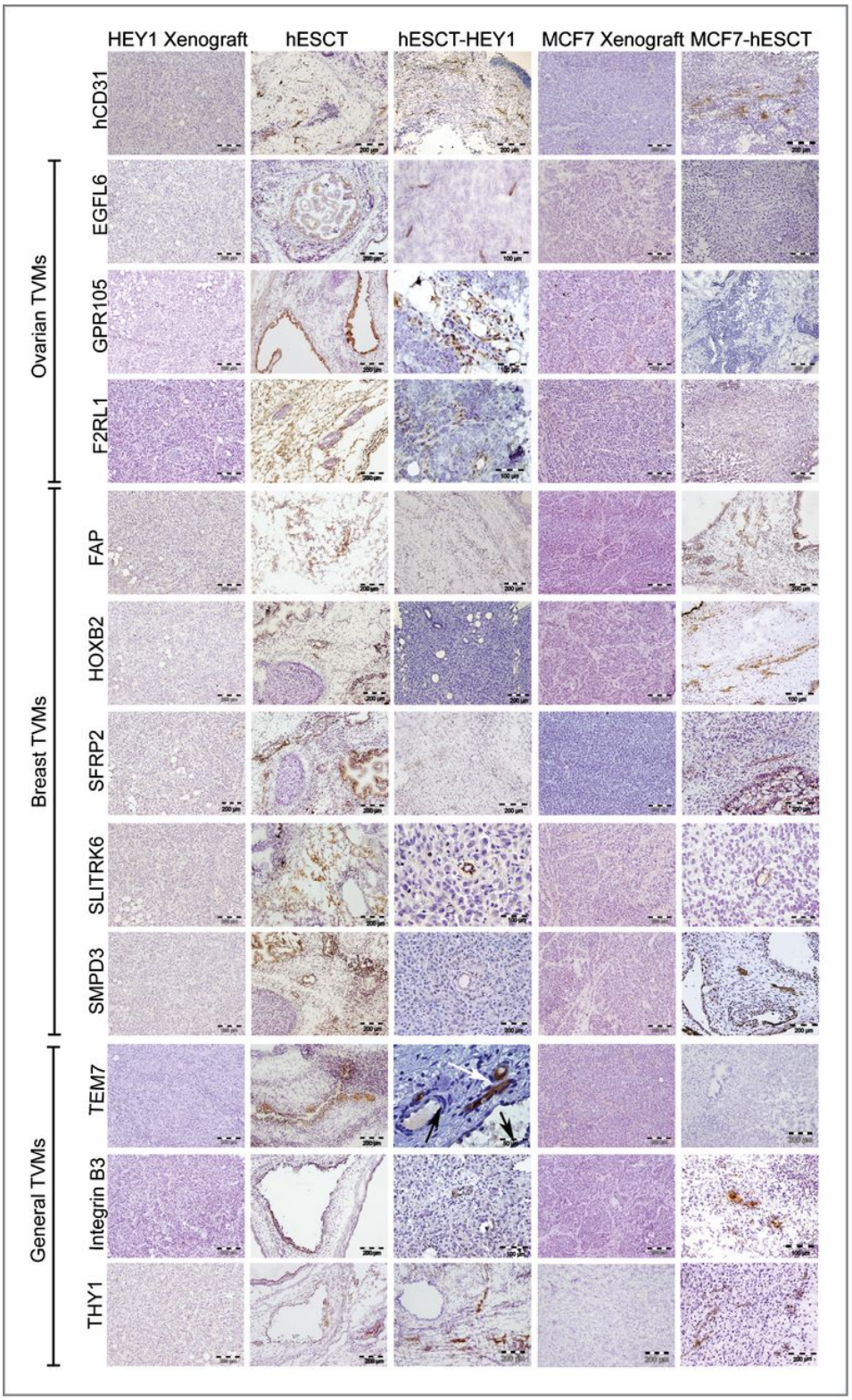

Figure I2. TVM expression in the vasculature is influenced by the cancer cells. IHC localization of ovarian cancer specific TVMs, breast cancer specific TVMs and non-tumor specific general TVMs in the indicated tumors. While TVMs are expressed in various

developmental tissues of the hESCT, vascular expression of TVMs is primarily seen only in the presence of cancer cells in a tumor type specific manner. n= 4 animals/group in two experiments. Black arrow indicates vessel containing red blood cells.

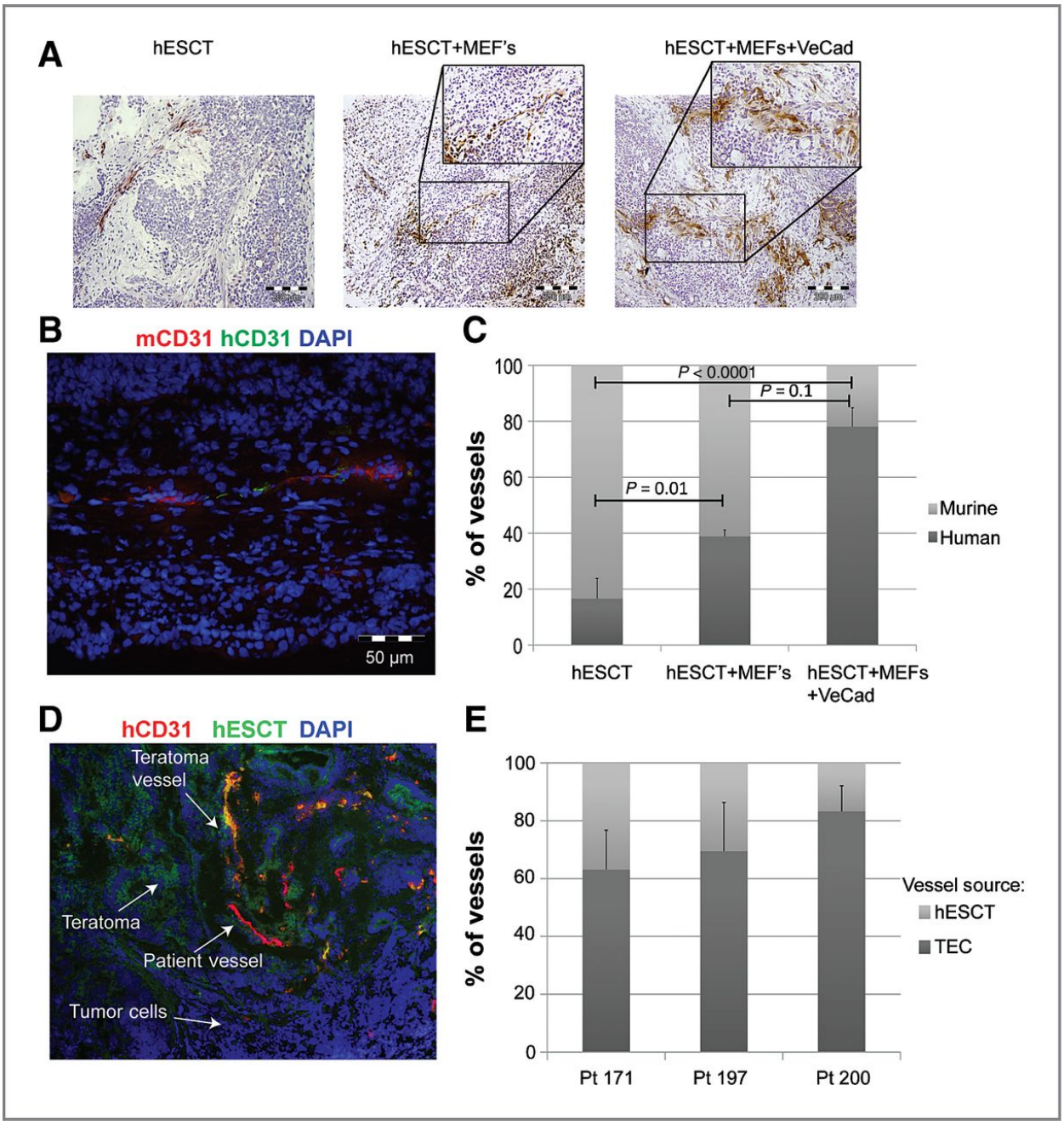

Figure I3. Enhancing the number of human vessels in the hESCT-cancer model. (A) IHC of hCD31 in hESCT-HEY1, hESCT-HEY1-MEFs, hESCT-HEY1+MEFs+VE-Cadherin^{+}. **(B)** IF showing inter-connection of mouse and human vessels. **(C)** Quantification of mouse and human vessels in the hESCT-cancer model alone, with MEFs, or with MEFS and VE-Cadherin^{+} cells. p values are indicated with error bars representing standard deviations. n=4 animal/group. **(D)** Co-IF demonstrating hCD31 stain (red) in both hESCT-GFP cells (green) resulting in yellow hESC derived vessels, and non-GFP cells originating from VE-Cadherin isolated patient tumor endothelial cells (patient vessels). **(E)** Quantification of the percentage of hESCT derived and patient tumor endothelial cell (TEC) derived vessels.

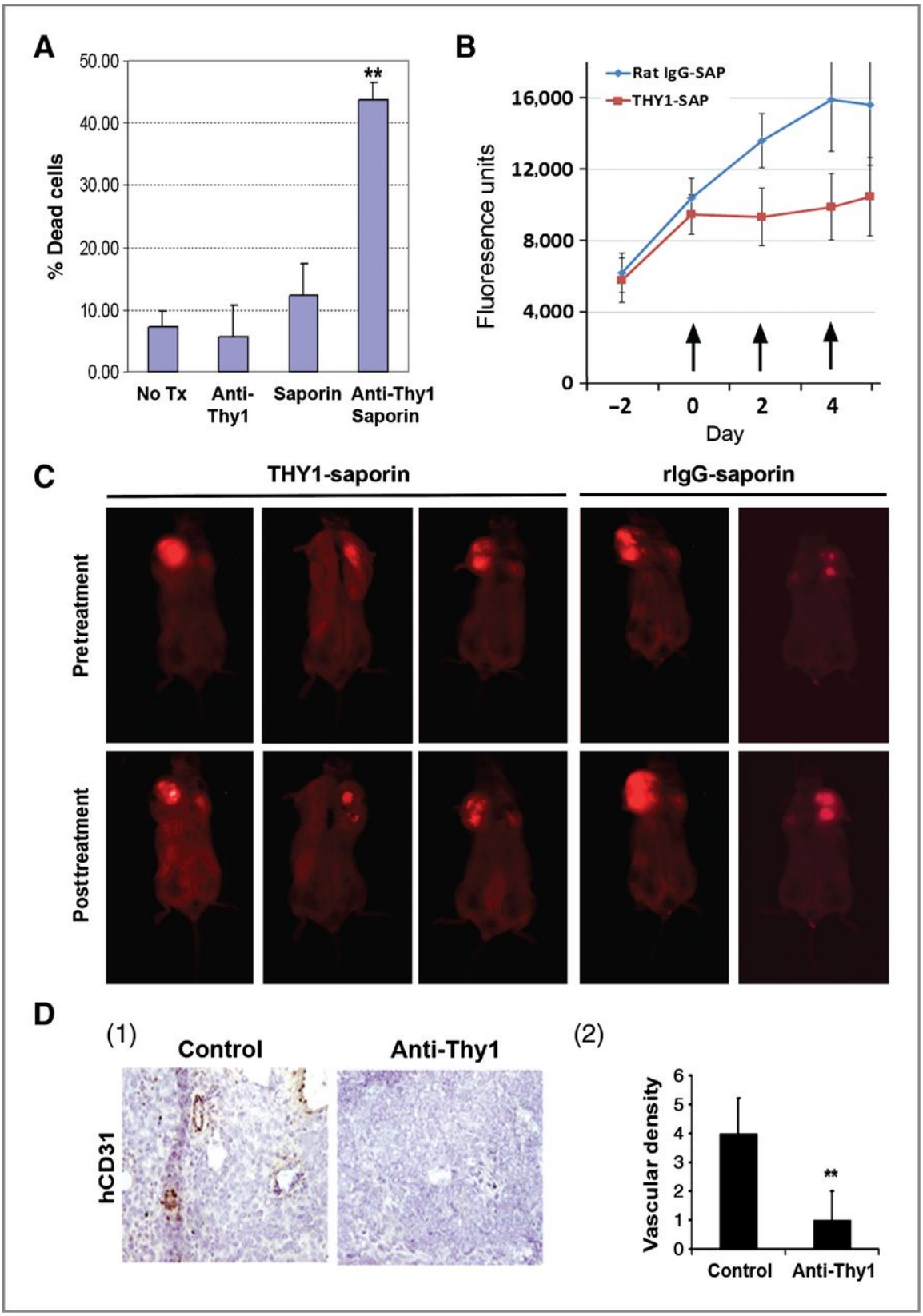
A
% Dead cells
50.00
40.00
30.00
20.00
10.00
0.00
**
No Tx
Anti-Thy1
Saporin
Anti-Thy1 Saporin
B
Rat IgG-SAP
THY1-SAP
Fluoresence units
16,000
12,000
8,000
4,000
0
−2
0
2
4
Day
C
THY1-saporin
rIgG-saporin
Pretreatment
Posttreatment
D
(1)
Control
Anti-Thy1
hCD31
(2)
Vascular density
6
5
4
3
2
1
0
**
Control
Anti-Thy1

Figure I4. Testing Anti-TVM Therapeutics in the hESCT-HEY1 ovarian tumor model. (A) Quantification of cellular death of THY1 expressing MSC treated with anti-THY1-saporin immunotoxin and controls. **(B)** Biofluorescence of hESCT-HEY1 DsRed ovarian tumor before and after two treatments with anti-THY1-saporin immunotoxin arrows indicated time of treatment. **(C)** Biofluorescent images of hESCT-HEY1 DsRED tumors before and after treatment with the indicated immunotoxins. **(D)** IHC images (1) and (2) quantification of human tumor vessels in control and Anti-THY1-saporin treated tumors. Error bars represent standard deviations.

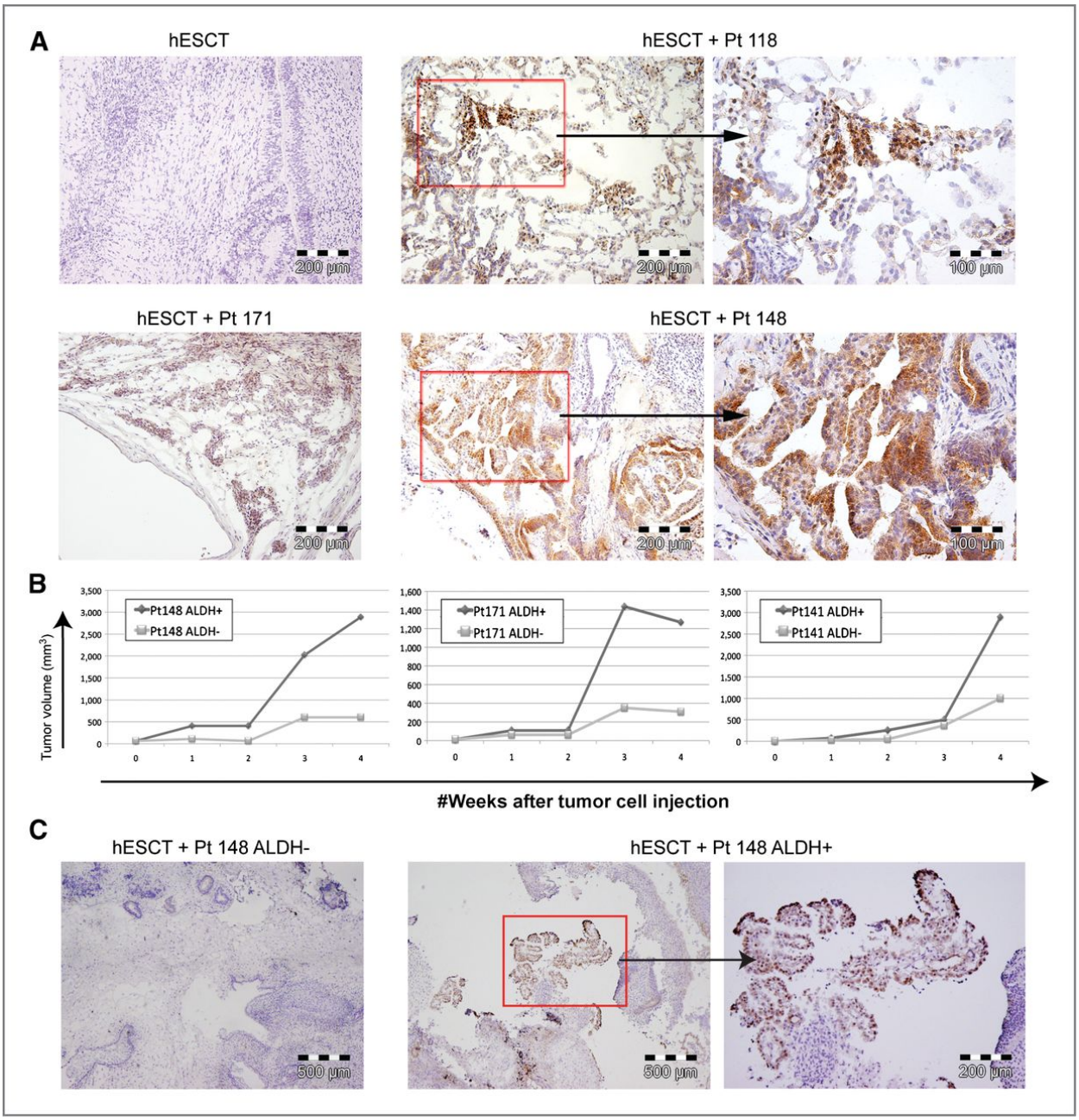

Figure I5. Growth of primary ovarian CSCs using the hESCT model. (A) TP53 IHC demonstrating ovarian cancer cells initiated by $ALDH^+$ CSC injected within the hESCT. hESCT alone and $ALDH^+$ cells from a patient with a benign fibroadenoma demonstrated no growth. (B) hESCT-ovarian tumor volumes from hESCT injected with 10,000 $ALDH^+$ or $ALDH^-$ ovarian cancer cells from three patients. (C) TP53 IHC of hESCT injected with $ALDH^-$ cancer cells and $ALDH^+$ cancer cells demonstrating $TP53^+$ papillary serous tumor growth from $ALDH^+$ tumor only.

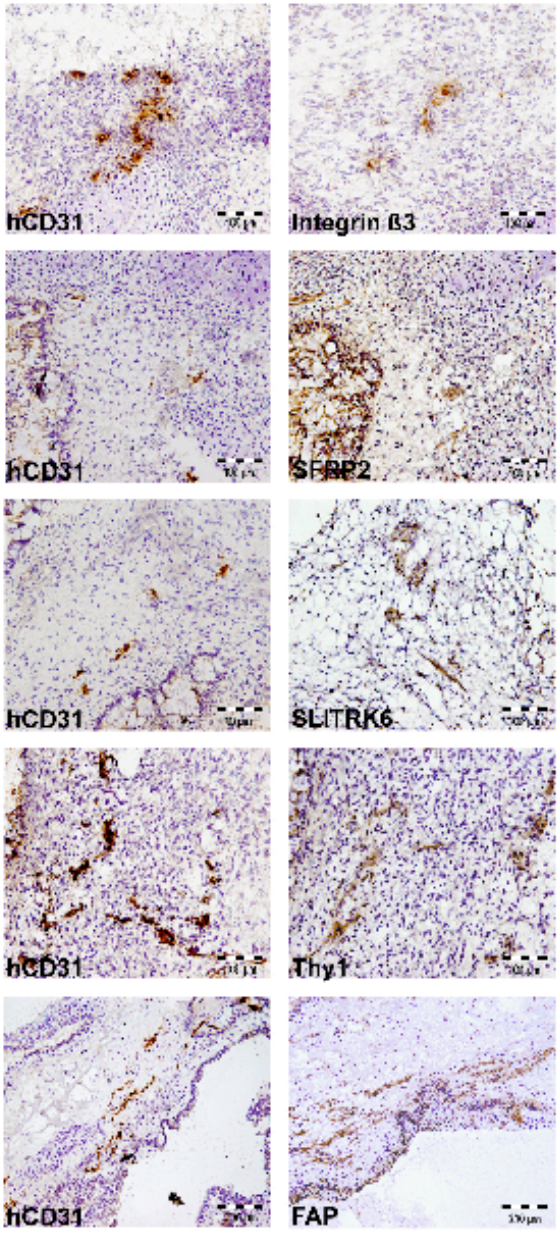

Supplemental Figure 1. Co-localization of TVM expression with hCD31 expression. IHC analysis of hCD31 (left panel) and the indicated TVMs (right panel) in serial sections from the hESCT-cancer model demonstrating co-localization.

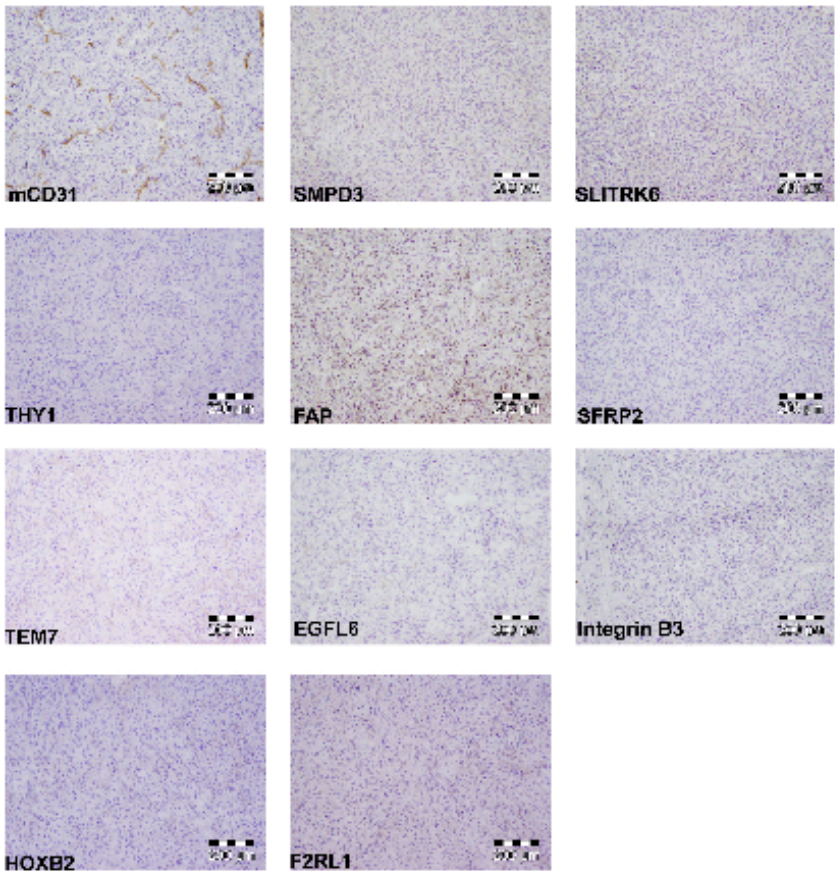

Supplemental Figure 2. TVM antibodies do not cross-react with murine tumor vessels. IHC for mCD31 (control) and human ovarian cancer and human breast cancer TVMs in a murine ovarian tumor demonstrating no vascular expression of human TVMs. FAP demonstrated reactivity with ovarian tumor cells.

Name	Clone	Dilution	Company	Method and Figure used	Cross-reactivity to Ms	Cross-reactivity to Hu
FITC anti-human CD31	WM59	1:600	BD Pharmigen	IF Fig 1A ; IF Fig 3B	No	Yes
PE Anti-mouse CD31	MEC13.3	1:50	Biolegend	IF Fig 3B	Yes	No
ms mab to CD31 (hCD31)	MEM-05	1:600	Abcam	IHC Fig 2; IHC Fig 3A; IHC Fig 4 D(1); IHC Sup Fig 1	No	Yes
Rat mab to CD31 (mCD31)	390	1:600	Abcam	IHC Sup Fig 2	Yes	No
FAP	Polyclonal	1:1000	Abcam	IHC Fig 2	Yes	Yes
GPR105	Polyclonal	1:400	Abcam	IHC Fig 2	No	Yes
SFRP-2	Polyclonal	1:200	Santa Cruz	IHC Fig 2	Yes	Yes
Anti-EGFL6	Polyclonal	1:600	Sigma-Aldrich	IHC Fig 2	No	Yes
Integrin ß3	Polyclonal	1:100	Cell Signaling Technology	IHC Fig 2	Yes	Yes
F2RL1	Polyclonal	1:500	Genway	IHC Fig 2	No	Yes
Tem7	197C193	1:2000	Imgenex	IHC Fig 2	Yes	Yes
CD90: Biotin	F15-42-1	1:200	Serotec	IHC Fig 2	No	Yes
SMPD3	N/A	1:4000	Gift from DeMore Lab	IHC Fig 2	N/A	Yes
SLITRK6	N/A	1:4000	Gift from DeMore Lab	IHC Fig 2	N/A	Yes
Biotinylated Anti-Goat IgG	BA-5000	1:400	Vector Laboratories	IHC Fig 2	No	No
Biotinylated Anti-Rabbit IgG	BA-1000	1:400	Vector Laboratories	IHC Fig 2	No	No
Biotinylated Anti-Mouse IgG	BA-2000	1:400	Vector Laboratories	All IHC	Yes	No
Biotinylated Anti-Rat IgG	BA-4000	1:400	Vector Laboratories	IHC Sup Fig 2	No	No
VE-Cadherin-PE	16B1	1:40	eBiosciences	Flow Cytometry Fig 3A	No	Yes
Alexa 594 Goat Anti-Mouse	A11005	1:500	Invitrogen Molecular Probes	IF Fig 3D	Yes	No
Anti-human p53	Monoclonal DO-7	1:50	Dako	IHC Fig 5A-C	No	Yes

Table 3. List of Antibodies Used

Gene	Forward	Reverse
C11ORF8	CTTCAAAGAGTGGGCTGTGTG	GAGGCATTGATGTACGTTGTG
CD31	TTTGGCTAGTCCTTGTTCTTTGG	CGGTGTCTTCAGGTTGGTATTC
Coll11α1	AGGGTGAAGATGGAGATCCTG	TTTCACCTTGTCTTCCCTCTG
EGFL6	AGAAGACCACGAGTGAGGATG	CCACGTTCTGCTTCAAAAATG
F2RL1	TGCTAGCAGCCTCTCTCTCC	TTTCCAGTGACGTGGGATG
FAP	CTTCTCATCCACGGAACAGC	GGATAAGCCGTGGTTCTGG
FZ10	CAGACTAAAACGCTGGACTGC	TCTTGGAGGTCCAAATCCAC
GPR105	GTCCCACCTTAAGTCAAGTCG	TCTTTGTGTAGGGGATTCTGG
HoxB2	CAGGACAAGAGCGTGTTCG	TCTGGTAACGTGTGTATGTCTGG
HPRT1	ATGCTGAGGATTTGGAAAGG	CAGAGGGCTACAATGTGATGG
Integrin B3	CATTGTCCAGCCTAATGACG	CAGTCATCAGCCCCAAAGAG
OLFML2B	CCAAAGGATGAGCGGATTTAC	GCTGTACGGGAGCTTGTAGG
SFRP2	TGACAACGACATAATGGAAACG	CACCGTTCAGCTTGTAAATGG
SLITKR6	TGTGCATTACAGATAACGTCAGG	CCTCTGGATGAGAGCACTGG
TEM7	ACACGCTGCCAGATAACAGG	TCGGCCACATCTACCCACA
THY1	TGAAGGTCCTCTACTTATCCGC	GCACTGTGACGTTCTGGGA

Table 4. PCR Primers Used

REFERENCES

1. St Croix B, Rago C, Velculescu V, Traverso G, Romans KE, Montgomery E, et al. Genes expressed in human tumor endothelium. Science. 2000;289:1197-202.
2. Pasqualini R, Moeller BJ, Arap W. Leveraging molecular heterogeneity of the vascular endothelium for targeted drug delivery and imaging. Semin Thromb Hemost. 2010;36:343-51.
3. Zhong X, Ran YL, Lou JN, Hu D, Yu L, Zhang YS, et al. Construction of human liver cancer vascular endothelium cDNA expression library and screening of the endothelium-associated antigen genes. World J Gastroenterol. 2004;10:1402-8.
4. Allinen M, Beroukhim R, Cai L, Brennan C, Lahti-Domenici J, Huang H, et al. Molecular characterization of the tumor microenvironment in breast cancer.[see comment]. Cancer Cell. 2004;6:17-32.
5. Bhati R, Patterson C, Livasy CA, Fan C, Ketelsen D, Hu Z, et al. Molecular Characterization of Human Breast Tumor Vascular Cells. Am J Pathol. 2008;172:1381-90.
6. Seaman S, Stevens J, Yang MY, Logsdon D, Graff-Cherry C, St Croix B. Genes that distinguish physiological and pathological angiogenesis. Cancer Cell. 2007;11:539-54.
7. Buckanovich RJ, Sasaroli D, O'Brien-Jenkins A, Botbyl J, Hammond R, Katsaros D, et al. Tumor Vascular Proteins as Biomarkers in Ovarian Cancer Journal of Clinical Oncology. 2007;25 852-61.
8. Lu C, Bonome T, Li Y, Kamat AA, Han LY, Schmandt R, et al. Gene alterations identified by expression profiling in tumor-associated endothelial cells from invasive ovarian carcinoma. Cancer Res. 2007;67:1757-68.
9. Madden SL, Cook BP, Nacht M, Weber WD, Callahan MR, Jiang Y, et al. Vascular gene expression in nonneoplastic and malignant brain. Am J Pathol. 2004;165:601-8.
10. Priebe A, Buckanovich RJ. Ovarian tumor vasculature as a source of biomarkers for diagnosis and therapy. Expert Rev Obstet Gynecol. 2007;3:65-72.
11. Nanda A, St Croix B. Tumor endothelial markers: new targets for cancer therapy. Current Opinion in Oncology. 2004;16:44-9.
12. Burgos-Ojeda D, Rueda BR, Buckanovich RJ. Ovarian cancer stem cell markers: prognostic and therapeutic implications. Cancer Lett. 2012;322:1-7.
13. Halin C, Rondini S, Nilsson F, Berndt A, Kosmehl H, Zardi L, et al. Enhancement of the antitumor activity of interleukin-12 by targeted delivery to neovasculature. Nat Biotechnol. 2002;20:264-9.
14. Cryan LM, Rogers MS. Targeting the anthrax receptors, TEM-8 and CMG-2, for anti-angiogenic therapy. Front Biosci. 2011;16:1574-88.
15. Chaudhary A, Hilton MB, Seaman S, Haines DC, Stevenson S, Lemotte PK, et al. TEM8/ANTXR1 blockade inhibits pathological angiogenesis and potentiates tumoricidal responses against multiple cancer types. Cancer Cell. 2012;21:212-26.
16. Milowsky MI, Nanus DM, Kostakoglu L, Sheehan CE, Vallabhajosula S, Goldsmith SJ, et al. Vascular targeted therapy with anti-prostate-specific membrane antigen monoclonal antibody J591 in advanced solid tumors. J Clin Oncol. 2007;25:540-7.

17. Sanz L, Cuesta AM, Salas C, Corbacho C, Bellas C, Alvarez-Vallina L. Differential transplantability of human endothelial cells in colorectal cancer and renal cell carcinoma primary xenografts. Lab Invest. 2009;89:91-7.
18. Bussolati B, Grange C, Tei L, Deregibus MC, Ercolani M, Aime S, et al. Targeting of human renal tumor-derived endothelial cells with peptides obtained by phage display. J Mol Med. 2007;85:897-906.
19. Nor JE, Peters MC, Christensen JB, Sutorik MM, Linn S, Khan MK, et al. Engineering and characterization of functional human microvessels in immunodeficient mice. Laboratory Investigation. 2001;81:453-63.
20. Calabrese C, Poppleton H, Kocak M, Hogg TL, Fuller C, Hamner B, et al. A perivascular niche for brain tumor stem cells. Cancer Cell. 2007;11:69-82.
21. Tzukerman M, Rosenberg T, Reiter I, Ben-Eliezer S, Denkberg G, Coleman R, et al. The influence of a human embryonic stem cell-derived microenvironment on targeting of human solid tumor xenografts. Cancer Res. 2006;66:3792-801.
22. Tzukerman M, Rosenberg T, Ravel Y, Reiter I, Coleman R, Skorecki K. An experimental platform for studying growth and invasiveness of tumor cells within teratomas derived from human embryonic stem cells. Proc Natl Acad Sci U S A. 2003;100:13507-12.
23. Winer I, Wang S, Lee YE, Fan W, Gong Y, Burgos-Ojeda D, et al. F3-targeted cisplatin-hydrogel nanoparticles as an effective therapeutic that targets both murine and human ovarian tumor endothelial cells in vivo. Cancer Res. 2010;70:8674-83.
24. Wu R, Hu TC, Rehemtulla A, Fearon ER, Cho KR. Preclinical testing of PI3K/AKT/mTOR signaling inhibitors in a mouse model of ovarian endometrioid adenocarcinoma. Clin Cancer Res. 2011;17:7359-72.
25. Wu R, Hendrix-Lucas N, Kuick R, Zhai Y, Schwartz DR, Akyol A, et al. Mouse model of human ovarian endometrioid adenocarcinoma based on somatic defects in the Wnt/beta-catenin and PI3K/Pten signaling pathways. Cancer Cell. 2007;11:321-33.
26. Silva IA, Bai S, McLean K, Yang K, Griffith K, Thomas D, et al. Aldehyde dehydrogenase in combination with CD133 defines angiogenic ovarian cancer stem cells that portend poor patient survival. Cancer Res. 2011;71:3991-4001.
27. Pulaski HL, Spahlinger G, Silva IA, McLean K, Kueck AS, Reynolds RK, et al. Identifying alemtuzumab as an anti-myeloid cell antiangiogenic therapy for the treatment of ovarian cancer. J Transl Med. 2009;7:49.
28. Tzukerman M, Skorecki KL. A novel experimental platform for investigating cancer growth and anti-cancer therapy in a human tissue microenvironment derived from human embryonic stem cells. Methods Mol Biol. 2006;331:329-46.
29. Tzukerman M, Skorecki K. A novel experimental platform for investigating tumorigenesis and anti-cancer therapy in a human microenvironment derived from embryonic stem cells. Discov Med. 2003;3:51-4.
30. Theriault C, Pinard M, Comamala M, Migneault M, Beaudin J, Matte I, et al. MUC16 (CA125) regulates epithelial ovarian cancer cell growth, tumorigenesis and metastasis. Gynecol Oncol. 2011;121:434-43.

31. Kolonin MG, Sun J, Do KA, Vidal CI, Ji Y, Baggerly KA, et al. Synchronous selection of homing peptides for multiple tissues by in vivo phage display. FASEB J. 2006;20:979-81.
32. Hajitou A, Pasqualini R, Arap W. Vascular targeting: recent advances and therapeutic perspectives. Trends Cardiovasc Med. 2006;16:80-8.
33. Spaeth EL, Dembinski JL, Sasser AK, Watson K, Klopp A, Hall B, et al. Mesenchymal stem cell transition to tumor-associated fibroblasts contributes to fibrovascular network expansion and tumor progression. PLoS One. 2009;4:e4992.
34. McLean K, Buckanovich RJ. Myeloid cells functioning in tumor vascularization as a novel therapeutic target. Transl Res. 2008;151:59-67.
35. McLean K, Gong Y, Choi Y, Deng N, Yang K, Bai S, et al. Human ovarian carcinoma-associated mesenchymal stem cells regulate cancer stem cells and tumorigenesis via altered BMP production. J Clin Invest. 2011;121:3206-19.

CHAPTER II

Targeting CD24$^+$ Ovarian Cancer Stem-Like Cells in a Transgenic Murine Model of Ovarian Cancer Restricts Metastasis

D. Burgos-Ojeda[1], R. Wu[2], K. McLean[4].Talpaz[3] K. Cho[2], R.J. Buckanovich[1,3,4]

Cellular and Molecular Biology Graduate Program[1], Department of Pathology Division of Gynecological Pathology[2], Department of Internal Medicine Division Hematology-Oncology[3], Department of Obstetrics-Gynecology Division of Gynecologic Oncology[4], University of Michigan, Ann Arbor, MI

ABSTRACT

A better understanding of ovarian CSC could lead to novel therapeutic. Unfortunately, the study of human CSC is hampered by heterogeneity of patients' tumor samples, long requirements for tumor growth in vivo, and the need for tumor growth in immune-deficient mice. We have therefore characterized CSC in a transgenic murine model of ovarian cancer. This mouse model with conditional deletion of APC, PTEN and TP53 tumor suppressor genes develop advanced ovarian cancer similar to that seen patients. Cell lines derived from this tumor express numerous putative CSC surface markers including CD24, CD44, CD90, CD117, CD133 and ALDH. CD24$^+$ and CD133$^+$ cells demonstrate increased tumor sphere forming capacity. CD133$^+$ cells demonstrated a trend for increased tumor initiation in vivo while CD24$^+$ cells vs

$CD24^-$ cells, had significantly greater tumor initiation and tumor growth capacity. No preferential tumor initiating or growth capacity was observed for $CD44^+$, $CD90^+$, $CD117^+$, or $ALDH^+$ versus their negative counterparts. Consistent with a stem cell phenotype we have found that $CD24^+$ cells, compared to $CD24^-$ cells, have increased expression of Nanog and c-myc and increased phosphorylation of STAT3. JAK2 inhibition eliminated STAT3 phosphorylation and preferential targeted $CD24^+$ cells. In vivo therapy with the JAK2 inhibitor TG101209 appeared to decrease tumor metastasis, and combined with chemotherapy, prolonged overall survival. These findings suggest that $CD24^+$ cells have a CSC phenotype and may play a role in tumor migration and metastasis.

INTRODUCTION

Ovarian cancer is the fifth leading cause of cancer-related death among women (132). Most ovarian cancer patients present with advanced stage disease such that treatment with surgery and chemotherapy results in a median progression-free survival of only 16-22 months and a 5-year survival rate of only 27% (3). There are four major histologic subtypes of epithelial ovarian cancer: serous, endometrioid, clear cell and mucinous (4). The different subtypes are characterized by distinct genetic alterations (6). A better understanding of the specific pathway defects in the different ovarian cancer types will lead us to improve standard chemotherapies by including molecular targeted therapies specific to each cancer type (101).

The clinical course of ovarian cancer, good initial response rates followed by high rates for relapse and the development of chemotherapy resistant disease, is consistent with the cancer stem cell model (115). Cancer stem-like cells (CSC) are a rare chemotherapy resistant cells within a tumor which can serve to repopulate the bulk of a tumor with more differentiated daughter cells and potentially contribute to recurrent disease (58). Several markers have been proposed as potential cancer stem cell markers in ovarian cancer including CD133, aldehyde dehydrogenase (ALDH), CD44, CD117 and CD24 (22, 54) (29, 64) (31) (24, 26, 115).

The study of human CSC is very challenging due to patient samples variability, need of immunosuppressive mice and a long-term growth requirement for in vivo studies. The study of CSC in a murine tumor model provides a more homogenous means to study CSC with well-defined genetic mutations in an immunocompetent microenvironment. There are currently

several genetic murine models of ovarian cancer, which utilize ovarian bursal injection of an adenovirus expressing cre recombinase (AdCre) to induce the deletion of specific 'Floxed' genes. Wu et al. developed a model of a high-grade endometrioid ovarian carcinoma, which develops after inactivation of APC, PTEN and TP53. This tumor model has 100% death due to widely metastatic disease similar to that of patients with advanced stage ovarian cancer patients (13).

In this study we characterized cell lines and primary tumors from the $Apc^{flox/flox}$; $Pten^{flox/flox}$; $Tp53^{flox/flox}$ ovarian tumor model for cells with ovarian CSC activity. We demonstrate that cells with expression of the cell surface marker CD24 have greater sphere formation capacity, ability to passage, and ability to initiate tumors in vivo. We report that similar to that observed for hepatocellular carcinoma, $CD24^+$ CSC demonstrate preferential expression of Nanog and phosphorylation of STAT3. $CD24^+$ cells are preferentially sensitive to inhibition of STAT3 phosphorylation with a JAK2 inhibitor. Finally, we show that JAK2 therapy in vivo using this tumor model seems to decrease tumor metastasis. This studies supports other work demonstrating $CD24^+$ cells as a metastatic CSC population and suggests that targeting JAK2 could reduce ovarian tumor metastasis.

MATERIALS AND METHODS

Cell Culture

Murine ovarian endometrioid adenocarcinoma cell lines were derived as previously described (133). Briefly, W2476T tumor cell line was established by mechanically dispersing ovarian tumor tissues with sterile scalpels followed by digestion at 37º C with 0.05% Trypsin-EDTA for 20 minutes. Cells were cultured for five passages in DMEM containing 10% FBS and 1% penicillin/streptomycin (p/s) in an incubator with 3% O_2; 5%CO_2. During the first five passages of primary culture, no adherent cells were discarded, and only adherent cells were passaged. W2476T cell line display epithelial (cobblestone) morphology. Cells were maintained and grown in RPMI containing 10% of FBS and 1% of p/s (Gibco, Grand Island, NY) at 37º C and 5%CO_2.

Isolation of Cancer Stem Cells from W2476T cell line and primary $Apc^{flox/flox}$; $Pten^{flox/flox}$; $Tp53^{flox/flox}$ ovarian tumors

Primary tumors were mechanically dissected into single-cell suspensions as previously described (29). Cells were isolated using fluorescence activated cell sorting (FACS). Briefly, primary ovarian tumor or cell lines single cell suspensions were counted and incubated with primary antibodies (CD24-PerCP Cy5.5, CD117-APC and CD133-PE from eBioscience San

Diego, CA) CD44-Pacific Blue (Biolegend, San Diego, CA), CD90-PE BD Pharmigen (San Jose, CA) for 30 min at 4º C. For $ALDH^+$ sample, ALDH enzymatic activity was defined using the ALDEFLUOR kit (Stem Cell Technologies, Canada) as previously described (29). FACS was performed with ~ 1 $x10^6$ cells using FACSAria (Becton Dickinson, Franklin Lakes, NJ) under low pressure in the absence of UV light when possible.

Sphere Assays

Sphere culture was performed as previously described (29, 131, 134). Briefly, FACS-isolated $CD24^{+/-}$, CD44, CD90, CD117, CD133 and ALDH cell populations were plated in triplicates in either 6-well or 24-well ultra-low attachment plates in serum-free DMEM/F12, epidermal growth factor (EGF) 20ng/mL, gentamycin 20µg/mL, insulin 5µg/mL, 1% p/s (Gibco, Grand Island, NY), hydrocortisone 1ng/mL, ß-Mercaptoethanol 100µM (Sigma, St. Lois, MO), fibroblast growth factor (bFGF) (Millipore, Billerica, MA) 10ng/mL. Either 300 or 2000 cells were seeded in ultralow attachment plates (Sigma, St. Louis, MO) depending on the availability of cells to perform the experiment triplicates. Primary spheres were counted on day 5 and then dissociated enzymatically with 0.025% Trypsin-EDTA (Gibco, Grand Island, NY) for 2 minutes at 37º C and mechanically with Pasteur pipette. The cells obtained from dissociation were analyzed microscopically for single cellularity and then replated sphere formation assays. Secondary spheres were counted on day 5 after passaging.

In vivo Tumor Models

Mice were housed and maintained in the University of Michigan Unit for Laboratory Animal Medicine and all studies were performed with the approval of the University Committee on the Use and Care of Animals. ~$5x10^4$ W2476T-Luc FACS sorted cells for each cancer stem cell marker were injected subcutaneously into the axilla of CIEA NOG mice (Taconic, Germantown, NY) with 100ul of PBS and 200ul of matrigel (BD Biosciences, San Diego, CA). Two weeks after injection tumor growth was monitored weekly using in vivo bioluminescence imaging and tumor monitoring using caliper. For primary murine ovarian cancer cells, $Apc^{flox/flox}$; $Pten^{flox/flox}$; $Tp53^{flox/flox}$ tumors were harvested and cells were dissociated and sorted for $CD24^+$, $CD24^-$ as stated above. $5x10^4$ $CD24^+$ and $CD24^-$ cells were injected into the contralateral flanks of NOG-SCID mice. Tumor growth was monitored by injecting D-Luciferin (Biosynth)/PBS solution to each mice as previously described (131). Mice were imaged using an IVIS Image System 200 Series (Xenogen Corporation). Image acquisition was initiated approximately 10 min after injection of D-luciferin. The bioluminescence signals (photons/s) emitted from the mice were collected using sequential mode until reaching peak values and analyzed by LivingImage 3.0 sofware (Xenogen Corporation). Tumors were harvested before reaching 2000 mm^3 and were measured for tumor volume, weighted and snap frozen for histologic analysis, RNA and protein. Tumor volumes were calculated using the L x W x W/2 formula.

$Apc^{flox/flox}$; $Pten^{flox/flox}$; $Tp53^{flox/flox}$ tumor bearing mice were generated via intra-bursal AdCre injection as previously described (13, 101). TG101209 was reconstituted in dimethyl sulfoxide (DMSO) at 10mM and stored at -20º C and further diluted in 40µl of DMSO before injection. TG101209 was injected i.p. at concentrations of 50mg/Kg in a final volume of 40µL

daily for 3 weeks. Control mice were treated with 40μL of DMSO alone. 21 days of TG101209 single agent therapy (50mg/kg n=5) or vehicle (n=5) was initiated 7 days after AdCre injection. For combined therapy with cisplatin, following AdCre injection mice were monitored until ovarian tumors were palpable (~4weeks). Mice were paired by tumor sized and then randomized to treatment with cisplatin alone (once a week 2mg/Kg x 2 weeks and vehicle daily) or cisplatin + daily TG101209 (n=6/group). Mice were monitored in conjunction with the University of Laboratory and Animal Management and euthanized when (i) animal appeared ill with signs of weight loss, (ii) significant bowel distention, (iii) or primary ovarian tumors were felt to be ~1000mm3.

RNA Isolation and qRT-PCR

W2476T cells were FACS isolated and RNA was extracted using PureLink RNA Mini kit, Ambion, Grand Island, NY) per manufacturer recommendations. RNA integrity was confirmed on the Agilent 2100 BioAnalyzer. Quantitative real-time PCR was performed for 40 cycles using SYBR green (Applied Biosystems, Carlsbad, CA) as recommended by the manufacturer, with primers at 100nM concentrations. Expression was normalized to Transferrin. All transcripts were confirmed using 3% agarose gel electrophoresis.

Western

To detect a differential expression of pSTAT3 in $CD24^{+}$ versus $CD24^{-}$ cells, ~$3x10^{5}$ W2476T cells and $CD24^{+/-}$ sorted cells were incubated overnight at 37ºC and 5% CO_2. Protein

lysates were obtained after 1 hr incubation with TG10209. Protein concentrations were determined using the Bradford Protein Assay (Bio-Rad) using Spectra max (Molecular Devices, Downingtown, PA) and SofMaxPro V5 sofware. 20µg of protein lysates were separated on 4-12% NuPAGE SDS gel (Invitrogen, Grand Island, NY) and detected using total STAT3 and pSTAT3 (1:1000 dilution, Cell Signaling Technology, Danvers, MA). Bands were visualized using the ECL Kit Pierce (Thermo Scientific, Waltham, MA).

In vivo Cytotoxicity Studies

MTT assays were performed as previously described (135). Briefly $5x10^3$ W2476T cells were plated in each of a 96 well plate overnight and treated with increasing concentrations of Stattic (Sigma, St.Louis, MO) and TG101209 (gift from Talpaz Laboratory from University of Michigan). 24, 48 and 72 hours after plating medium was replaced with PBS + 2% FBS and 10µl of 12mM MTT from Vybrant MTT Proliferation Assay kit (Molecular Probes, Grand Island, NY) and incubated for 4 hrs. After a second incubation with DMSO for 10min at 37º C absorbance was read at 540nm using Spectra max (Molecular Devices, Downingtown, PA) and SofMaxPro V5 sofware. **Cell Adherent culture:** $5x10^5$ W2476T cells were seeded and treated with increasing concentrations of cisplatin (0, 0.1, 0.3, 1 and 3 µg/mL) daily for three consecutive days. TG101209 cells (0, 0.3, 0.6, 1 and 1.3µM) were administered on day 1 only. Cell number as a percentage of untreated control was assessed after 72 hours. **Cells in suspension:** For drug treatment in spheres, W2476T cells were first sorted for CD24 positive and negative populations then subjected them for sphere assay. 24hrs later, cells were treated

with Stattic or TG101209 for three consecutive days and then sphere were counted and subjected to passaging studies as above on day 5 after sorting.

RESULTS

In order to identify putative CSC in the $Apc^{flox/flox}$; $Pten^{flox/flox}$; $Tp53^{flox/flox}$ ovarian cancer tumor model, we first used flow cytometry to analyze the expression of commonly reported CSC markers in the $Apc^{flox/flox}$; $Pten^{flox/flox}$; $Tp53^{flox/flox}$ primary tumor derived W2476T tumor cell line (Fig.II1A and B). We detected clear expression of CD24 (20-30%), CD44 (22-35%), CD90 (1-2%), and limited expression of ALDH, CD117, and CD133 (0.5-1% each).

As stem cells are characterized by the ability to grow in suspension and form spheres without the need of serum, we next tested the ability of FACS isolated cells expressing the specific CSC markers above to generate tumor spheres. $CD24^+$ and $CD133^+$ cells generated more primary tumor spheres, and demonstrated a greater ability to passage to form secondary spheres (Fig. II2).

CD24 Identifies Cells with Tumor Initiating Capacity

In vivo tumor initiation remains the gold standard for the identification of CSC. We therefore next sorted luciferase labeled W2476T cells for each marker positive and their negative counterpart. Specifically, $CD24^+$ Vs $CD24^-$, $CD44^+$ Vs $CD44^-$, $CD90^+$ Vs $CD90^-$, $CD117^+$ Vs $CD117^-$ and $ALDH^+$ Vs $ALDH^-$. We then injected 5,000 cells of each population subcutaneously in the axilla of NOG/SCID mice (n=5) and monitored tumor formation by bioluminescence.

Only $CD24^+$ Vs $CD24^-$ cells had a statistically significant increase in tumor growth rates. $CD133^+$ Vs $CD133^-$ cells demonstrated a trend for increased tumor growth. (Fig.II3 A-C). CD44, CD90, CD117, and ALDH demonstrated no significantly different tumor growth capacity between both marker positive and marker negative populations (See Supp Fig 3). Notice that in Fig II3A there is tumor formation by CD24- cells but it was not showed by bioluminescence. This is one of the limitations of the luciferase model for monitoring tumors. Importantly we performed weekly tumor monitoring measurement with caliper and when mice reached euthanization guidelines all tumors were measured and weighted.

Given the improved tumor initiation capacity of $CD24^+$ cells, we next performed tumor initiation studies with 200 $CD24^+$ versus $CD24^-$ cells. Consistent with a CSC phenotype, 200 $CD24^+$ cells Vs $CD24^-$ cells had a greater rate of tumor initiation (Fig. II4A-C). In addition, $CD24^+$ cells were capable of serial passage through at least three generations (data not shown). 50,000 $CD24^+$ cells of primary $Apc^{flox/flox}$; $Pten^{flox/flox}$; $Tp53^{flox/flox}$ tumors formed 5/5 tumors whereas $CD24^-$ cells formed 2/5 tumors (data not shown).

CD24 Cells Preferentially Express Stem Cell Genes and Phosphorylate STAT3

Given greater tumor sphere formation capacity, passaging potential, and greater tumor initiation rates in vivo we next characterized stem cell gene expression in $CD24^+$ and $CD24^-$ population (Fig II5A). W2476T whole cell line, and sorted cells $CD44^+$ and CD44- were used as controls (Supplemental Fig 4). While no differential expression was noted in controls qRT-PCR analysis demonstrated $CD24^+$ Vs $CD24^-$ cells had increased expression of Nanog, c-myc and Cyclin D1.

Interestingly, CD24 has been reported as a CSC marker in hepatic cancer. $CD24^+$ cells in hepatic cancer similarly had increased expression of Nanog, and it was found that Nanog promoted cellular self-renewal via phosphorylation of STAT3. We therefore next evaluated pSTAT3 in $CD24^+$ and $CD24^-$ cells. Whole cell line W2476T chemosensitization was performed (Fig II5 B). $CD24^+$ cells showed increased basal levels of STAT3 phosporylation compared to the $CD24^-$ cells (Fig II5C). We next treated whole W2476T, or FACS isolated $CD24^+$ and $CD24^-$ cells with the direct STAT3 inhibitor Stattic, or the JAK2 inhibitor TG101209 which indirectly inhibits STAT3 phosphorylation. Surprisingly, TG101209 inhibited pSTAT3 more efficiently in isolated $CD24^+$ cells than Stattic (Fig II5C). In order to determine the functional importance of STAT3 phosphorylation, we treated $CD24^+$ and $CD24^-$ spheres with both Stattic and TG101209. Both Stattic and TG101209 preferentially decreased $CD24^+$ primary sphere growth, and essentially eliminated passaging potential, suggesting an important functional role of STAT3 in $CD24^+$ ovarian tumor cells (Fig II5 D-E).

In order to confirm anti-tumor activity of inhibiting STAT3 phosphorylation via JAK2 inhibition in vivo we assessed the impact of JAK2 inhibition on $Apc^{flox/flox}$; $Pten^{flox/flox}$; $Tp53^{flox/flox}$ ovarian established tumors. Tumors were established and monitored until tumors reached ~500mm3. Tumors were paired based on size and then randomized to cisplatin Vs. cisplatin + TG101209 for 21 days. Combinatory treatment of cisplatin plus TG101209 improved survival of mice compared with mice treated with cisplatin only (Fig II6A-B).

We next treated 'early onset' ovarian cancer mice with TG101209. TG101209 or control therapy was initiated one week after injection of AdCre (Fig II7A). Unexpectedly, while control mice had tumor nodules in the intestine, liver and peritoneum, mice treated with TG101209 had

little or no tumor nodules (Fig II7B-D). This study will be repeated with a higher number of mice in order to confirm our findings.

DISCUSSION

Genetic models of cancer represent a homogenous and reproducible means to study CSC. Murine models also offer the advantage of an immunocompetent host. We found that in the $Apc^{flox/flox}$; $Pten^{flox/flox}$; $Tp53^{flox/flox}$ murine tumor model that $CD24^+$ cells that contain a subset of cells with increased tumor sphere forming and tumor-initiating capacity. $CD24^+$ cells preferentially express the stem cell genes Nanog, cyclin-D1, and c-myc and have increased pSTAT3 levels. Interestingly, Nanog (42, 136), Cyclin D1 and c-myc (137, 138) have been previously reported to be regulated by STAT3.

In this study we found that $CD24^+$ cells have increased basal pSTAT3 and that in vitro blockade of pSTAT3 was associated with decreased proliferation. Blockade of STAT3 phosphorylation in vivo was associated with near complete loss of metastasis, implicating $CD24^+$ cells in metastasis. This is supported by numerous other reports, Gao and colleagues reported that $CD24^+$ primary human ovarian cancer in addition to having the stem cell characteristics of quiescence, chemoresistance, and tumor initiation (26) also exhibited a epithelial-mesenchymal-transition (EMT) (133) phenotype, with high invasive capacity. Suggesting a direct role for CD24 in EMT, shRNA depletion of CD24 suppressed cell invasion and reversed the EMT phenotype (139). While there is increasing evidence of the role of CD24 in metastasis, the exact mechanism remains uncertain. CD24 may act both as an adhesion molecule to promote cellular migration. CD24 can bind to P-selectin and directly support the rolling of breast carcinoma cells

on endothelial cells. Similarly CD24 has been reported to directly support the adhesion, migration and invasion in colon and pancreatic cell lines (140).

CD24 also appears to play an important role in signal-transduction to promote metastasis. CD24 is reported to physically interact with c-src in both breast and ovarian cancer to regulate STAT3 (141-143). In hepatocellular carcinoma, CD24 has been shown to promote self-renewal through Nanog mediated by STAT3 phosphorylation (42). Our studies suggest that the activation of STAT3 plays a critical role in $CD24^+$ cell metastasis. STAT3 phosphorylation can be mediated by either Src or JAK2 (42, 143). Unlike previous studies, which implicated Src in CD24 mediated STAT3 phosphorylation, our studies indicate a critical role for JAK2.

For our in vitro studies we used both Stattic, direct pSTAT3 inhibitor and TG101209 a JAK2 inhibitor that prevent STAT3 phosphorylation. Interestingly, while both Stattic and TG101209 block STAT3 phosphorylation in isolated $CD24^+$ cells, TG101209 effectively blocked STAT3 phosphorylation more efficiently. We observed no change in p-Src (Y416) in the W2476T cell line, $CD24^+$ and $CD24^-$ treated with Stattic or TG101209, suggesting that in this particular cell line, phosphorylation of STAT3 goes through JAK2 and not Src. It is important to note that TG101209, in addition to inhibition JAK2, also inhibits FLT3, RET kinases (144). Further studies will be necessary to determine if inhibition of either FLT3 or RET is contributing to the metastasis inhibiting role of TG101209. Furthermore, in our in vivo studies we cannot rule out an important contribution of TG101209 activity on the tumor microenvironment contributing to inhibition of metastasis.

Ovarian cancer has been classified in type I and type II. Endometrioid, clear cell, muscinous and low grade serous carcinomas are classified as type I ovarian cancer (11, 13). In

contrast, type II ovarian cancers are high grade, biologically aggressive tumors from the beginning, with a tendency for metastasis from small-volume primary lesions (11, 13). High-grade serous ovarian carcinomas are type II ovarian carcinomas, which possess TP53 mutations (9, 10). Interestingly, type I and type II ovarian cancer have overlapping features suggesting that a subset of epithelial ovarian cancer may undergo type I to type II progression along with the acquisition of somatic TP53 mutations (13). The $Apc^{flox/flox}$; $Pten^{flox/flox}$; $Tp53^{flox/flox}$ mouse model of ovarian cancer used in this study carry the genetic mutations *APC/PTEN* commonly observed in type I tumors, however, with the addition of the *TP53* mutation assuming a much more aggressive/metastatic phenotype consistent with progression from type I to type II. Interestingly, with the administration of TG101209 there appears to be a pharmacologic reversion of these aggressive tumors back to a type I phenotype with disease essentially confined to the ovary.

Our data would indicate a potentially important role for JAK2 inhibitors in patients with ovarian cancer; the ability to prevent metastasis could dramatically improve the outcomes of patients with ovarian cancer and prevent complications such as bowel obstruction. However, as JAK2 inhibition did not affect the growth of primary tumors, novel endpoints for trial design will need to be consider as resist criteria alone may discount an important therapeutic benefit.

One clinical setting in which JAK2 inhibition could be very potent in ovarian cancer is as a chemoprophylaxis. JAK2 inhibitors are oral, relatively well tolerated medications. The use of JAK2 inhibitors in women at high risk for ovarian cancer to prevent metastatic spread prior to prophylactic oophorectomy could potential prevent metastatic disease.

CONCLUSION

In conclusion, we show that CD24 is a putative CSC marker of the $Apc^{flox/flox}$; $Pten^{flox/flox}$; $Tp53^{flox/flox}$ mouse model of ovarian cancer. This model will be a useful means to study ovarian CSC in an immunocompetent host. Using this model we have found that JAK2 inhibition improves survival when combined with standard chemotherapy and may play a role in tumor metastasis.

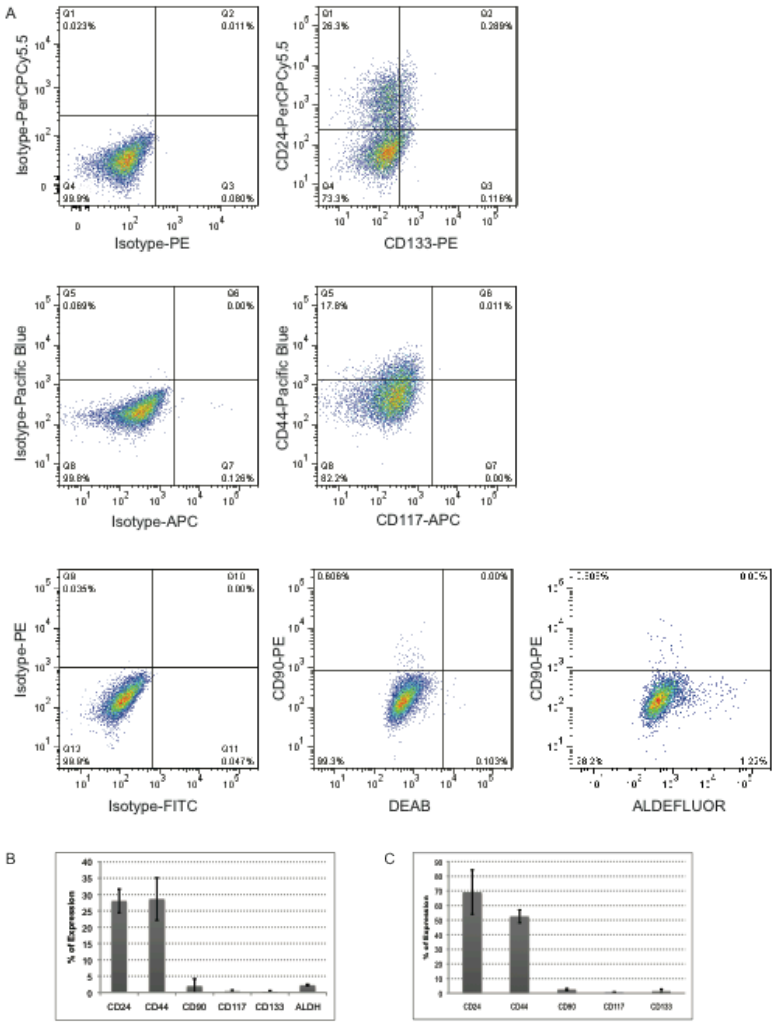

Figure II1. Analysis of stem cell marker expression in cell lines and primary tumors derived from the $Apc^{flox/flox}$; $Pten^{flox/flox}$; $Tp53^{flox/flox}$ ovarian **mouse model.** (A) FACS plots of the indicated markers and isotype controls of W2476T cell line (B) Summary of average percentage of CSC marker expressing cells (C) Summary of average percentage of CSC marker expressing cell in W2476T cell line and primary tumors n=5)

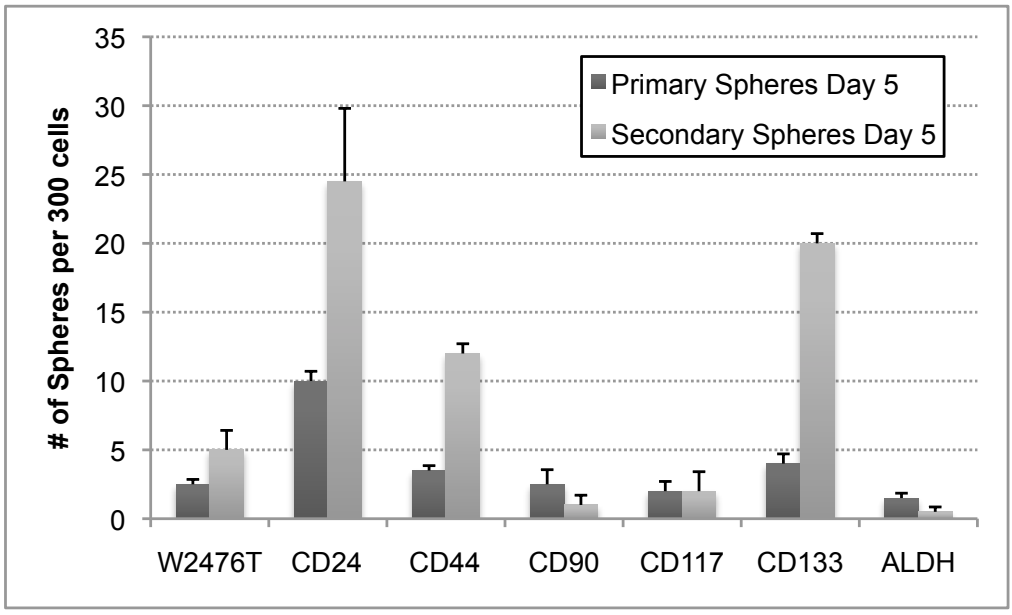

Figure II2. Functional Asssessment of CSC activity. Summary of average numbers of primary and secondary tumors spheres formed 300 FACs isolated cells expressing the indicated CSC marker. Results are representative of at least 3 assays with 3 replicates for each group

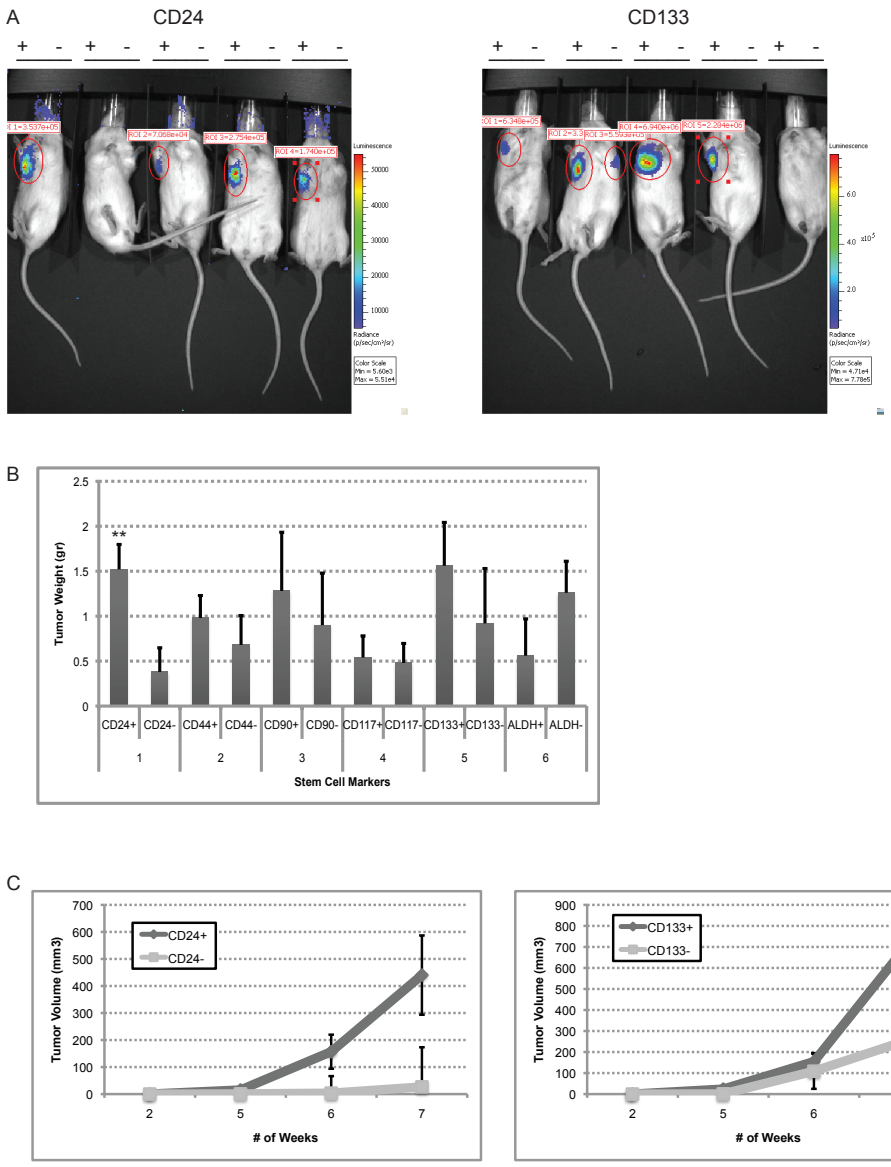

Figure II3. CD24+ demonstrate preferential tumor initiation capacity. (A) Bioluminescent images of W2476T-Luc tumors formed from cells, which express or do not express the indicated CSC marker. (Right axilla CSC marker positive cells and left axilla CSC marker negative cells) (B) Tumor weight of tumors generated from different stem cell markers (C) Tumor volume of CD24 +/- and CD133+/- tum

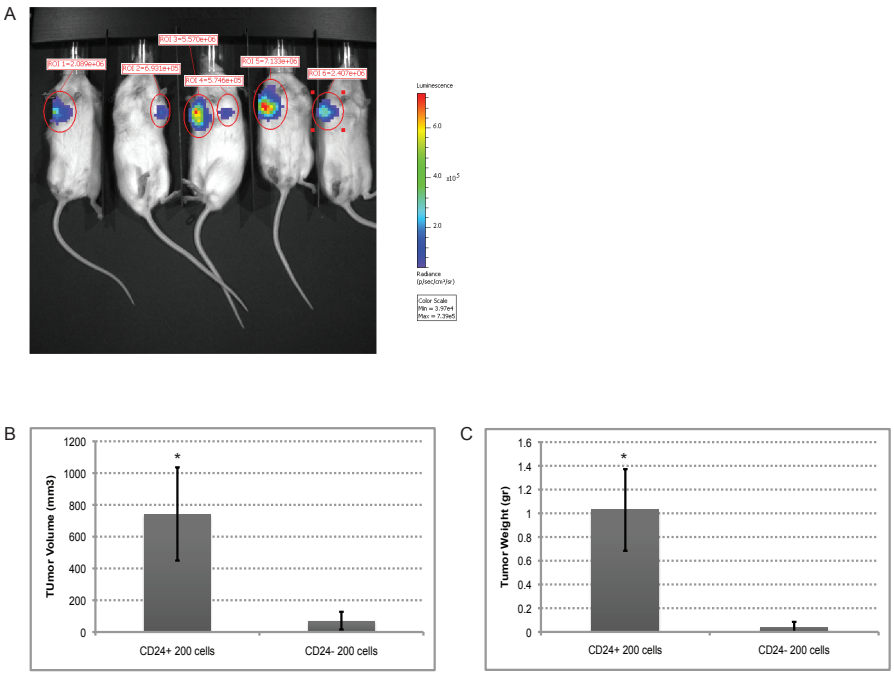

Figure II4. W2476T-Luc Dilution experiment for CD24 stem cell marker. (A) Luminescence expression of 200 CD24+ and CD24- cells tumor volumes (C) and weight (D) $p<0.05$ n=5

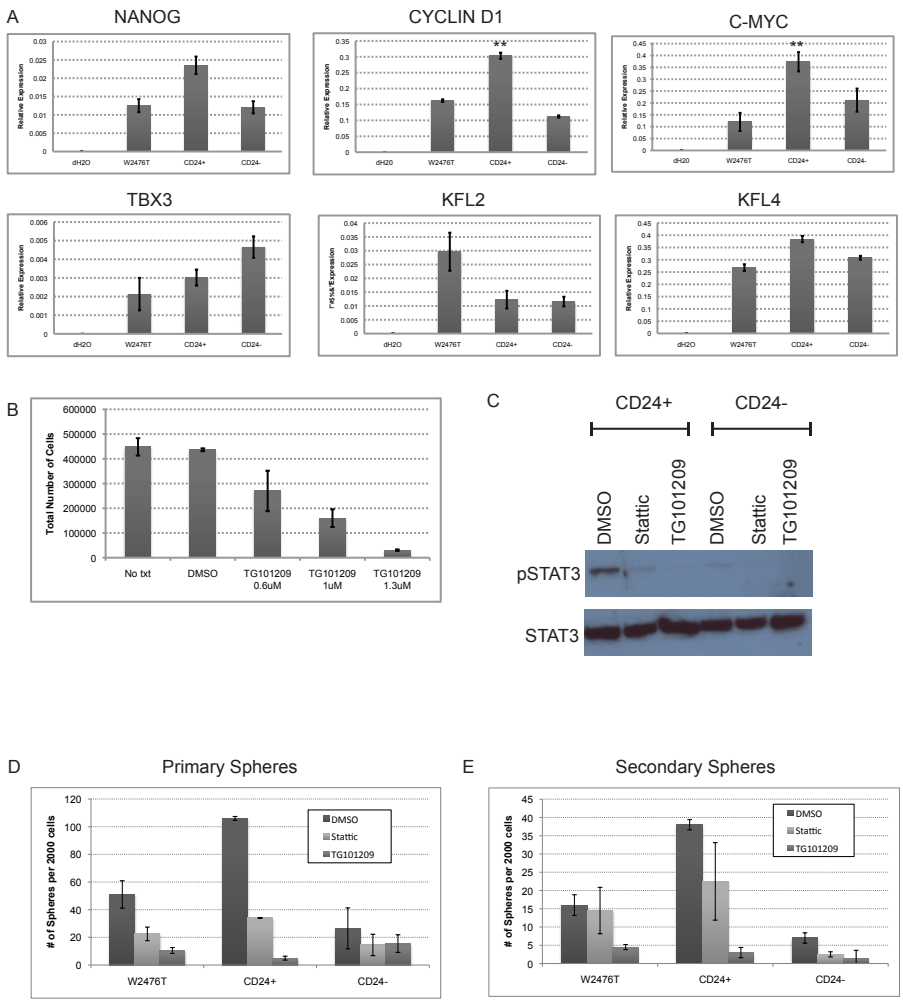

Figure II5. CD24+ cells preferentially expresses stem cell genes and have increased levels of pSTAT3. (A) qRT-PCR Comparison of stem cell gene expression in W2476T whole cell line and sorted CD24+ and CD24- cells. (B) Chemosensitization assay of W2476T cells with TG101209 (C) Western blot showing differential phosphorylation of STAT3 in CD24+ and CD24- cells and inhibition by Stattic and TG101209 (D) Primary and secondary (E) spheres treated with Stattic and TG101209 for three consecutive days and counted on day 5. Showing preferential inhibition of spheres formed from CD24+ cells

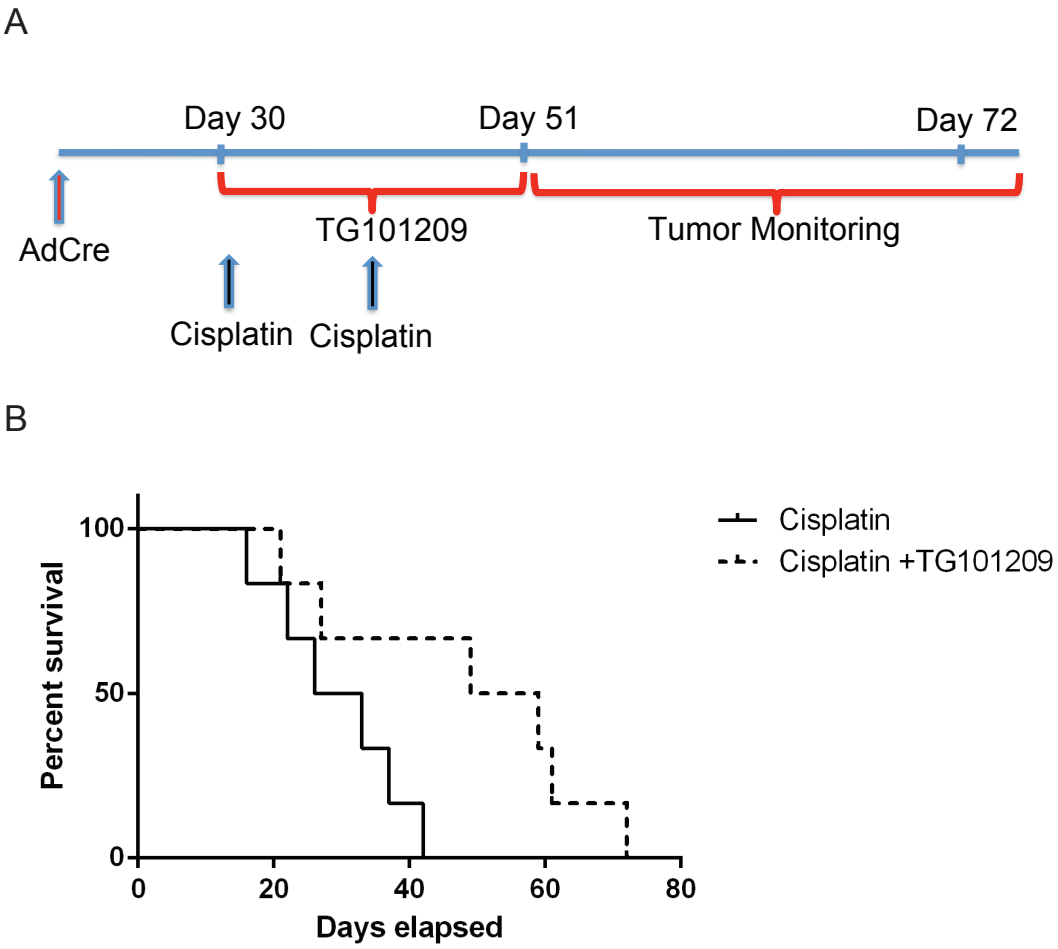

Figure II6. Combination of cisplatin and TG101209 treatment in Apc$^{flox/flox}$; Pten$^{flox/flox}$; Tp53 $^{flox/flox}$ mice improves survival. (A) Timeline of cisplatin and TG101209 treatment (B) Survival curves for mice treated with Cisplatin vs Cisplatin + TG101209 p=0.04 n=6

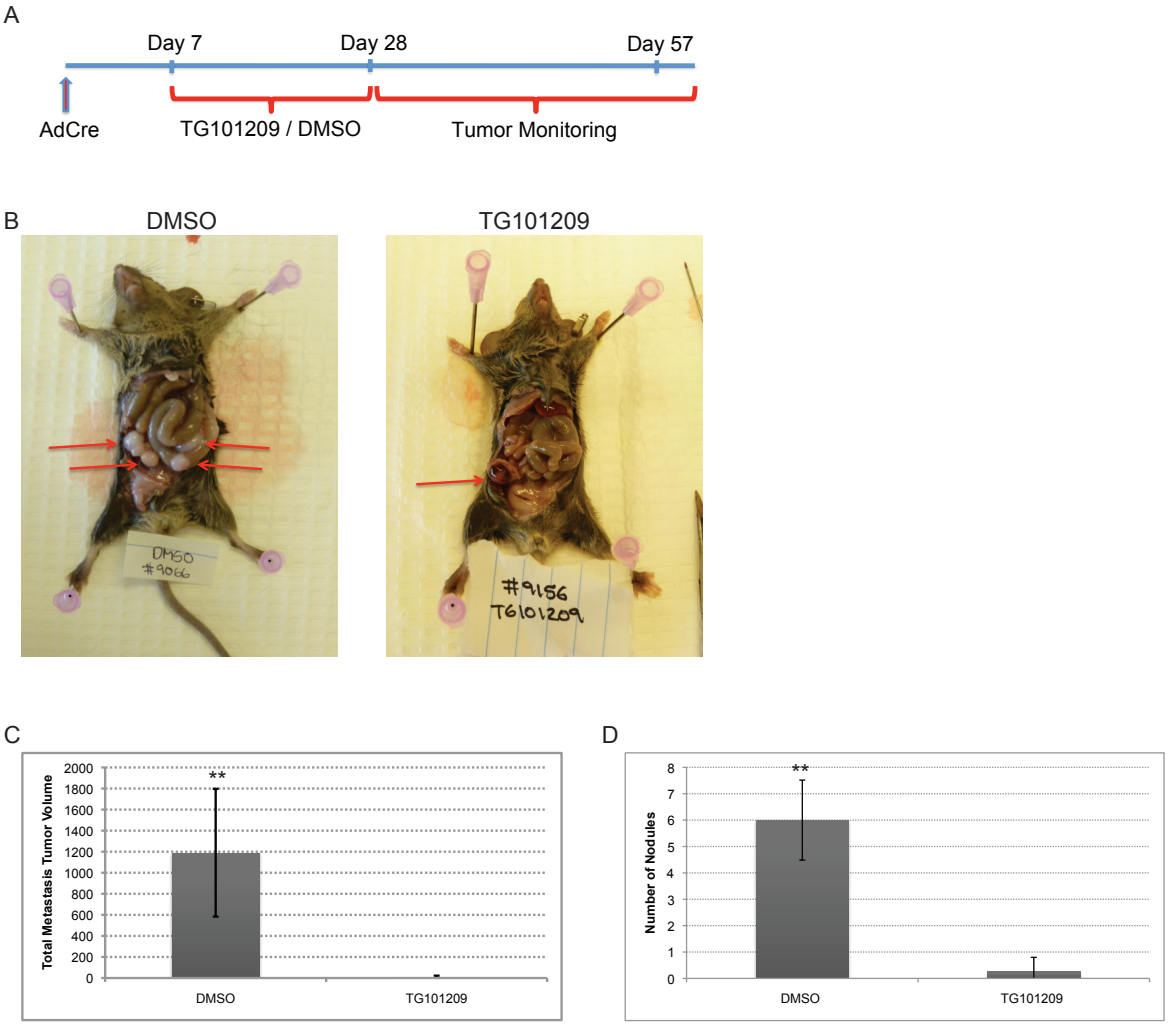

Figure II7. Treatment of Apc$^{flox/flox}$; Pten$^{flox/flox}$; Tp53 $^{flox/flox}$ mice with TG101209 restricts metastasis. (A) Timeline of TG101209 treatment (B) Mice treated with TG101209 and contro (DMSO). Arrows indicate metastasis and primary tumor (C) Total metastasis volume $p< 0.001$ and (D) number of metastatic nodules $p < 0.0001$ n=5

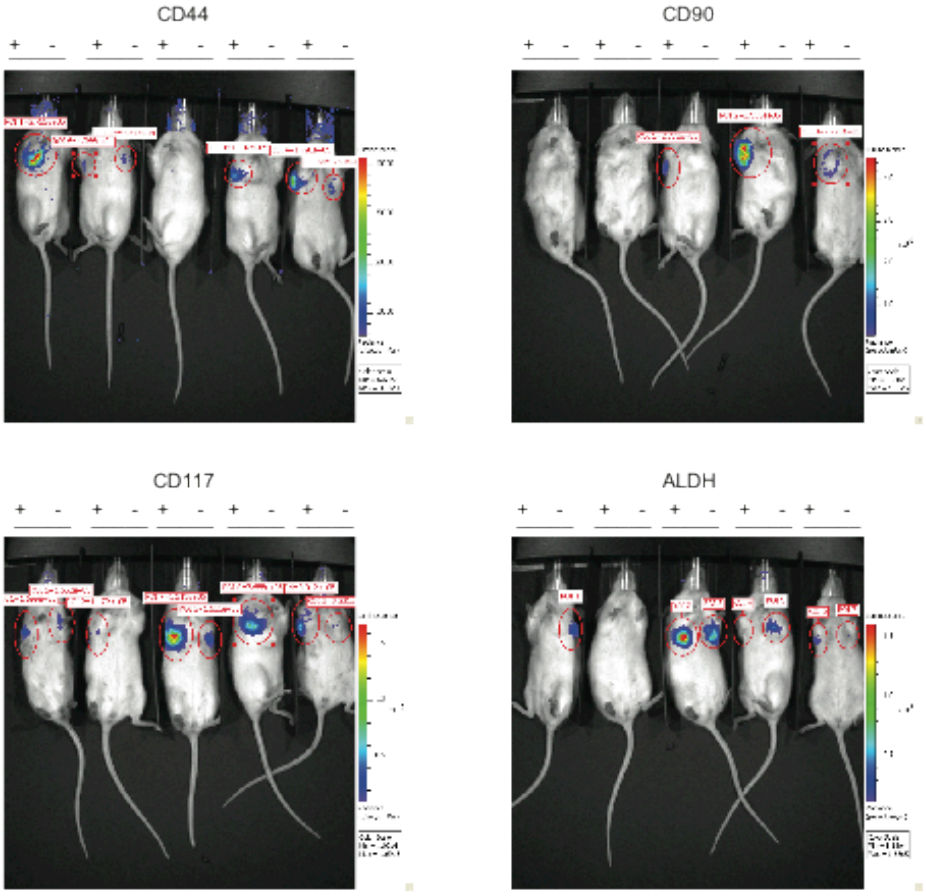

Supplemental Figure 3. Tumor formation by CD44, CD90, CD117 and ALDH.
W2476T-Luc sorted for different stem cell markers and injected in NOG/SCID mice.
Right axilla positive cells and left axilla negative cells for the indicated marker

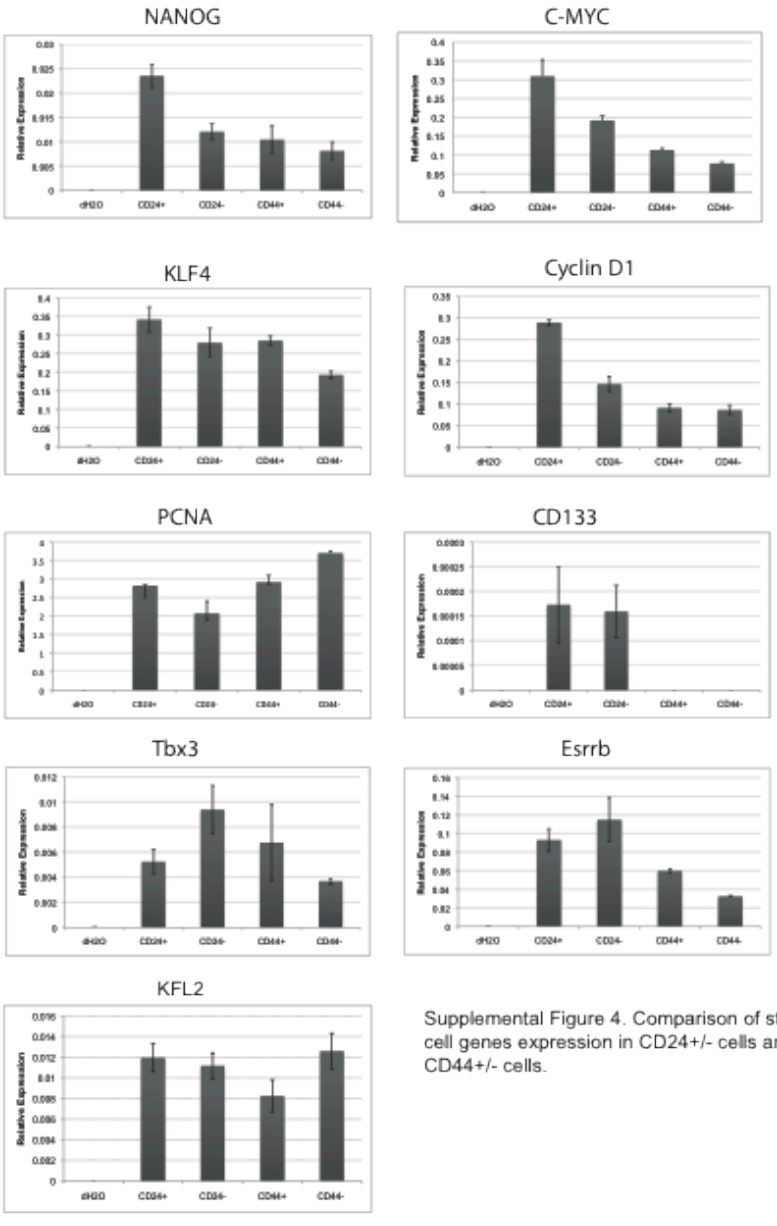

Supplemental Figure 4. Comparison of stem cell genes expression in CD24+/- cells and CD44+/- cells.

REFERENCES

1. Jemal A, Siegel R, Ward E, Hao Y, Xu J, Thun MJ. Cancer statistics, 2009. CA Cancer J Clin. 2009;59:225-49.
2. Kipps E, Tan DS, Kaye SB. Meeting the challenge of ascites in ovarian cancer: new avenues for therapy and research. Nat Rev Cancer. 2013;13:273-82.
3. Guppy AE, Nathan PD, Rustin GJ. Epithelial ovarian cancer: a review of current management. Clin Oncol (R Coll Radiol). 2005;17:399-411.
4. Bell DA. Origins and molecular pathology of ovarian cancer. Mod Pathol. 2005;18 Suppl 2:S19-32.
5. Wu R, Hendrix-Lucas N, Kuick R, Zhai Y, Schwartz DR, Akyol A, et al. Mouse model of human ovarian endometrioid adenocarcinoma based on somatic defects in the Wnt/beta-catenin and PI3K/Pten signaling pathways. Cancer Cell. 2007;11:321-33.
6. Burgos-Ojeda D, Rueda BR, Buckanovich RJ. Ovarian cancer stem cell markers: prognostic and therapeutic implications. Cancer Lett. 2012;322:1-7.
7. Al-Hajj M, Wicha MS, Benito-Hernandez A, Morrison SJ, Clarke MF. Prospective identification of tumorigenic breast cancer cells. Proc Natl Acad Sci U S A. 2003;100:3983-8.
8. Ferrandina G, Martinelli E, Petrillo M, Prisco MG, Zannoni G, Sioletic S, et al. CD133 antigen expression in ovarian cancer. BMC Cancer. 2009;9:221.
9. Baba T, Convery PA, Matsumura N, Whitaker RS, Kondoh E, Perry T, et al. Epigenetic regulation of CD133 and tumorigenicity of CD133+ ovarian cancer cells. Oncogene. 2009;28:209-18.
10. Silva IA, Bai S, McLean K, Yang K, Griffith K, Thomas D, et al. Aldehyde dehydrogenase in combination with CD133 defines angiogenic ovarian cancer stem cells that portend poor patient survival. Cancer Res. 2011;71:3991-4001.
11. Kryczek I, Liu S, Roh M, Vatan L, Szeliga W, Wei S, et al. Expression of aldehyde dehydrogenase and CD133 defines ovarian cancer stem cells. Int J Cancer. 2012;130:29-39.
12. Zhang S, Balch C, Chan MW, Lai HC, Matei D, Schilder JM, et al. Identification and characterization of ovarian cancer-initiating cells from primary human tumors. Cancer Res. 2008;68:4311-20.
13. Alvero AB, Chen R, Fu HH, Montagna M, Schwartz PE, Rutherford T, et al. Molecular phenotyping of human ovarian cancer stem cells unravels the mechanisms for repair and chemoresistance. Cell Cycle. 2009;8:158-66.
14. Gao MQ, Choi YP, Kang S, Youn JH, Cho NH. CD24+ cells from hierarchically organized ovarian cancer are enriched in cancer stem cells. Oncogene. 2010;29:2672-80.
15. Wu R, Baker SJ, Hu TC, Norman KM, Fearon ER, Cho KR. Type I to type II ovarian carcinoma progression: mutant *Tp53* or Pik3ca confers a more aggressive tumor phenotype in a mouse model of ovarian cancer. Am J Pathol. 2013;182:1391-9. 16. Wang H, Galban S, Wu R, Bowman BM, Witte A, Vetter K, et al. Molecular imaging reveals a role for AKT in resistance to cisplatin for ovarian endometrioid adenocarcinoma. Clin Cancer Res. 2013;19:158-69.

17. McLean K, Gong Y, Choi Y, Deng N, Yang K, Bai S, et al. Human ovarian carcinoma-associated mesenchymal stem cells regulate cancer stem cells and tumorigenesis via altered BMP production. J Clin Invest. 2011;121:3206-19.
18. Dontu G, Abdallah WM, Foley JM, Jackson KW, Clarke MF, Kawamura MJ, et al. In vitro propagation and transcriptional profiling of human mammary stem/progenitor cells. Genes Dev. 2003;17:1253-70.
19. Yang K, Mooney C, Spahlinger G, Schuetze S, Arias-Pulido H, Verschraegen C, et al. DR6 as a diagnostic and predictive biomarker in adult sarcoma. PLoS One. 2012;7:e36525.
20. Lee TK, Castilho A, Cheung VC, Tang KH, Ma S, Ng IO. CD24(+) liver tumor-initiating cells drive self-renewal and tumor initiation through STAT3-mediated NANOG regulation. Cell Stem Cell. 2011;9:50-63.
21. Suzuki A, Raya A, Kawakami Y, Morita M, Matsui T, Nakashima K, et al. Nanog binds to Smad1 and blocks bone morphogenetic protein-induced differentiation of embryonic stem cells. Proc Natl Acad Sci U S A. 2006;103:10294-9.
22. Dauer DJ, Ferraro B, Song L, Yu B, Mora L, Buettner R, et al. Stat3 regulates genes common to both wound healing and cancer. Oncogene. 2005;24:3397-408.
23. Yu H, Pardoll D, Jove R. STATs in cancer inflammation and immunity: a leading role for STAT3. Nat Rev Cancer. 2009;9:798-809.
24. Kang KS, Choi YP, Gao MQ, Kang S, Kim BG, Lee JH, et al. CD24(+) ovary cancer cells exhibit an invasive mesenchymal phenotype. Biochem Biophys Res Commun. 2013;432:333-8.
25. Sagiv E, Starr A, Rozovski U, Khosravi R, Altevogt P, Wang T, et al. Targeting CD24 for treatment of colorectal and pancreatic cancer by monoclonal antibodies or small interfering RNA. Cancer Res. 2008;68:2803-12.
26. Baumann P, Cremers N, Kroese F, Orend G, Chiquet-Ehrismann R, Uede T, et al. CD24 expression causes the acquisition of multiple cellular properties associated with tumor growth and metastasis. Cancer Res. 2005;65:10783-93.
27. Bretz N, Noske A, Keller S, Erbe-Hofmann N, Schlange T, Salnikov AV, et al. CD24 promotes tumor cell invasion by suppressing tissue factor pathway inhibitor-2 (TFPI-2) in a c-Src-dependent fashion. Clin Exp Metastasis. 2012;29:27-38.
28. Bretz NP, Salnikov AV, Perne C, Keller S, Wang X, Mierke CT, et al. CD24 controls Src/STAT3 activity in human tumors. Cell Mol Life Sci. 2012;69:3863-79.
29. Pardanani A, Hood J, Lasho T, Levine RL, Martin MB, Noronha G, et al. TG101209, a small molecule JAK2-selective kinase inhibitor potently inhibits myeloproliferative disorder-associated JAK2V617F and MPLW515L/K mutations. Leukemia. 2007;21:1658-68. 30.
Kurman RJ, Shih Ie M. Pathogenesis of ovarian cancer: lessons from morphology and molecular biology and their clinical implications. Int J Gynecol Pathol. 2008;27:151-60.
31. Ahmed AA, Etemadmoghadam D, Temple J, Lynch AG, Riad M, Sharma R, et al. Driver mutations in TP53 are ubiquitous in high grade serous carcinoma of the ovary. J Pathol. 2010;221:49-56.
32. Integrated genomic analyses of ovarian carcinoma. Nature. 2011;474:609-15.

GENERAL DISCUSSION

We have described two models to study ovarian CSC. Previously human ovarian CSC studies have been hampered by the low engraftment rate in xenografts using immunosuppressed mice. Therefore we developed a model system in which human embryonic stem cells offer a human microenvironment by forming a teratoma in the mouse. We improved this model by adding tumor endothelial cells to enrich the percentage of human tumor vessels and therefore provide an enhanced microenvironment/CSC niche for human ovarian CSC growth. This model system offers a new tool to study human ovarian CSC growth and test therapeutics specifically targeting human tumor vessels.

While the hESC model overcomes poor engraftment rates associated with in vivo human ovarian CSC growth, in vivo study human ovarian CSC remains challenging due to significant patient heterogeneity, the need to use of an immunosuppressive microenvironment, and a long latency before tumor formation. Therefore we studied a second model for ovarian cancer. We characterized ovarian CSC in a mouse model of ovarian cancer with genetic mutations in APC PTEN and TP53 that resembles type II ovarian cancer. The advantages of this model are: it is homogeneous, it has defined genetic defects reflecting human disease, tumors develop rapidly, and it offers an immunocompetent microenvironment. From this mouse model of ovarian cancer we found that $CD24^+$ cells have characteristics of CSC including sphere formation in vitro and increased tumor initiation and growth in vivo. Studies have shown that CD24 promotes self-renewal through Nanog mediated activation of STAT3. $CD24^+$ cells were demonstrated

preferential activation of STAT3. In vivo treatment with TG101209, which is an indirect inhibitor of STAT3 phosphorylation, significantly decreased metastasis associated with this aggressive ovarian cancer model. Finally, when TG101209 was combined with chemotherapy, we observed prolonged overall survival. These findings indicate that CD24 population have a CSC phenotype and may play a role in tumor migration and invasion in other organs. Moreover, these findings suggest that combination of chemotherapy and CSC targeted therapies can potentially improve survival by inhibiting metastasis.

Tumor Vascular Markers, the Extracellular Matrix and the CSC niche

Tumor vasculature has a markedly different gene expression pattern than normal vasculature. Most of differentially expressed tumor vascular genes are involved in extracellular matrix formation or remodeling. For example, St. Croix et al. compared endothelium from colon cancer to normal endothelium and found that at least seven of the differentially expressed genes encoded proteins were involved in extracellular matrix formation and remodeling (3). Similarly, glioma endothelial cells study upregulate tumor endothelium extracellular matrix components such as heparan sulfate proteoglycan 2, type II collagen and matrix metalloprotease 14 (4). In breast cancer endothelial cells, genes that regulated the extracellular matrix were found to be osteonectin and matrix metalloprotease 9, and tissue inhibitor of metalloproteinase 1 (5). In ovarian cancer, tumor endothelial cells showed a differential expression on adlican (matrix remodeling associated 5, MXRA5); C11orf8 (metallophosphoesterase domain containing 2, MPPED2 and Collagen typeXI alpha-1 (Col11A1) (6).

The unique extracellular matrix created by tumor endothelial cells likely contributes to the CSC niche. Niches play a protective role by shielding stem cells from environmental insults as well as regulating stem cell proliferation and cell fate decisions (7). It has been suggested that the vascular niche protects CSC from chemotherapy and radiotherapy to promote tumor recurrence (7-9). Brain CSC have been shown to grow near the tumor vasculature (7) where the endothelial cells provide secreted factors that maintain these cells in a self-renewing and undifferentiated state. Furthermore, Calabrese et al. showed that antiangiogenic therapies which reduce tumor blood vessels arrested tumor growth with a restriction in CSC number (7). These findings suggest that the vascular niche represents a therapeutic target to impact CSC.

Given the role of the vascular cells, both in providing nutrients for cancer growth and in creating a niche for CSC, inhibiting or destroying tumor vessels using either anti-angiogenic agents or vascular disrupting agents is a very attractive treatment approach. However, given many human tumor vascular targets are not expressed on murine tumor vessels, most murine tumor models are insufficient for anti-human tumor vascular targeted therapy studies. Therefore our model system offers a microenvironment with human tumor vessels where we can test the efficacy of targeted therapies specifically to human tumor vessels. Similarly, this model can also be used to test the in vivo binding activity of vascular-targeted peptides (10). We proved the power of this model using both human specific vascular targeting antibodies (1) and vascular targeted nanoparticles (11). Future studies will be necessary to assess the impact of vascular targeting on the CSC niche in this tumor model.

Future Experiments with the hESCT Tumor Model

This work lays an important foundation for numerous future studies. The hESCT-tumor model can be further developed and ultimately individualized for a given patient with the goal of identifying therapeutic response. We have previously identified other components of the human CSC niche including tumor associated macrophages and mesenchymal stem cells. The hESCT model system could be expanded to include addition of these cellular components directly derived from a patient's primary debulking sample. With the addition of tumor endothelial cells, mesenchymal stem cells, tumor associated macrophages, and cancer stem cells a human tumor could be nearly completely reconstructed within the mouse. Such a system could then be used to test therapeutics targeting either tumor vasculature, CSC or both. This will allow us to re-create the tumor in a more similar environment where it was and test therapeutics and find the most efficacious one and eventually if these drugs are approved then give to the patient.

The sources to of human vessels in the mouse such human embryonic stem cells and human tumor endothelial cells to grow in the mouse have certain disadvantages. First of all human embryonic stem cells in vitro growth are time consuming and patient tumor endothelial cells are difficult to obtain and are very difficult to expand in vitro therefore need to be injected into mice as soon as possible. Another easier option to potentially grow human vessels in the mouse is the use of endothelial cell lines. One very good candidate cell line is infantile hemangioma cell line. Infantile hemangioma is a vascular neoplasm resulting from abnormal proliferation of endothelial cells. Hemangioma stem cell lines have been developed and when injected into immunosuppresed mice recapitulate a hemangioma tumor with human vessels (12). It will be appealing to inject hemangioma cells, with ovarian tumor cells and evaluate if these express ovarian TVMs. Also, following the before mentioned approach we could inject these

along with mesenchymal stem cells and CSC and having an easier model system than the need of hESCT.

While the hESCT model system has advantages, it is highly laborious, uses immunosuppresed mice and there is patient to patient CSC variability. The transgenic mouse model of ovarian cancer represents an important additional model for more expeditious studies of ovarian CSC in parallel with the hESTC model since we know the genetic deficits, which resemble human disease, is homogeneous and represents an immunocompetent microenvironment.

CD24, Cancer Stem cells and Epithelial Mesenchymal Transition

Emerging data have highlighted shared molecular characteristics of CSC and EMT cells (13, 14). EMT is also believed to enhance metastasis due to the increased migratory capacity of mesenchymal cells. EMT has a central role in embryogenesis and is well recognized for its close connection to cancer metastasis also in ovarian cancer (15). In ovarian cancer, cells with a mesenchymal phenotype have been shown to be more resistant to chemotherapy than epithelial cells (16-18). It was previously shown by Kang et al. that $CD24^+$ population of human ovarian cancer cell line and primary ovarian cancer clone exhibit an EMT phenotype, high invasive capacity, and CXCR4/SDF-1 mediated chemotactic migration (19). Furthermore, depletion of CD24 by shRNA suppressed cell invasion and resulted in a loss of an EMT phenotype (19). In our hands, preliminary data shows that W2476T $CD24^+$ cells similarly have a mesenchymal phenotype with increased expression of mesenchymal genes compared to $CD24^-$ population (data not shown). We also found that these cells were more invasive in vitro (data not shown). Furthermore, treatment of tumor in vivo resulted in fewer metastases. However, we cannot

definitively determine if this is secondary to $CD24^+$ cell specific toxicity. In order to assess if the loss of metastases is specifically due to toxicity of $CD24^+$ cells, $CD24^+$ and $CD24^-$ cells could be injected in the ovarian bursa orthotopically and test if there are metastatic differences among the two different populations.

CD24, IL6/JAK/STAT pathway and Metastasis

Our studies show that CD24 is a stem cell marker in this mouse model of ovarian cancer in which pSTAT3 may play a role in stem cell self renewal and in tumor metastasis. CD24 has been shown to promote self renewal through STAT3 mediated Nanog (20). Additionally, CD24 is linked to tumor invasion (21) and metastatic progression (22, 23). It has been shown that CD24 on the surface of tumor cells can bind P-selectin on vascular endothelial cells and platelets to promote tumor metastasis (24, 25). Therefore, cancer cells with high CD24 expression might invade the vessel lumen and bind with platelets, resulting in vascular or lymphatic metastasis (24).

It has been previously reported that IL-6 plays a role in progression of epithelial ovarian cancer (26, 27), suggesting IL-6/JAK/STAT pathway may play a role in ovarian cancer metastasis. Supporting a role for IL6 in metastasis, IL-6 augments the tumorigenic potential and invasiveness of EOC cells by inducing the secretion of metalloproteinase-9 (28). Moreover, in a 3D co-culture of mesenchymal stem cells and ovarian cancer cells IL-6 promoted invasion and migration of ovarian cancer cells (29). In breast cancer there is an autocrine/paracrine IL-6/JAK/STAT3 feed-forward loop, which participates in tumor proliferation, shaping of the tumor microenvironment, and metastasis (30). Chang et al. examined the levels and distribution of IL-6

expression by immunohistochemistry in human primary breast cancers including those with metastatic involvement in matched axillary lymph nodes (30). They found that the highest levels of IL-6 were found in the tumor edge enriched in stromal/immune cells, areas of lymmphovascular invasion, and axillary lymph nodes (30). Moreover, they found a correlation between high levels of IL-6 on the tumor edge and the number of lymph nodes affected by metastatic disease.

Normal stem cells are regulated by their microenvironment and CSC are regulated by cells in the tumor microenvironment. These interactions involve inflammatory cytokines, such as IL-1, Il-6 and Il-8 which in turn activate STAT3/NF-kB pathways in both stromal and tumor cells (31). Activation of these pathways stimulates further cytokine production, generating positive feedback loops that in turn drive CSC self renewal (31) . Interestingly, these pathways are normally activated during inflammation and wound healing and may contribute to the known link between inflammations and cancer. Inhibitors if these cytokines and their receptors have been developed as anti-inflammatory agents. By blocking signals from the tumor microenvironment these agents have the potential to target CSC. In our studies, we decreased metastasis by targeting JAK2 and consequently phosphorylation of STAT3. One may hypothesize that STAT3/NF-kB pathways are activated by ovulation induced inflammation/wound healing. If aberrant inclusion cysts are created, these may lead to chronic inflammation and ultimately initiate ovarian cancer.

IL6 signaling is mediated by inflammation and IL6 receptor activation results in the phosphorylation of the receptor and JAK2, which recruits its substrate proteins such as signal transducers and activators of transcriptions (STATs). STATs, especially STAT3 and STAT5, translocate to the nucleus and transactivate many genes involved in cell proliferation and

survival (ex. Cyclin D1). Like IL6, the JAK/STAT signaling is strongly linked with oncogenesis. The JAK/STAT signaling pathway is frequently activated in leukemia and other hematological disorders. This may occur via activating mutations upstream cytokine receptors, including FLT3, c-kit and G-CSFR, and constitutively active JAK kinases, such as JAK2 V617F and TEL-JAK2. In addition, alterations of the downregulator of this pathway could also contribute to aberrant activation (32).

Our findings contribute to a growing body of literature of the role of the JAK/STAT pathway in cancer. We found that the JAK2 inhibitor TG101209: [1] Decreases $CD24^+$ sphere formation, [2] Inhibits phosphorylation of STAT3 in W2476T ovarian cancer cell line, [3] Blocks metastasis in vivo and [4] If combined with cisplatin improves survival in a mouse model of ovarian cancer.

Consistent with our studies, Chang et al. found that the JAK2 inhibitor ruxolitininb inhibited tumor growth, metastatic nodules and reduction of phosphorylation of STAT3, infiltrating endothelial cells and fibroblast/myoepithelial cells (30).

It is important to note that, while TG101209 is most active against JAK2 (IC_{50}=6nM), it also inhibits FLT3, RET and JAK3 kinases with IC_{50} of 25-169 nM in vitro kinase assays (33). Thus, while we used TG101209 at low doses in vivo, we cannot rule out that some of the anti-metastatic effect of TG101209 is secondary to effects on these other kinases. In addition, while we observed no significant changes in the number/types of host cells in the tumor microenvironment in the presence and absence of TG101209 treatment, it is also possible TG101209 is exerting some of its impact via an effect on the microenvironment.

Dedifferentiation

Recently, two independent studies show that if normal stem cells are depleted, differentiated cells of the stomach (34) and lung (35) can act as adult stem cells, generating various cell types of the tissues including a pool of stem cells. Further studies need to be done if this is also applicable in CSC. In our hands, W2476T $CD24^-$ cells formed less and smaller tumors than $CD24^+$ population (See Fig II3 and II4). When we analyzed the tumor cells we observed that $CD24^-$ tumors primary tumor cells contained $CD24^+$ and $CD24^-$ cells (data not shown). This could be due contamination from the FACS (meaning $CD24^-$ cell pool mistakenly harbored $CD24^+$ cells) or that $CD24^-$ cells formed $CD24^+$ cells. In the above recent studies, Tata et al. shows that in the trachea contact between differentiated Clara lung cells and lung basal stem cells inhibits dedifferentiation of Clara cells. Suggesting maybe $CD24^-$ cells dedifferentiated due to the absence of $CD24^+$ cells and regenerated $CD24^+$ and $CD24^-$ cells. However further studies need to be accomplished to understand why primary $CD24^-$ tumors generated $CD24^+$ and $CD24^-$ cells.

Applying these Findings in Other Ovarian Cancer Types

It will be interesting to obtain endometrioid adenocarcinoma patient tumor samples and analyze if CD24 is a good candidate for CSC in that specific epithelial ovarian cancer type. Previously it has been shown by us (2) and others (36-40) that the most common stem cell marker candidates for serous ovarian cancer are ALDH and CD133. It will be worthy of note to test if CD24 is higher in the CSC hierarchy in endometrioid ovarian cancer type in comparison with ALDH and CD133.

Origin of ovarian cancer

Epidemiologic studies have shown a significant reduction in risk of ovarian cancer directly related to increased parity and the use of contraceptive pills. This suggests an important factor in ovarian cancer is ovulation (41). One hypothesis on the origin of ovarian cancer is that normal fallopian tube epithelium from the fimbria implants at the site of rupture of OSE when ovulation occurs, leading to the development of a cortical inclusion cyst (CIC) that may undergo malignant transformation (42). There appear to be two types of ovarian CICs. One type results from invagination of OSE with a flattened epithelium. The second type is lined by ciliated columnar epithelium which is histological identical to the fallopian tube epithelium (42). Suggestive that CICs are derived from fallopian tube epithelium is the finding of leukocyte populations, including CD3+ T cells, CD8+ T lymphocytes and CD68R+ macrophages are present in CICs (42, 43); Fallopian tube epithelium contain these immune cell populations while OSE does not. These leukocyte populations may be involved in immune mucosal protection and through their role in inflammation, may contribute to neoplastic transformation (42). This may be due to the destruction and repair of OSE during ovulation, which is accompanied by inflammation that probably plays a role in ovarian cancer (44).

If fallopian tube derived CICs are a putative source of ovarian cancer and CSC are also important for ovarian cancer initiation, then it would be anticipated that stem like cells would be present in the fallopian tube and CICs. Indeed, recently Auersperg showed that even though the fimbrial epithelial cells are highly differentiated, some cells express stem cell markers such as Nanog, ALDH1A1 and ALDH1A2 and these markers are also present in the human (45) and mouse (46) OSE. Importantly these markers were present in the distal parts of fimbrial epithelium, which are also the sites of serous tubal intraepithelial carcinomas (STICs), the

putative precursors of high grade serous ovarian cancer (45, 47). If the fimbrial epithelium expresses Nanog (45) and the ovarian surface inclusion cysts expresses Nanog and CD24 (45, 48), then one may speculate that serous ovarian cancer may originate from altered Nanog expressing distal fimbria that has translocated into the OSE and then becoming entrapped within the ovarian stroma. This may happen during ovulation because the fimbria and the OSE are in closer contact during ovulation of inflammation (49). It will be interesting to determine whether the normal mouse ovaries have CICs expressing Nanog and CD24 and compared it to different time points after induction of ovarian cancer after injection of AdCre in the ovarian bursa inactivating APC, PTEN and TP53 genes. These findings will help us understand the recently published results were Schereiber at al. showed that CD24 and Nanog were in the cyst walls of 81% of human serous ovarian carcinomas and the source of this disease.

Future Directions for detecting CSC in Mouse Model of Ovarian Cancer

In this study we show that mice bearing ovarian cancer with APC PTEN TP53 mutations have a decrease in metastasis when treated with TG101209. At this time we lack the information of how specifically the drug is preventing metastasis. In order to address this issue several studies need to be accomplished. First, it will be important to confirm TG101209 is acting on tumor cells primarily and not on the host cells. If treatment effects are primarily due to inhibition of JAK2 on the tumor cell then knockdown of JAK2, in the W2476T cell line and evaluate if this cells are able to migrate/invade and metastasize in vitro and in vivo. To further confirm that the impact is due to targeting JAK2 and not off target effects on JAK1 or FLT3, we could also use specific inhibitors of JAK1 or FLT3 and evaluate if these decrease metastatic nodules as well as

TG101209. Further evaluation of CD24 and metastasis is needed. Knocking out CD24 in W2476T cell line and evaluation of this in vitro and in vivo may give us some answers how specifically is TG101209 inhibiting metastasis.

REFERENCES

1. Burgos-Ojeda D, McLean K, Bai S, Pulaski H, Gong Y, Silva I, et al. A novel model for evaluating therapies targeting human tumor vasculature and human cancer stem-like cells. Cancer Res. 2013;73:3555-65.
2. Silva IA, Bai S, McLean K, Yang K, Griffith K, Thomas D, et al. Aldehyde dehydrogenase in combination with CD133 defines angiogenic ovarian cancer stem cells that portend poor patient survival. Cancer Res. 2011;71:3991-4001.
3. St Croix B, Rago C, Velculescu V, Traverso G, Romans KE, Montgomery E, et al. Genes expressed in human tumor endothelium. Science. 2000;289:1197-202.
4. Madden SL, Cook BP, Nacht M, Weber WD, Callahan MR, Jiang Y, et al. Vascular gene expression in nonneoplastic and malignant brain. Am J Pathol. 2004;165:601-8.
5. Parker BS, Argani P, Cook BP, Liangfeng H, Chartrand SD, Zhang M, et al. Alterations in vascular gene expression in invasive breast carcinoma. Cancer Res. 2004;64:7857-66.
6. Buckanovich RJ, Sasaroli D, O'Brien-Jenkins A, Botbyl J, Hammond R, Katsaros D, et al. Tumor vascular proteins as biomarkers in ovarian cancer. J Clin Oncol. 2007;25:852-61.
7. Calabrese C, Poppleton H, Kocak M, Hogg TL, Fuller C, Hamner B, et al. A perivascular niche for brain tumor stem cells. Cancer Cell. 2007;11:69-82.
8. Garcia-Barros M, Paris F, Cordon-Cardo C, Lyden D, Rafii S, Haimovitz-Friedman A, et al. Tumor response to radiotherapy regulated by endothelial cell apoptosis. Science. 2003;300:1155-9.
9. Paris F, Fuks Z, Kang A, Capodieci P, Juan G, Ehleiter D, et al. Endothelial apoptosis as the primary lesion initiating intestinal radiation damage in mice. Science. 2001;293:293-7.
10. Winer JL, Liu CY, Apuzzo ML. The use of nanoparticles as contrast media in neuroimaging: a statement on toxicity. World Neurosurg. 2012;78:709-11.
11. Winer I, Wang S, Lee YE, Fan W, Gong Y, Burgos-Ojeda D, et al. F3-targeted cisplatin-hydrogel nanoparticles as an effective therapeutic that targets both murine and human ovarian tumor endothelial cells in vivo. Cancer Res. 2010;70:8674-83.
12. Tang Y, Liu W, Yu S, Wang Y, Peng Q, Xiong Z, et al. A novel in vivo model of human hemangioma: xenograft of human hemangioma tissue on nude mice. Plast Reconstr Surg. 2007;120:869-78.
13. Floor S, van Staveren WC, Larsimont D, Dumont JE, Maenhaut C. Cancer cells in epithelial-to-mesenchymal transition and tumor-propagating-cancer stem cells: distinct, overlapping or same populations. Oncogene. 2011;30:4609-21.
14. Mani SA, Guo W, Liao MJ, Eaton EN, Ayyanan A, Zhou AY, et al. The epithelial-mesenchymal transition generates cells with properties of stem cells. Cell. 2008;133:704-15.
15. Lili LN, Matyunina LV, Walker LD, Wells SL, Benigno BB, McDonald JF. Molecular profiling supports the role of epithelial-to-mesenchymal transition (EMT) in ovarian cancer metastasis. J Ovarian Res. 2013;6:49.

16. Ahmed N, Abubaker K, Findlay J, Quinn M. Epithelial mesenchymal transition and cancer stem cell-like phenotypes facilitate chemoresistance in recurrent ovarian cancer. Curr Cancer Drug Targets. 2010;10:268-78.
17. Latifi A, Abubaker K, Castrechini N, Ward AC, Liongue C, Dobill F, et al. Cisplatin treatment of primary and metastatic epithelial ovarian carcinomas generates residual cells with mesenchymal stem cell-like profile. J Cell Biochem. 2011;112:2850-64.
18. Marchini S, Fruscio R, Clivio L, Beltrame L, Porcu L, Nerini IF, et al. Resistance to platinum-based chemotherapy is associated with epithelial to mesenchymal transition in epithelial ovarian cancer. Eur J Cancer. 2013;49:520-30.
19. Kang KS, Choi YP, Gao MQ, Kang S, Kim BG, Lee JH, et al. CD24(+) ovary cancer cells exhibit an invasive mesenchymal phenotype. Biochem Biophys Res Commun. 2013;432:333-8.
20. Lee TK, Castilho A, Cheung VC, Tang KH, Ma S, Ng IO. CD24(+) liver tumor-initiating cells drive self-renewal and tumor initiation through STAT3-mediated NANOG regulation. Cell Stem Cell. 2011;9:50-63.
21. Mierke CT, Bretz N, Altevogt P. Contractile forces contribute to increased glycosylphosphatidylinositol-anchored receptor CD24-facilitated cancer cell invasion. J Biol Chem. 2011;286:34858-71.
22. Overdevest JB, Thomas S, Kristiansen G, Hansel DE, Smith SC, Theodorescu D. CD24 offers a therapeutic target for control of bladder cancer metastasis based on a requirement for lung colonization. Cancer Res. 2011;71:3802-11.
23. Baumann P, Cremers N, Kroese F, Orend G, Chiquet-Ehrismann R, Uede T, et al. CD24 expression causes the acquisition of multiple cellular properties associated with tumor growth and metastasis. Cancer Res. 2005;65:10783-93.
24. Zhu J, Zhang G, Lu H. CD24, COX-2, and p53 in epithelial ovarian cancer and its clinical significance. Front Biosci (Elite Ed). 2012;4:2745-51.
25. Lim SC, Oh SH. The role of CD24 in various human epithelial neoplasias. Pathol Res Pract. 2005;201:479-86.
26. Scambia G, Testa U, Benedetti Panici P, Foti E, Martucci R, Gadducci A, et al. Prognostic significance of interleukin 6 serum levels in patients with ovarian cancer. Br J Cancer. 1995;71:354-6.
27. Scambia G, Testa U, Panici PB, Martucci R, Foti E, Petrini M, et al. Interleukin-6 serum levels in patients with gynecological tumors. Int J Cancer. 1994;57:318-23.
28. Rabinovich A, Medina L, Piura B, Segal S, Huleihel M. Regulation of ovarian carcinoma SKOV-3 cell proliferation and secretion of MMPs by autocrine IL-6. Anticancer Res. 2007;27:267-72.
29. Touboul C, Lis R, Al Farsi H, Raynaud CM, Warfa M, Althawadi H, et al. Mesenchymal stem cells enhance ovarian cancer cell infiltration through IL6 secretion in an amniochorionic membrane based 3D model. J Transl Med. 2013;11:28.
30. Chang Q, Bournazou E, Sansone P, Berishaj M, Gao SP, Daly L, et al. The IL-6/JAK/Stat3 feed-forward loop drives tumorigenesis and metastasis. Neoplasia. 2013;15:848-62.
31. Korkaya H, Liu S, Wicha MS. Regulation of cancer stem cells by cytokine networks: attacking cancer's inflammatory roots. Clin Cancer Res. 2011;17:6125-9.

32. Lo MC, Peterson LF, Yan M, Cong X, Hickman JH, Dekelver RC, et al. JAK inhibitors suppress t(8;21) fusion protein-induced leukemia. Leukemia. 2013.
33. Pardanani A, Hood J, Lasho T, Levine RL, Martin MB, Noronha G, et al. TG101209, a small molecule JAK2-selective kinase inhibitor potently inhibits myeloproliferative disorder-associated JAK2V617F and MPLW515L/K mutations. Leukemia. 2007;21:1658-68.
34. Stange DE, Koo BK, Huch M, Sibbel G, Basak O, Lyubimova A, et al. Differentiated troy(+) chief cells act as reserve stem cells to generate all lineages of the stomach epithelium. Cell. 2013;155:357-68.
35. Tata PR, Mou H, Pardo-Saganta A, Zhao R, Prabhu M, Law BM, et al. Dedifferentiation of committed epithelial cells into stem cells in vivo. Nature. 2013.
36. Kuroda T, Hirohashi Y, Torigoe T, Yasuda K, Takahashi A, Asanuma H, et al. ALDH1-high ovarian cancer stem-like cells can be isolated from serous and clear cell adenocarcinoma cells, and ALDH1 high expression is associated with poor prognosis. PLoS One. 2013;8:e65158.
37. Baba T, Convery PA, Matsumura N, Whitaker RS, Kondoh E, Perry T, et al. Epigenetic regulation of CD133 and tumorigenicity of CD133+ ovarian cancer cells. Oncogene. 2009;28:209-18.
38. Curley MD, Therrien VA, Cummings CL, Sergent PA, Koulouris CR, Friel AM, et al. CD133 expression defines a tumor initiating cell population in primary human ovarian cancer. Stem Cells. 2009;27:2875-83.
39. Landen CN, Jr., Goodman B, Katre AA, Steg AD, Nick AM, Stone RL, et al. Targeting aldehyde dehydrogenase cancer stem cells in ovarian cancer. Mol Cancer Ther. 2010;9:3186-99.
40. Kryczek I, Liu S, Roh M, Vatan L, Szeliga W, Wei S, et al. Expression of aldehyde dehydrogenase and CD133 defines ovarian cancer stem cells. Int J Cancer. 2012;130:29-39.
41. Risch HA, Weiss NS, Lyon JL, Daling JR, Liff JM. Events of reproductive life and the incidence of epithelial ovarian cancer. Am J Epidemiol. 1983;117:128-39.
42. Nik NN, Vang R, Shih IM, Kurman RJ. Origin and Pathogenesis of Pelvic (Ovarian, Tubal, and Primary Peritoneal) Serous Carcinoma. Annu Rev Pathol. 2013.
43. Pothuri B, Leitao MM, Levine DA, Viale A, Olshen AB, Arroyo C, et al. Genetic analysis of the early natural history of epithelial ovarian carcinoma. PLoS One. 2010;5:e10358.
44. Fathalla MF. Incessant ovulation--a factor in ovarian neoplasia? Lancet. 1971;2:163.
45. Auersperg N. The stem-cell profile of ovarian surface epithelium is reproduced in the oviductal fimbriae, with increased stem-cell marker density in distal parts of the fimbriae. Int J Gynecol Pathol. 2013;32:444-53.
46. Gamwell LF, Collins O, Vanderhyden BC. The mouse ovarian surface epithelium contains a population of LY6A (SCA-1) expressing progenitor cells that are regulated by ovulation-associated factors. Biol Reprod. 2012;87:80.
47. Crum CP, McKeon FD, Xian W. The oviduct and ovarian cancer: causality, clinical implications, and "targeted prevention". Clin Obstet Gynecol. 2012;55:24-35.
48. Schreiber L, Raanan C, Amsterdam A. CD24 and Nanog identify stem cells signature of ovarian epithelium and cysts that may develop to ovarian cancer. Acta Histochem. 2013.
49. Kurman RJ, Shih Ie M. Molecular pathogenesis and extraovarian origin of epithelial ovarian cancer--shifting the paradigm. Hum Pathol. 2011;42:918-31.

APPENDIX

F3-targeted cisplatin-hydrogel nanoparticles as an effective therapeutic that targets both murine and human ovarian endothelial tumor cells in vivo

I. Winer[1], S. Wang[2], Y-E K. Lee[2], W. Fan[2], Y. Gong[3], D. Burgos-Ojeda[3], G. Spahlinger[3], R. Kopelman[2], and Ronald J. Buckanovich, MD, PhD[1,3]

[1]Division of Gynecologic Oncology, Department of Obstetrics and Gynecology

[2]Department of Chemistry

[3]Division of Hematology Oncology, Department of Internal Medicine

University of Michigan Medical Center, Ann Arbor, MI 48109

ABSTRACT

Recent studies indicate that ovarian cancer may be highly responsive to anti-vascular therapeutics. We have developed an anti-vascular tumor therapeutic using the F3 peptide to target cisplatin loaded nanoparticles (F3-Cis-Np) to tumor vessels. We demonstrate that while F3-Cis-Np bind with high specificity to both human ovarian tumor cells and tumor endothelial cells *in vitro*, they only demonstrate cytotoxic activity against the tumor endothelial cells. *In vivo* these nanoparticles bind primarily to tumor endothelial cells. Therapeutic studies in both flank and orthotopic intraperitoneal murine ovarian tumor models, as well as human tumor xenograft models, demonstrate rapid tumor regression with treatment. Treatment was associated with significant vascular necrosis consistent with an anti-vascular effect. Furthermore treatment

was active in both platinum sensitive and platinum resistant cell lines. Importantly we demonstrate that F3-Cis-Np bind to human tumor endothelial cells *in vitro* and to human tumor vessels *in vivo*. Therapy targeting human vasculature *in vivo* with F3-Cis-Np led to near complete loss of all human tumor vessels in a murine model of human tumor vasculature. Our studies indicate that F3-targeted vascular therapeutics may be an effective treatment modality in human ovarian cancer.

INTRODUCTION

Ovarian cancer is a deadly disease for which there have been few new therapies. For the past decade platinum and taxane chemotherapy regimens remain the mainstay of therapy. The development of targeted and biologic therapies for ovarian cancer has lagged behind other tumor types. Recent studies have suggested angiogenic pathways are important therapeutic targets in ovarian cancer. Phase II trials suggest a significant response rate of ovarian cancer to anti-VEGF therapy (174-177). This is unlike other solid tumors such as colon, lung, and breast cancer which showed no response to single agent anti-VEGF therapy. When anti-VEGF therapy is used in combination with chemotherapy in ovarian cancer, response rates are even higher (178, 179). Unfortunately, even when used in combination with chemotherapy, response to anti-VEGF therapy is relatively short. This is due in part to host cell up-regulation of alternate angiogenic pathways (180).

Targeting vascular cells directly represents a means to target numerous angiogenic pathways which act ultimately at the endothelial cell. In addition, unlike traditional anti-angiogenic therapies which prevent new vasculature, and therefore typically lead to disease stabilization but not regression, targeting active tumor vascular cells could potentially lead to tumor necrosis and disease regression. Ovarian tumor vasculature has been demonstrated to be unique from normal resting vasculature (112, 181). Several peptides have been identified and developed which bind with relatively high affinity and specificity to tumor vessels. RGD (arginine–glycine–aspartic acid) motif containing peptides have been developed which bind to

integrin molecules which are up-regulated on tumor vessels and sometimes tumor cells (182, 183). Similarly, aspargine-glycine-arginine peptides can be used to target CD13 isoforms expressed in tumor vasculature (184). The 31 amino acid F3 peptide has also been shown to bind to nucleolin protein expressed on the surface of tumor endothelial cells as well as on the surface tumor cells (185-187).

These peptides have been used to target nanoparticles carrying various therapeutic payloads to the tumor, such as MRI contrast agents and photodynamic drugs (188, 189). This approach allows the therapeutic agent to be concentrated at the tumor site, while reducing systemic exposure and potentially reducing drug related side effects. RGD targeted cisplatin nanoparticles were found to inhibit endothelial cell proliferation *in vitro* (190). RGD targeted paclitaxel containing nanoparticles were demonstrated to target ovarian cancer cells *in vitro* and *in vivo* and effectively restrict ovarian tumor growth(191). Similarly, in several tumor models including ovarian cancer, vascular targeted liposomal doxorubicin was found to be a more effective therapeutic than traditional doxorubicin or liposomal doxorubicin (192). Interestingly, a targeting peptide (iRGD) has been developed that combines the RGD motif with a protease site and a neuropilin targeting motif to create a peptide that promotes trans-endothelial passage of nanoparticles to enhance tissue penetration and targeting to tumor cells (193). The F3 peptide has also been used to deliver nanoparticles to the tumor microenvironment. A rat model of glioblastoma multiforme suggested that F3 targeted nanoparticles can be used for both tumor imaging and tumor therapeutics (186).

Studies to date have all focused on *in vitro* studies or studies in rodents. One shortcoming of these studies is the lack of a demonstration of activity against human tumor vessels *in vivo*. A model of human tumor vasculature has recently been developed (92, 93). This

model uses human embryonic stem cells as a source of vascular cells, thus the vascular cells are human. Vessels that are generated in this model demonstrate that they have both human endothelial and vascular smooth muscle cells.

We used the F3 peptide to deliver cisplatin loaded polyacrylamide (PAA) nanoparticles to tumor vessels in both murine and human ovarian cancer models. We demonstrate that these nanoparticles bind to murine and human tumor endothelial cells both *in vitro* and *in vivo*. When used as a therapeutic, these nanoparticles lead to significant tumor regression and then stabilization of tumor burden. Nanoparticles were effective in both xenograft and orthotopic tumor models. Our data strongly support the efficacy of vascular targeted nanoparticle therapy in ovarian cancer and represent the first demonstration of chemo-nanoparticle binding to human tumor vessels *in vivo*.

MATERIALS AND METHODS

Nanoparticle (NP) Preparation

Chemicals

Acrylamide, N,N,N',N'- tetraethylmethylenediamine (TEMED), Ammonium persulfate (APS), Polyethylene glycol dodecyl ether (Brij 30), 3-(acryloyloxy)-2-hydroxypropylmethacrylamide (AHM), hexane, and dioctyl sulfosuccinate (AOT) were purchased from Sigma Aldrich. 3-(aminopropyl) methacrylamide (APMA) was obtained from Polysciences Inc.and ethanol (190 proof) was obtained from Fisher Scientific. Cisplatin was purchased from SICOR pharmaceuticals Inc. (Irvine, CA), while Sulfosuccinimidyl 4-[N-maleimidomethyl] cyclohexane-1-carboxylate (Sulfo-SMCC), Traut's reagent (2-IT), amine reactive fluorescein isothiocyanate (FITC) and AlexaFluor 594 were from Thermo Scientific Inc. All solutions were prepared from 18 MΩ water purified by a Barnstead/Thermolyne Nanopure II system except where otherwise stated.

Blank Np polymerization

Hexane (45 mL) was added into a dried 100 mL round bottom flask and stirred under a constant purge of argon. AOT (1.6 g) and Brij 30 (3.1 g) were added to the reaction flask and stirring was continued under argon for 20 min. In the mean time, acrylamide (0.711 g) and APMA (0.055 g) were dissolved in PBS (pH=7.4) in a glass vial by sonication. AHM (0.428 g)

was added to the acrylamide solution and the reaction mixture was sonicated for 5 min to obtain a uniform solution. The solution was then added to the hexane reaction mixture and vigorously stirred for 20 min at room temperature under argon protection. Polymerization reaction was initiated by adding freshly prepared ammonium persulfate (10% aqueous solution, 40 μL) and TEMED (40 μL) and the resulting solution was stirred vigorously at room temperature overnight (12 hour). At the completion of polymerization, hexane was removed by rotary evaporation and the particles were precipitated by addition of ethanol. The surfactant and unreacted monomers were washed away from the particles by washing with ethanol (5×160mL) followed by washing with water (5×100 mL) in an Amicon ultra-filtration cell (200mL, equipped with a Biomax 100kDa cutoff membrane). The concentrated Np were lyophilized for two days before use.

Cisplatin-Encapsulated and FITC or AlexaFluor linked Np

The polymerization procedures for cisplatin-encapsulated Np were the same as above except that 2mL cisplatin (SICOR Pharnaceuticals Inc, Irvine, California, obtained via the Department of Pharmacy at the University of Michigan) drug solution (1mg/mL) was used to dissolve all the monomers. The cisplatin-encapsulated nanoparticles were protected from light during the production process. An inductively coupled plasma (ICP) (Perkin-Elmer Optima 2000 DV with Winlab software) was used to determine the concentration of cisplatin encapsulated. The cisplatin concentration was measured by ICP to be 0.75±0.02 ug/mg Np. The nanoparticle solution for each injection was prepared to allow consistent dosing of cisplatin among experiments.

For fluorophore linked Np, 1mg of FITC or 5mg of AlexaFluor 594 was added into monomer solution and the mixture were kept stirring at 37°C for an hour before injected into

hexane. The rest of the procedures were same as Cisplatin encapsulated Np. Blank, fluorophore conjugated, or cisplatin encapsulated PAA Np, were prepared with a final average size of 24.4nm (polydispersity index equals to 0.120).

F3 targeted Np

Cisplatin encapsulated (or fluorophore linked or blank) Np were suspended in PBS (pH 7.2) solution by sonication, followed by adding suitable amount of Sulfo-SMCC. After half an hour reaction under stirring, the SMCC conjugated Np were washed by using Amicon centrifugal filter unit for 3 times. Prescribed amount of F3 peptide and 2-IT was dissolved in DI water under stirring for 2 hours at 37°C, and was added into the SMCC conjugated Np suspension. The mixture was stirred at room temperature overnight and then washed again to obtain the concentrated Np.

In vitro Studies

ID8, SKOV3, A2008 cells were a generous gift from Dr. George Coukos and A2780 ovarian cancer cell lines were a generous gift of Dr. Rebecca Liu. Tumor endothelial cells (TEC's) were freshly generated from VE-Cadherin+/CD146+ cells FACS isolated from mechanically dissected tumors as previously described (194, 195). TEC were then grown in EBM2 media (Clonetech). Monocytes were isolated from 2ml of donor blood based upon their ability to adhere to plastic following ACK lysis. All cells except TEC were grown in RPMI/10%FBS/5% penicillin-streptomycin, medium and split two days prior to experiments to 40% confluency. For binding experiments, cells were incubated with a range of F3 targeted

AlexaFluor 594 linked Np (F3-Alex-Np), or blank Np (10-100 mg/ml) for 4 hours with intermittent rocking. Cells were then washed three times with PBS under sterile conditions and returned to the incubator for 30 minutes and then imaged using a Nikon fluorescent microscope (Nikon) attached to CoolSNAP CCD camera (Roper Scientific). In order to determine *in vitro* killing efficiency cells were incubated with F3 targeted blank Np (F3-Np), F3 targeted cisplatin encapsulated Np (F3-Cis-Np, 0.15 μg/ml final cisplatin concentration), parental cisplatin compound (at 5μg/ml final concentration for cell line experiments and at 1 ug/ml for TEC and PBMC experiment) or mock treated with PBS. The cells were washed after 4 hours and then allowed to grow for a total of 72 hours prior to harvesting for cell counting via trypan blue exclusion.

Mouse Studies

All mice were housed at the University of Michigan Medical School in the Unit for Laboratory Medicine (ULAM) and protocols were approved under the University Committee on the Use and Care of Animals (UCUCA). Tumor cell lines were grown in DMEM/10%FBS/5% penicillin-streptomycin, medium.

Axillary and flank tumor models: $10x10^6$ cells were injected with 0.2 ml of PBS and 300ul of matrigel (BD Biosciences). In the initial targeting experiments, axillary tumors were allowed to grow for 10 days and then 100 mg/Kg F3 targeted Alexa-488 linked Np (F3-FITC-Np) or Alexa-488 linked Np (FITC-Np,) were administered intravenously. 24 hr after injection the mice were sacrificed and tumors, liver, lung, kidney, heart and spleen were harvested and examined for fluorescent nanoparticle uptake. For therapeutic studies Hey1 tumor cells were stably transduced with a DsRed expressing lentivirus (plentiloxEV-DsRed virus, provided by the

vector core at the University of Michigan). Tumor cells were injected subcutaneously into either the flank (ID8 studies) or axilla (SKOV3, A2780-GFP, and DsRED HEY1) of either C57Bl6 or nu/nu mice respectively. Axillary injection was used in the case of the human tumor xenografts as we find axillary tumors have a greater microvascular density than flank tumors. Xenografts were allowed to establish as indicated and were treated with either (1) IP cisplatin at 250 μg/kg alone or (2) IP cisplatin combined with with F3-Np via tail vein injection or (3) with F3-Cis-Np via tail vein injection (IV) at 100mg/kg of nanoparticles (final cisplatin concentration 75 μg/kg). Mice were treated initially at Day 10 and Day 14 (all tumor xenografts) and Day 21 (for ID8 and SKOV3 xenografts only). Tumor volume was monitored via caliper (W^2 x L/2). A2780-GFP mice were imaged with whole body imaging utilizing the Maestro imaging system. Mice were sacrificed on either day 18 or day 28. Axillary and flank tumors were harvested for histology and immunohistochemistry.

Intraperitoneal (IP) models: Mice were randomized by weight to the various treatment groups for IP injections. 2.0 x10^6 ID8 cells harvested in exponential growth were injected intraperitoneally in 0.2 ml of PBS. Tumor cells were then allowed to grow for 10 days prior to first treatment. Control mice were then treated with either IP cisplatin at 250 μg/kg alone or along with (1) IP blank F3-Np, (2) IV blank F3-Np, or (3) both IP and IV administered blank F3-Np. Alternatively mice were treated with F3-Cis-NP (1) delivered IV, (2) IP, or (3) both IV and IP. Nanoparticles were dosed with final cisplatin does of 150 μg/kg; 150 μg/kg for IV or IP alone, or 75 μg/kg IV and 75 μg/kg IP for IV/IP treated animals. Mice were treated at days 10, 14, 21 and 28. Mice were followed for weight gain/ascites and sacrificed after a 10 gram weight gain or when they appeared moribund. Kaplan-Meier curves were plotted and statistical analysis performed via log rank test.

Teratoma Model: Hey-1/teratomas were generated as previously described (92, 93). Briefly, H9 embryonic stem cells (ESC) were cultured on mouse embryonic fibroblasts, manually dispersed, and passaged. $1x10^6$ undifferentiated H9 embryonic stem cells were injected subcutaneously into the axilla of NOD-SCID mice with matrigel and allowed to grow until teratomas were palpable. 100,000 DsRed-HEY1 cells were then injected within teratoma. Tumors were imaged using bio-immunofluorescence. Given the large size of the tumor/teratomas and their rapid growth rates, mice were then treated with intravenous F3-Np or F3-Cis-Np 75μg/kg every 48 hour, 4 times, for a total of 8 days. Tumors were harvested 24 hours after the 4^{th} NP treatment. Controls were treated with F3-FITC-Np 1 hour prior to sacrifice to confirm F3-NP targeting to human vessels. Tumors were then analyzed with Co-IF with anti- human CD31-PE.

RESULTS

Targeting of F3-targeted nanoparticles to tumor endothelial cells and tumor cells in vitro

Blank, fluorophore conjugated or cisplatin encapsulated PAA Np, were prepared with a final average size ranging from 20-30 nm (Figure A1). The PAA nanoparticle is a hydrogel that has a high aqueous solubility and long plasma circulation time, being suitable for *in vivo* applications (186, 188, 196). It also has excellent engineerability within both nanoparticle core and surface, which allowed conjugation of fluorophores and/or multiple targeting/visualization peptides for the current studies. F3 peptide was conjugated to the Np for targeting. This peptide is a subcomponent of the HMGN2 protein and has demonstrated specificity for both human tumor cells and vasculature (185-187). Alexafluor-594 was bound to the nanoparticles (Alex-Np) for visualization in initial targeting experiments. To test the ability of the F3 peptide to target ovarian tumor cells, both mouse and human ovarian cancer lines (Mouse ID8 and Human SKOV3, A2008, A2780) were incubated with either F3-Alex-Np (100μg/ml) or Alex-Np (1mg/ml). We observed significant binding of the F3 targeted Np to all ovarian tumor cell lines tested (Figure A2A). Little or no binding was observed with Np that lacked the targeting F3 peptide. We next tested the ability of F3-Np to bind to tumor endothelial cells (TECs) (Figure A2A). F3-Alex-Np demonstrated strong binding to both mouse and human TECs. Once again, non-targeted Np showed little or no binding.

In vitro cytotoxicity of F3 targeted cisplatin encapsulated Np:

In order to determine the cytotoxic potential of F3 targeted Np, tumor cell lines were treated with either PBS, F3-Cis-Np, blank F3-Np combined with cisplatin, for four hours and then washed. The final concentration of cisplatin in the F3-Cis-Np was 0.15 μg/ml and that of cisplatin combined with the blank F3-Np was 1 μg/ml for TEC/PBMC experiments and 5 μg/ml for A2780 and SKOV3 experiments. The cells were then allowed to grow for an additional 72 hours and harvested. We then assayed the number of viable cells in each treatment group relative to the PBS control. Consistent with previous studies of nanoparticles targeting tumor cells, our experiments demonstrated little cell death in the nanoparticle experimental groups (Figure A2B) (197-199).

We then repeated these experiments using tumor endothelial cells isolated from both murine ID8-VEGF ovarian tumors and human ovarian cancers. Unlike what was observed for the tumor cell lines, we observed significant induction of cell death with F3-Cis-Np on both mouse and human tumor endothelial cells. No cell death was noted when treating control PBMCs (Figure A2B). Thus F3 targeted Np appear to be more toxic to tumor endothelial cells than to tumor cell lines.

F3 –Np target tumor vessels in vivo

To test the efficacy of F3 targeting *in vivo* we used the highly vascular ID8-VEGF ovarian tumors model (200). Mice bearing ID8-VEGF tumors were treated intravenously with increasing concentrations of either non-targeted Alexa488-Np or F3 targeted Alexa488 Np. Mice were sacrificed 24 hours after infusion and multiple tissue and tumor specimens were

harvested and examined via fluorescence for nanoparticle localization. Highest specific binding to tumor vessels without significant uptake in liver and kidney was determined at a dose of 100mg/kg (range tested 25-200 mg/kg, Figure 2C and data not shown). At this dose, non-targeted FITC-Np demonstrated little tumor specific uptake, but were found at significant levels in the liver and kidney. In contrast, at this concentration we observed significant uptake of F3-FITC-Np in tumor vessels and some uptake within tumor parenchyma. We noted minimal uptake of F3-FITC-Np in kupffer cells of the liver and within the renal collecting tubules (Figure A2C and data not shown). No significant binding was observed in other tissues including the lung, heart, spleen, intestine, or brain (data not shown).

Therapeutic efficacy of F3-Cis-Np

Next, to test the therapeutic efficacy of the nanoparticles, ID8-VEGF tumors were grown in the axillas of mice for 14 days. Mice were then treated intravenously with two weekly doses of F3-Cis-NPs, with a final cisplatin concentration of 70 μg/kg, IP cisplatin at 250 μg/kg or IP cisplatin at 250 μg/kg, combined with intravenous blank F3-NPs (total n= 15 for cisplatin or cisplatin and F3-Np and n=20 for F3-Cis-Np in two independent experiments) and then sacrificed one week later. Following the initial administration of F3-Cis-Np we observed a rapid and significant decline in tumor volume. This was maintained throughout the experiment. IP cisplatin alone and IP cisplatin/IV F3-NPs yielded identical results (data not shown). At the conclusion of the experiment, a 2.5 fold reduction in overall weight of the tumors and ~3.5 fold reduction in volume were noted when compared to IP cisplatin alone or IP cisplatin/IV F3-NPs (Figure 3A and data not shown). Histological analysis of these tumors demonstrated (1) large

regions of hemorrhage and necrosis consistent with a potent anti-vascular effect and (2) a significant reduction in the size of tumor islets with an increase in stromal tissues (Figure A3B).

In order to determine the potential toxicity of this therapy, we collected serum from 3 animals in each treatment group 24 hours after the last intravenous treatment. Serum creatinine (a marker of renal function), aspartate aminotransferase and alanine aminotransferase (markers of hepatic function) and complete blood counts were not significantly different among untreated and F3-Cis-NP treated mice (Figure A3C). This suggests these Np are not excessively toxic to normal tissues. Further supporting the safety of the Np, unlike mice treated with systemic cisplatin, we observed no significant weight loss for F3-Cis-Np treated mice nor any other adverse effects (data not shown).

We next tested the impact of Np on tumor growth using an orthotopic intraperitoneal tumor model. Tumors were allowed to engraft for 10 days and then mice were treated with either IP cisplatin at 250 μg/kg along and F3-Np IV, IP cisplatin alone, or F3-Cis-Np IV with a final concentration of 75ug/kg cisplatin. We observed a significant increase in the overall survival of animals treated with the F3-Cis-Np as compared to IP cisplatin alone or along with F3-NPs (Figure A3D(1) and data not shown). To determine if combining IV F3-Cis-Np with IP F3-Cis-Np therapy could improve survival further by targeting both tumor vasculature (via IV dosing) and tumor cells (via IP dosing), we repeated the orthotopic tumor studies and compared various combinations of Blank F3-Np and cisplatin delivered IV, IP or combined IP and IV versus F3-Cis-Np via IV, IP, or IV and IP administration at 150 μg/kg (for IV or IP alone) or 75 μg/kg for the both IV and IP treatments for a total cisplatin concentration of 150 μg/kg. Mice were treated on days 10, 14, 21 and 28. We observed a significant survival advantage for all groups which received F3-Cis-Np intravenously as compared to mice receiving blank F3-Np

combined with cisplatin. Interestingly, combined IV and IP treatment with F3-Cis-Np did not show a significant difference in survival (Figure A3D). This suggest that vascular exposure is the primary means of therapy as the addition of intraperitoneal therapy which could directly target tumor cells, had no added benefit.

We also tested the impact of F3-Cis-Nps using subcutaneous human tumor cell line xenograft tumor models. We used cisplatin sensitive Hey1, and cisplatin resistant A2780-GFP cells (IC_{50} 7mM) and SKOV3 (IC_{50} 4mM) ovarian tumor cell lines (n=11 in treatment and control groups). As the human tumor xenografts with Hey1 and A2780 cells grow more rapidly than ID8 cells we used a more frequent treatment schedule, treating mice on Days 7, 10, and 14 after tumor engraftment with either F3-Cis-Np or blank Np and systemic cisplatin as described above. In the platinum sensitive Hey1 and A2780-GFP tumors there was clear arrest of tumor growth during the course of therapy as indicated both by tumor volumes and *in vivo* biofluorescent imaging (Figure A4A, B and data not shown). Consistent with an antivascular effect rather than an anti-tumor effect, we observed a similar growth arrest with therapy of the platinum resistant SKOV3 tumors. Also consistent with a loss of tumor vascular perfusion, tumors resected from these mice were extremely pale compared to controls (Figure A4B). Histochemical analysis of tumors demonstrated a significant loss reduction in microvasculature the F3-Cis-Np treated mice and significant tumor necrosis similar to that observed with the ID8 tumors (data not shown).

F3-Cis-Np target and eliminate human tumor vessels in vivo

Finally, as we demonstrated that the F3 targeted Np were capable of binding to human tumor endothelial cells *in vitro*, we wished to determine if the Np could bind to human tumor vessels *in vivo*. In order to test this we used a recently developed model of human tumor vasculature which utilizes Hey1 tumors cells injected into H9 ESC derived teratomas. In this model tumor vascular cells are derived from the human ESC and thus are human in origin. We performed intravenous injections of F3-Alexa-Np in H9-ESC-Hey1 tumor bearing mice. Importantly, we observed clear binding of the F3-Alexa-Np to the human $CD31^+$ tumor vessels, confirming the ability of these F3 targeted Np to bind to human vessels *in vivo*. We therefore used this model to test the therapeutic efficacy of F3-Cis-Nps. To track tumor cell growth we used immunofluorescent DsRED Hey1 tumor cells. Once again we treated animals with either IV F3-Np and systemic cisplatin or F3-Cis-Np (n=3 controls and n=3 treatment groups in two independent experiments). Animals were treated on day 10, 14, 17 and 21. Like the previous tumor models, treatment with F3-Cis-Np lead to an initial loss of fluorescence and then stabilization of disease, whereas tumors treated with systemic cisplatin demonstrated progressive growth (Figure A5)

DISCUSSION

In this study, we used an F3-targeted polymeric nanoparticle formulation consisting of encapsulated cisplatin in a polyacrylamide nanoparticle to target tumor vessels as a cancer therapeutic. While vascular targeted nanoparticle studies have been reported previously, to our knowledge ours is the first to demonstrate the ability to bind to human tumor vessels *in vivo*.

F3-Cis-Np therapy appeared safe with minimal side effects. *In vitro* studies demonstrated specific binding to tumor and tumor endothelial cells. *In vivo* studies also demonstrated predominant binding to microvascular tumor endothelial cells with lesser uptake on tumor cells. We observed some minimal non-specific uptake in kupffer cells of the liver and nanoparticles were excreted via the kidneys. However, non-specific binding was minimized with titration of dose and minimal toxicity was noted with F3-Cis-Np treatment as evidenced by stable creatinine, liver function tests and complete blood counts. This is not surprising given the total cisplatin dose used in the nanoparticle studies (75 or 150 mg/Kg) was ~1/20th the traditional dose of cisplatin (1-5mg/kg).

In addition to being safe, F3-targeted nanoparticles appear to be a highly effective as a therapeutic. While F3 peptides can bind both tumor cells and endothelial cells, our studies suggest that the primary effect of therapy was anti-vascular: Similar to prior studies, minimal *in vitro* cytotoxicity was noted with F3-Cis-Np treatment of human tumor cell lines (197-199). This

may be due to the higher concentration of drug needed to kill tumor cells as evidenced by their higher IC50. In contrast we observed significant *in vitro* cytotoxicity of F3-Cis-Np on human tumor endothelial cells (Figure 2C). In addition we observed a rapid impact of therapy, associated with large regions of necrosis and hemorrhage, and a loss of clearly defined microvasculature consistent with an anti-vascular effect. Moreover, F3-Cis-Np were effective even in cisplatin resistant tumors. Finally, like other anti-angiogenics, continuous treatment was associated with stable disease and no further reduction of tumor was noted.

F3-Cis-Np therapy was effective in both solid tumor and IP tumor models. While the impact of therapy on flank tumors was most dramatic, a clear survival advantage was noted in the IP tumor model. The survival advantage was primarily associated with IV treatment. Interestingly, the combination of both IP and IV nanoparticles did not demonstrate a clear advantage over IV only nanoparticles. This may be because the cisplatin dose in the F3-Cis-Nps is sub-therapeutic to kill tumor cells as observed in vivo. Alternatively, while we did not see significant systemic Np exposure with IP delivery (data not shown), it is possible the Np delivered IP are still primarily taken up in the tumor vasculature.

We speculate that anti-vascular cell therapy may be much more effective clinically than specific molecular biologic anti-angiogenic therapies; resistance to therapies targeting specific molecular pathways can develop through the up-regulation of one of numerous redundant angiogenic pathways. However, the endothelial cell is the final target of all angiogenic pathways, thus elimination of the endothelial cell should inhibit all of these angiogenic pathways.

Based on previous observations that F3 peptide can target tumor cells, we chose to load our nanoparticles with cisplatinum, the most active anti-ovarian tumor cell agent. Given our observations that the F3 targeted nanoparticles appear to be primarily targeting tumor vascular cells, cisplatin may not be the most active chemotherapeutic. Cisplatin is a DNA targeting agent and is most active against actively proliferating cells; more established non-dividing vascular cells would be less sensitive to this agent. This would explain the stable disease we observed with repeat therapy. We hypothesize that therapy with a microtubule targeting agent, such as the taxanes, may demonstrate even greater activity. Furthermore, an iRGD peptide was recently described (193). This peptide targets the vasculature and is then cleaved to allow release of the peptide with a now exposed neuropilin-1 binding motif which mediates penetration of the peptide through the vasculature to target tumor cells. Thus a combination of F3-Taxane nanoparticle and iRGD peptide targeted cisplatin nanoparticles could be particularly effective—targeting neo-vasculature, established tumor vessels, and tumor cells. Given the extremely low doses of chemotherapeutic agents necessary for effectiveness of the Np as demonstrated in the current study, such a combination could be possible with an acceptable side effect profile. Further experiments will be necessary to determine the appropriate sequencing for combining these agents; vascular disruption prior to the administration of anti-tumor agents could in theory reduce intratumoral drug delivery and thereby reduce efficacy. In this context, dynamic imaging studies may be useful also to address the optimal schedule of administration of combination therapies.

Finally, we show for the first time, the ability of vascular targeted Np to effectively target human tumor endothelial cells, not only *in vitro*, but more importantly *in vivo*. We used a human ESC based tumor model in which a subset of the tumor vascular cells are derived from

the human ESC and are therefore human tumor vessels (93). We have demonstrated that the vessels in this model are indeed tumor vessels, expressing unique tumor vascular markers (201). Thus we believe that this model represents an excellent tool for the study of therapeutics targeting human tumor vasculature.

In conclusion we have demonstrated that F3-targeted nanoparticles are a safe and potently effective anti-vascular therapeutic. Activity appears primarily due to the elimination of tumor microvasculature. This proof of principle study demonstrates the ability to overcome ovarian cancer chemoresistance using vastly reduced drug concentrations by targeting nanoplatforms to the tumor neovasculature/microenvironment. Importantly, we demonstrate that these nanoparticles are effective in binding and eliminating human tumor endothelial cells. These preclinical studies indicate that further anti-vascular study in human tumors is warranted.

ACKNOWLEDGEMENTS

This work was initiated with the generous support of the Ovarian Cancer Research Fund Liz Tilberis' Award and the Damon Runyon Cancer Research Foundation Clinical Investigator Award. This work was completed with the support of the NIH New Investigator Innovator Directors Award grant #00440377. We would like to thank the embryonic stem cell core at the University of Michigan for assistance with ESC culture.

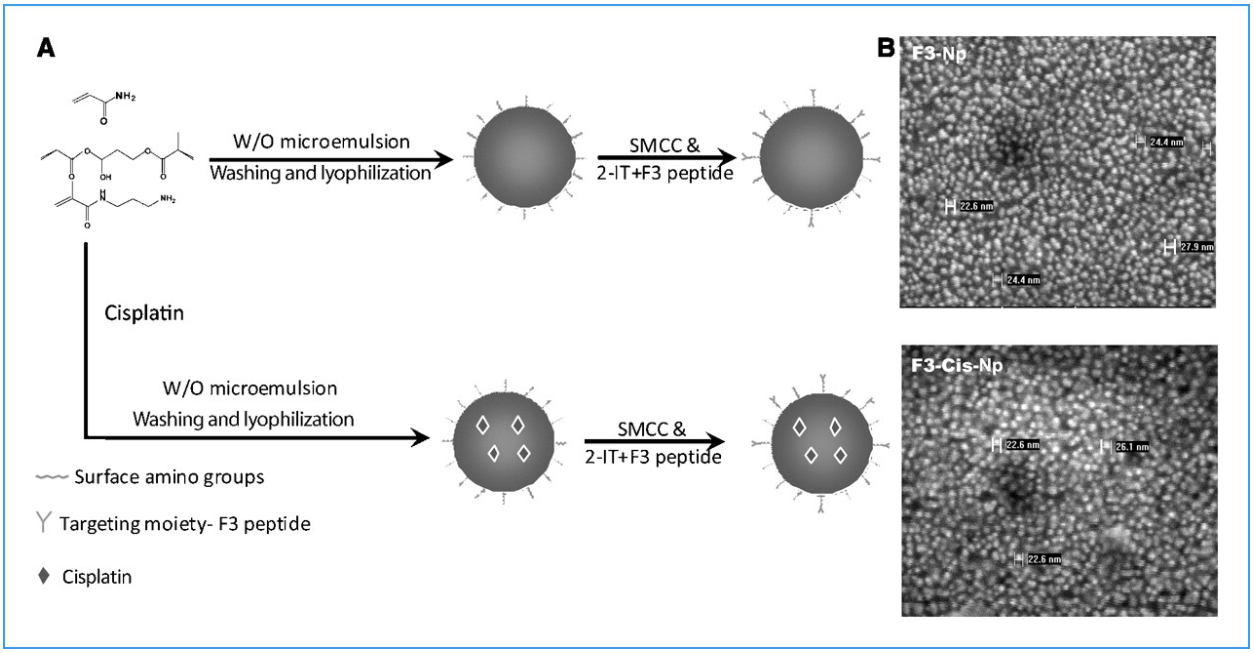

Figure A1. Development of nanoparticles. **A** Schematic demonstration of the production of both blank and cisplatin containing F3 targeted nanoparticles. **B**. The scanning electron micrographs showing the size of the nanoparticle after modification.

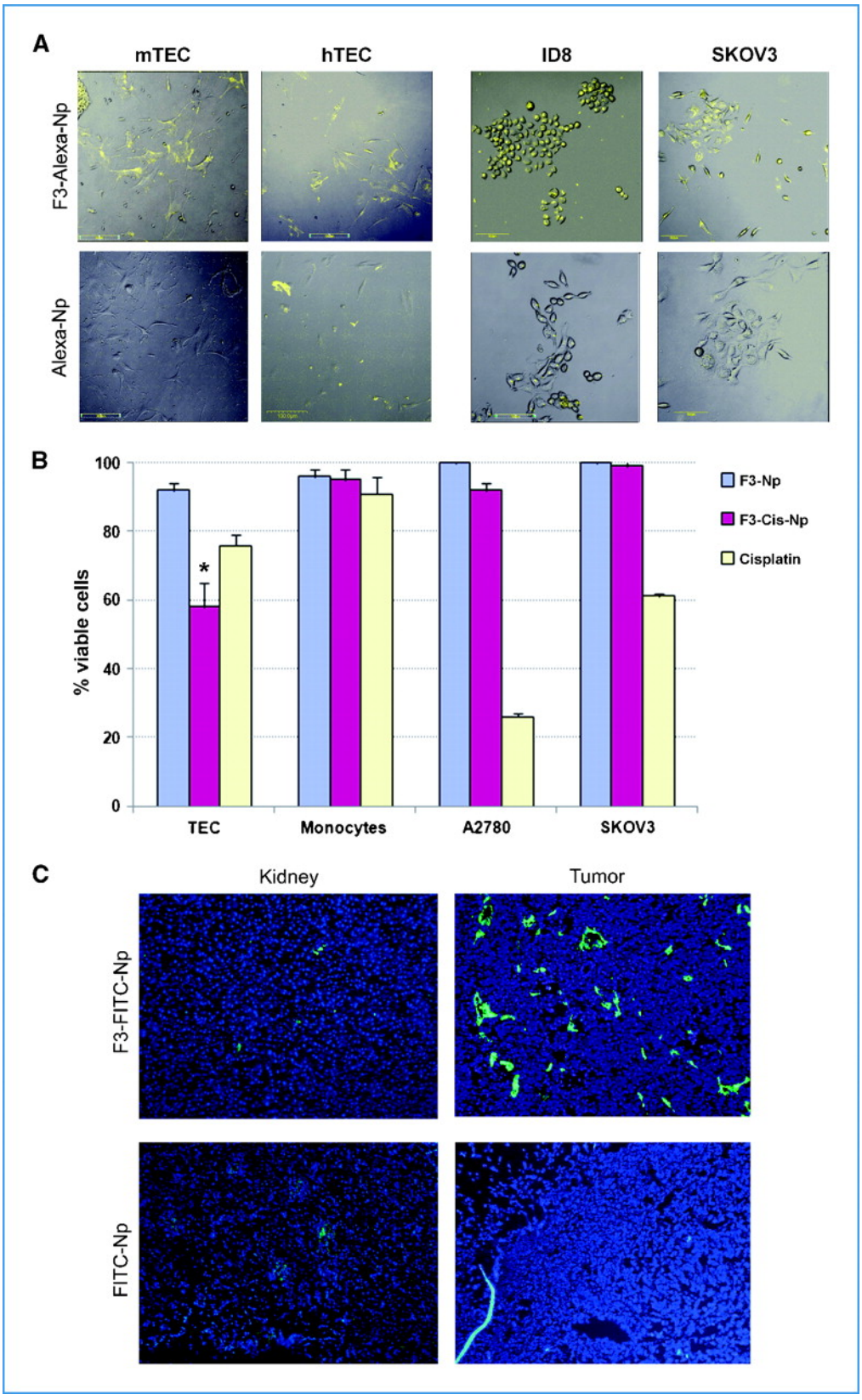
A
mTEC
hTEC
ID8
SKOV3
F3-Alexa-Np
Alexa-Np
B
% viable cells
100
80
60
40
20
0
*
TEC
Monocytes
A2780
SKOV3
F3-Np
F3-Cis-Np
Cisplatin
C
Kidney
Tumor
F3-FITC-Np
FITC-Np

Figure A2. Binding and cytotoxicity of F3 targeted nanoparticles. **A.** *In vitro* binding of fluorescent nanoparticles demonstrating effective binding of F3 targeted Alexa-594 nanoparticles (F3-Alexa-Np) but not for non-targeted Alexa-594 control nanoparticles (Alexa-Np) to murine and human tumor endothelial cells (mTEC and hTEC) and murine (ID8) and human (SKOV3) tumor cell lines. **B**. Percent viable cells (relative to PBS controls) following treatment with F3-Cis-Np, blank F3 targeted nanoparticles (F3-Np), or cisplatin (1 mg/ml for TECs and 5mg/ml for tumor cells) targeting human tumor endothelial cells (TEC), human peripheral blood monocytes, and ovarian tumor cells (SKOV3 and A2780). **C.** *In vivo* binding of F3-Alexa488-Np and non-targeted control Alexa-488 Np in murine ID8 flank tumors and kidneys of treated mice.

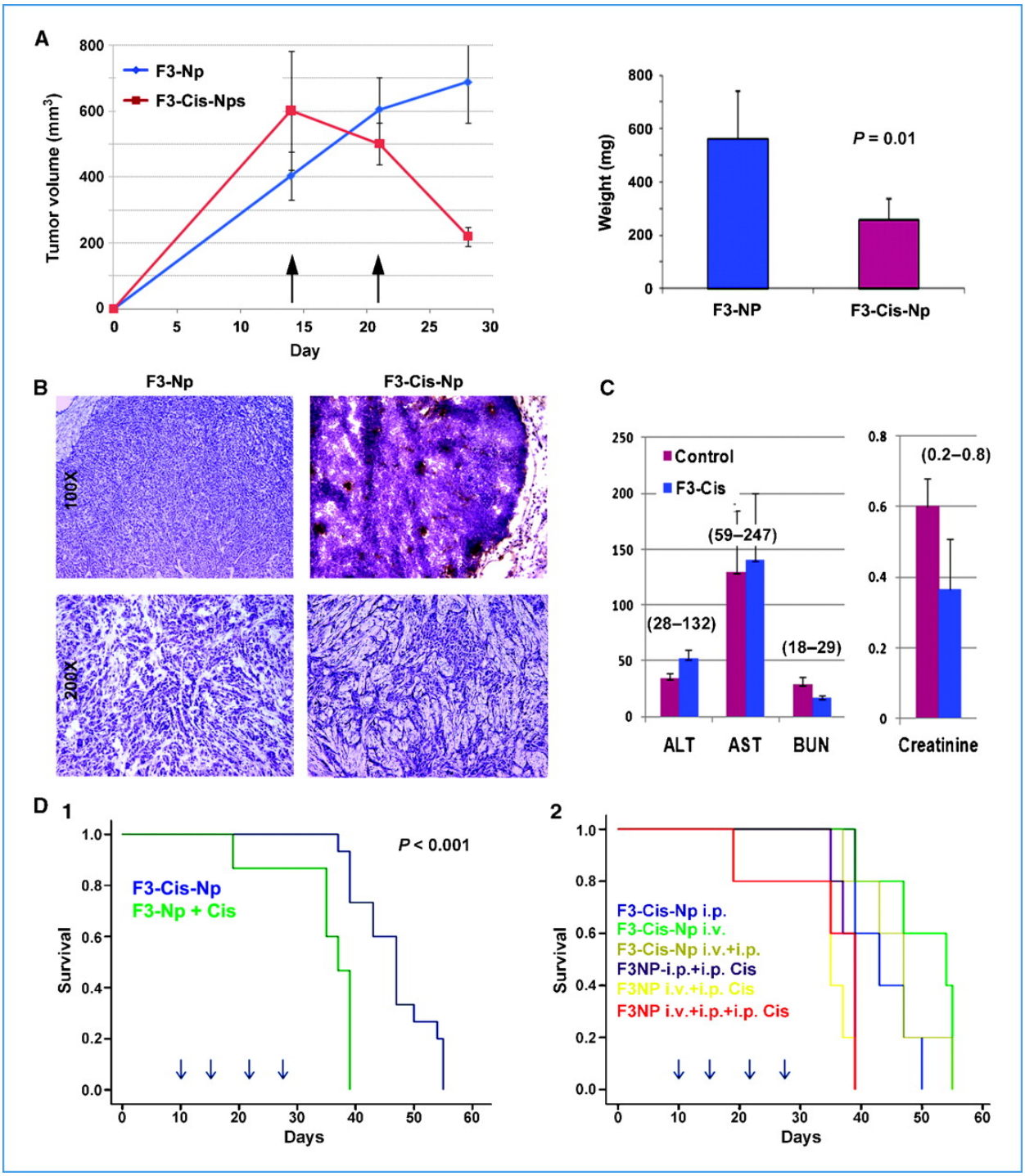

Figure A3. **Therapeutic efficacy and toxicity of F3-Cisplatin-nanoparticles in a murine ovarian tumor model. A.** Tumor growth curves and weights of ID8 xenografts treated with F3-Cis-Np or blank F3-Np and systemic cisplatin (n=15 animals per group). Arrows indicate time of treatment. **B**. Tissue histology of tumors from control animals treated with blank F3-Np and systemic cisplatin (F3-Np + Cis) or F3-Cis-Np. Low power image demonstrates large area

ofvascular necrosis (upper right) in treated tumors. High power images demonstrate significant reductions in tumor islets in treated tumors (lower right). **C.** Lack of toxicity in F3-Cis-Np treated animals as demonstrated alanine aminotranferease (ALT) and aspartate aminotransferase (AST), blood urea nitrogen (BUN) and serum creatinine from mice treated with F3-Cis-Nps or F3-Np controls. Normal ranges are indicated (parentheses). **D.** Kaplan Meier curves indicating survival using an orthotopic intraperitoneal tumor model (1) comparing intravenous (IV) F3-Cis-Np *vs* IV control nanoparticles + systemic cisplatin delivered intraperitoneally (F3-Np + Cis), and (2) comparison of indicated treatment groups comparing IV and IP treatment of F3-Cis-Np and various controls. Greatest survival advantage was seen in the IV F3-Cis-Np group. Addition of IP F3-Cis-Np added no survival advantage (n=10 animals per group). Arrows indicate time of treatment.

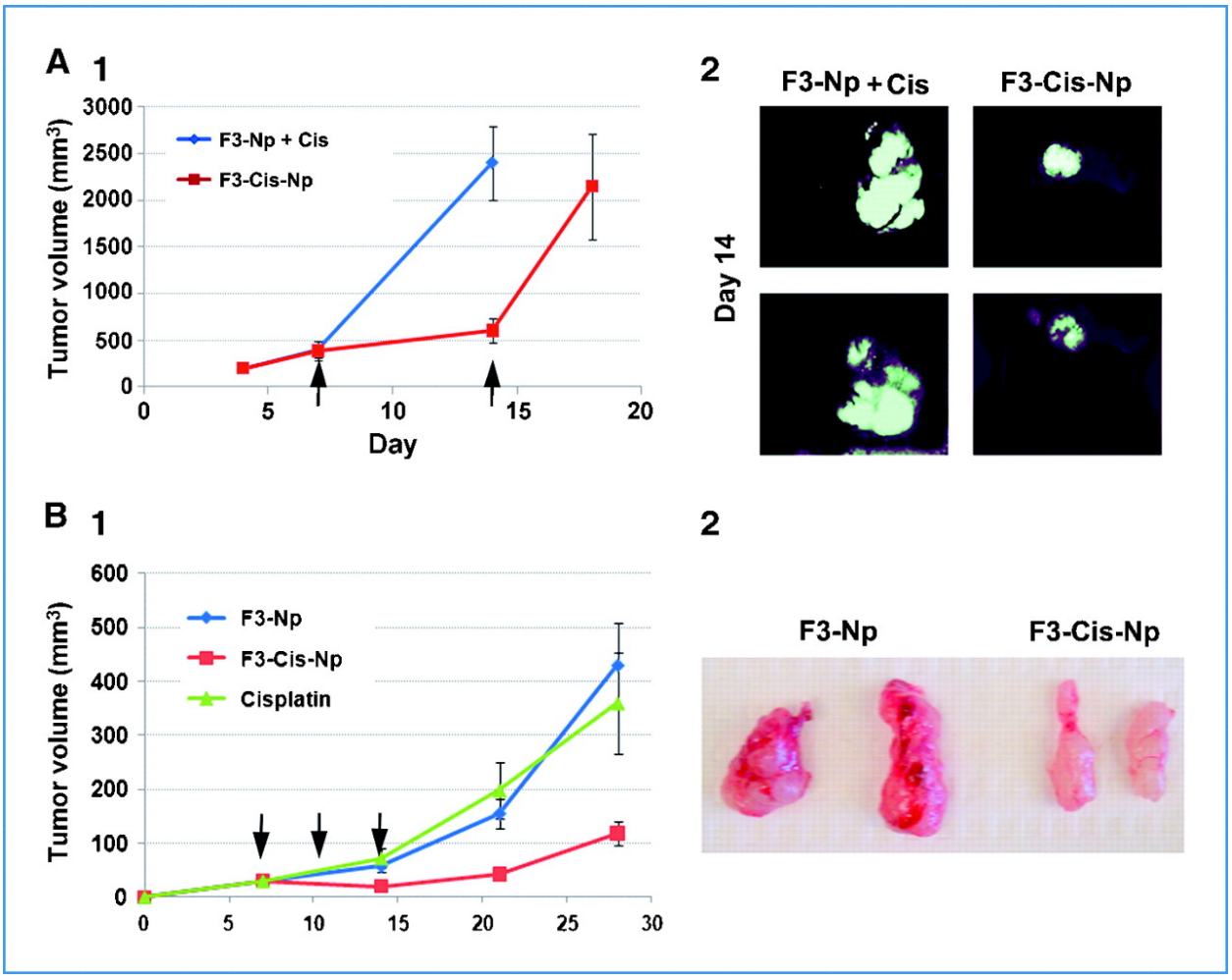

Figure A4. Therapeutic efficacy of F3-Cis-Np against human tumor xenografts. A. (1) Tumor growth curves and **(2)** *in vivo* fluorescent imaging of control (F3-NP and IP cisplatin treated) and F3-Cis-Np treated A2780 cisplatin sensitive tumor xenografts. **B (1)** and **(2)**. Tumor growth curves and gross tumor pathology of F3-Cis-Np treated and control F3-Np and IP cisplatin (F3-Np + Cis) treated cisplatin resistant SKOV3 tumor xenografts. F3-Cis-Np treated tumors were significantly smaller and appeared pale and avascular (n=5/group in two independent experiments).

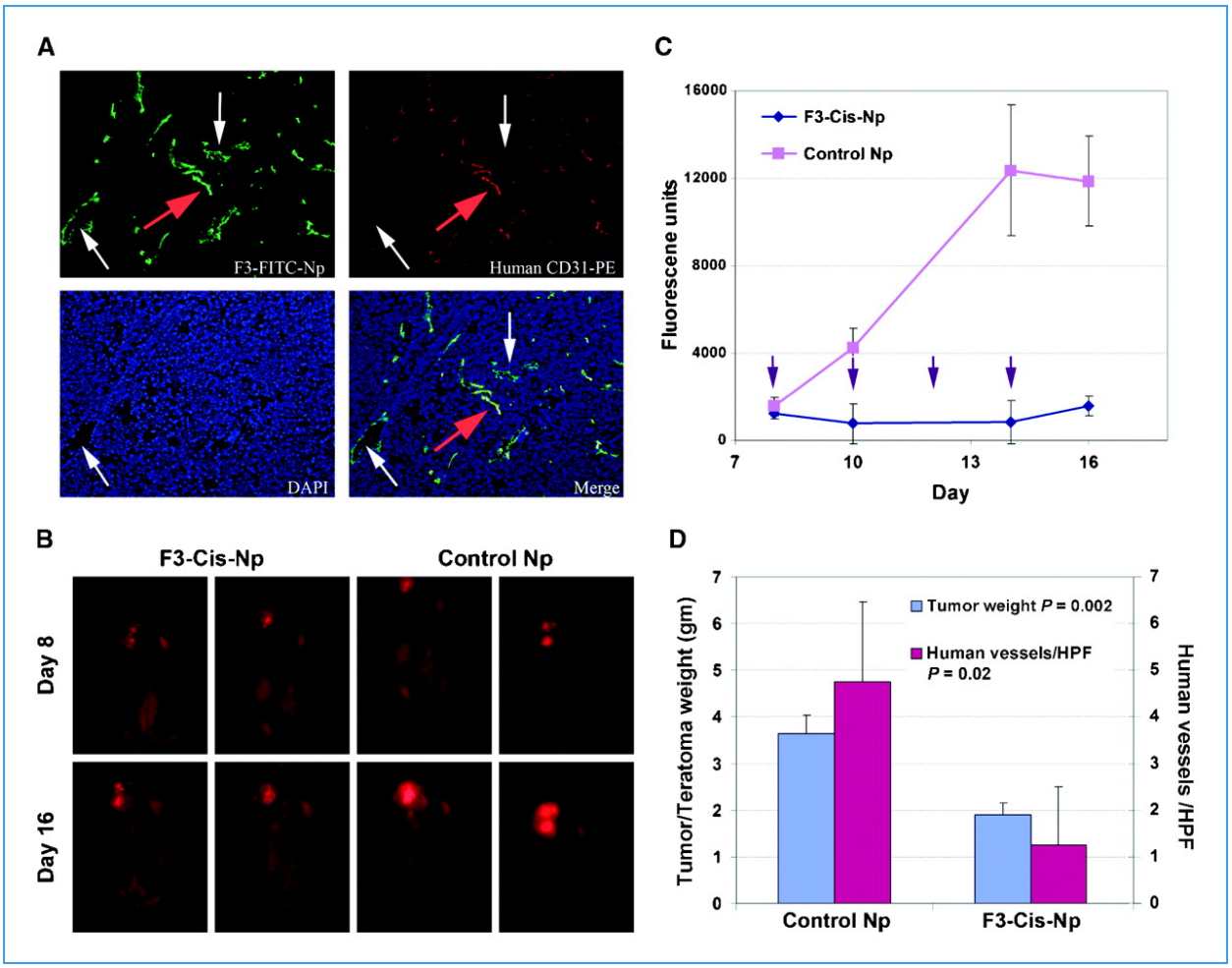

Figure A5. F3 targeted Np effectively target human tumor vessel s *in vivo.* A. Immunofluorescence demonstrating the F3 targeted Alexa488-Np (F3-Alexa-Np) bind to human CD31+ (hCD31) vessels *in vivo* using a human embryonic stem cell tumor model with human vessels. Red arrow indicates hCD31+ human vessel. White arrows identify hCD31(-) murine vessels. **B**. *In vivo* fluorescent imaging of F3-Cis-Np and control (blank F3-Np) treated ESC-DsREd Hey1 tumors just prior to the first IV treatments (day 8) and at the time of sacrifice two days after the last IV treatment (day 16). **C.** Tumor growth curves of F3-Cis-Np treated and control (F3-Np) treated ESC-DsREd Hey1 tumors with human tumor vessels. Arrows indicate times of IV NP treatments (n=3 per group in two independent experiments). **D**. Tumor weight and density of human vessels in F3-Cis-Np treated and control (F3-Np) treated ESC-DsREd Hey1 tumors. Both were statistically significantly reduced as indicated.

REFERENCES

1. Aghajanian C. The role of bevacizumab in ovarian cancer--an evolving story. Gynecol Oncol 2006;102(2):131-3.
2. Bidus MA, Webb JC, Seidman JD*, et al.* Sustained response to bevacizumab in refractory well-differentiated ovarian neoplasms. Gynecologic oncology 2006;102(1):5-7.
3. Monk BJ, Han E, Josephs-Cowan CA*, et al.* Salvage bevacizumab (rhuMAB VEGF)-based therapy after multiple prior cytotoxic regimens in advanced refractory epithelial ovarian cancer.[see comment]. Gynecologic oncology 2006;102(2):140-4.
4. Numnum TM, Rocconi RP, Whitworth J, Barnes MN. The use of bevacizumab to palliate symptomatic ascites in patients with refractory ovarian carcinoma. Gynecol Oncol 2006;102(3):425-8.
5. Garcia AA, Hirte H, Fleming G*, et al.* Phase II clinical trial of bevacizumab and low-dose metronomic oral cyclophosphamide in recurrent ovarian cancer: a trial of the California, Chicago, and Princess Margaret Hospital phase II consortia. J Clin Oncol 2008;26(1):76-82.
6. Cohn DE, Valmadre S, Resnick KE, Eaton LA, Copeland LJ, Fowler JM. Bevacizumab and weekly taxane chemotherapy demonstrates activity in refractory ovarian cancer. Gynecol Oncol 2006;102(2):134-9.
7. Shojaei F, Wu X, Malik AK*, et al.* Tumor refractoriness to anti-VEGF treatment is mediated by CD11b+Gr1+ myeloid cells. Nat Biotechnol 2007;25(8):911-20.
8. Buckanovich RJ, Sasaroli D, O'Brien-Jenkins A*, et al.* Tumor Vascular Proteins as Biomarkers in Ovarian Cancer Journal of Clinical Oncology 2007;25 (7):852-61.
9. Lu C, Bonome T, Li Y*, et al.* Gene alterations identified by expression profiling in tumor-associated endothelial cells from invasive ovarian carcinoma. Cancer Research 2007;67(4):1757-68.
10. Temming K, Schiffelers RM, Molema G, Kok RJ. RGD-based strategies for selective delivery of therapeutics and imaging agents to the tumour vasculature. Drug Resistance Updates 2005;8(6):381-402.
11. Janssen ML, Oyen WJ, Dijkgraaf I*, et al.* Tumor targeting with radiolabeled alpha(v)beta(3) integrin binding peptides in a nude mouse model. Cancer Research 2002;62(21):6146-51.
12. Garde SV, Forte AJ, Ge M*, et al.* Binding and internalization of NGR-peptide-targeted liposomal doxorubicin (TVT-DOX) in CD13-expressing cells and its antitumor effects. Anticancer Drugs 2007;18(10):1189-200.
13. Christian S, Pilch J, Akerman ME*, et al.* Nucleolin expressed at the cell surface is a marker of endothelial cells in angiogenic blood vessels. Journal of Cell Biology 2003;163(4):871-8. 14. Reddy GR, Bhojani MS, McConville P*, et al.* Vascular targeted nanoparticles for imaging and treatment of brain tumors. Clin Cancer Res 2006;12(22):6677-86.
15. Porkka K, Laakkonen P, Hoffman JA, Bernasconi M, Ruoslahti E. A fragment of the HMGN2 protein homes to the nuclei of tumor cells and tumor endothelial cells in vivo.

Proceedings of the National Academy of Sciences of the United States of America 2002;99(11):7444-9.
16. Koo YE, Reddy GR, Bhojani M*, et al.* Brain cancer diagnosis and therapy with nanoplatforms. Adv Drug Deliv Rev 2006;58(14):1556-77.
17. Kopelman R, Koo YEL, Philbert M*, et al.* Multifunctional nanoparticle platforms for in vivo MRI enhancement and photodynamic therapy of a rat brain cancer. J Magn Magn Mater 2005;293:404-10.
18. Mukhopadhyay S, Barnes CM, Haskel A, Short SM, Barnes KR, Lippard SJ. Conjugated platinum(IV)-peptide complexes for targeting angiogenic tumor vasculature. Bioconjug Chem 2008;19(1):39-49.
19. Lu Z, Tsai M, Lu D*, et al.* Tumor-penetrating microparticles for intraperitoneal therapy of ovarian cancer. Journal of Pharmacology & Experimental Therapeutics 2008;327(3):673-82.
20. Pastorino F, Di Paolo D, Piccardi F*, et al.* Enhanced antitumor efficacy of clinical-grade vasculature-targeted liposomal doxorubicin. Clinical Cancer Research 2008;14(22):7320-9.
21. Sugahara KN, Teesalu T, Karmali PP*, et al.* Tissue-penetrating delivery of compounds and nanoparticles into tumors. Cancer Cell 2009;16(6):510-20.
22. Tzukerman M, Rosenberg T, Reiter I*, et al.* The influence of a human embryonic stem cell-derived microenvironment on targeting of human solid tumor xenografts. Cancer Res 2006;66(7):3792-801.
23. Tzukerman M, Rosenberg T, Ravel Y, Reiter I, Coleman R, Skorecki K. An experimental platform for studying growth and invasiveness of tumor cells within teratomas derived from human embryonic stem cells. Proc Natl Acad Sci U S A 2003;100(23):13507-12.
24. Pulaski HL, Spahlinger G, Silva IA*, et al.* Identifying alemtuzumab as an anti-myeloid cell antiangiogenic therapy for the treatment of ovarian cancer. Journal of Translational Medicine 2009;7:49.
25. Conejo-Garcia JR, Buckanovich RJ, Benencia F*, et al.* Vascular leukocytes contribute to tumor vascularization. Blood 2005;105(2):679-81.
26. Koo YE, Fan W, Hah H*, et al.* Photonic explorers based on multifunctional nanoplatforms for biosensing and photodynamic therapy. Appl Opt 2007;46(10):1924-30.
27. Jin W, Xu P, Zhan Y*, et al.* Degradable cisplatin-releasing core-shell nanogels from zwitterionic poly(beta -aminoester)-graft-PEG for cancer chemotherapy. Drug Deliv 2007;14(5):279-86.
28. Uchino H, Matsumura Y, Negishi T*, et al.* Cisplatin-incorporating polymeric micelles (NC-6004) can reduce nephrotoxicity and neurotoxicity of cisplatin in rats. Br J Cancer 2005;93(6):678-87.
29. Nishiyama N, Okazaki S, Cabral H*, et al.* Novel cisplatin-incorporated polymeric micelles can eradicate solid tumors in mice. Cancer Res 2003;63(24):8977-83.
30. Zhang L, Yang N, Garcia JR*, et al.* Generation of a syngeneic mouse model to study the effects of vascular endothelial growth factor in ovarian carcinoma. American Journal of Pathology 2002;161(6):2295-309. 31. McLean K, Pulaski HS, Wang Y, Spahlinger G, Nor JE, RJ. B. Development of a Mouse Ovarian Cancer Model with Human Tumor Vessels to Test Novel Anti-Vascular Therapeutics. Gynecologic oncology 2009;112(2):S10-S1.